

UNCLASSIFIED

AD 258 883

*Reproduced
by the*

ARMED SERVICES TECHNICAL INFORMATION AGENCY
ARLINGTON HALL STATION
ARLINGTON 12, VIRGINIA



UNCLASSIFIED

NOTICE: When government or other drawings, specifications or other data are used for any purpose other than in connection with a definitely related government procurement operation, the U. S. Government thereby incurs no responsibility, nor any obligation whatsoever; and the fact that the Government may have formulated, furnished, or in any way supplied the said drawings, specifications, or other data is not to be regarded by implication or otherwise as in any manner licensing the holder or any other person or corporation, or conveying any rights or permission to manufacture, use or sell any patented invention that may in any way be related thereto.

258883

CATALOGED BY ASTIA
AS AD NO. _____

30 May 1961

REPORT NO. 0411-10Q-1

STUDY OF MECHANICAL PROPERTIES
OF SOLID ROCKET PROPELLANT

Contract AF 33(600)-40313 S. A. No. 1

Period Covered:

30 January through 30 April 1961

Aerojet-General CORPORATION
SOLID ROCKET PLANT • SACRAMENTO, CALIFORNIA

COPY NO. 27

9.10

30 May 1961

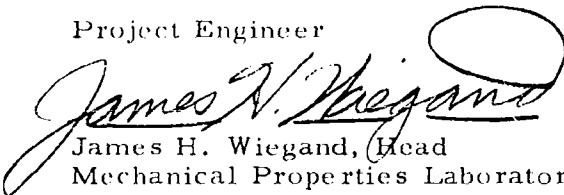
REPORT NO. 0411-10Q-1

STUDY OF MECHANICAL PROPERTIES
OF SOLID ROCKET PROPELLANT

Contract AF 33(600)-40314 S. A. No. 1

Period Covered: 30 January through 30 April 1961

Project Engineer



James H. Wiegand, Head
Mechanical Properties Laboratory

Aerojet-General CORPORATION
SOLID ROCKET PLANT . SACRAMENTO, CALIFORNIA

ABSTRACT

This program was initiated to bring together recent advances in mechanical property measurement with progress in stress analysis procedures and establish methods of predicting the structural performance of simple solid propellant grains of the case-bonded type. The availability of such methods, even though empirical and approximate, would allow an integration of propellant development and ballistic design with such a structural analysis to give an integrated approach to the design of optimum propellant charges for rocket motors. Progress has been made in focusing the measurement problem on the binder-oxidizer interaction, for which volume change on straining due to dewetting and void formation appears to be an important tool. This dilatation is shown to be the chief factor affecting strains in temperature cycling of motors and acts to reduce the maximum strains observed in cylindrical configurations. The localization of dewetting causes excessively high strains and such strained regions become the sites of final failure. The failure elongations, though highly variable, appear to offer a basis of correlating tensile test failure data with small motor temperature cycling failure, with a marked difference of such failure elongations occurring between different batches of the same formulation. The integration of the several parts of this work through a PERT type of network analysis offers promise as a basis of analysis of input, output, and interrelation of the many parts of each activity concerned with grain design.

FOREWORD

The program covered by this series of quarterly reports covers specific experiments and theoretical studies at both the Sacramento and Azusa facilities of Aerojet-General Corporation, at the University of California in Berkeley, and at the Massachusetts Institute of Technology. These reports will include also data taken on various motor development projects, where such data support or extend this program, and attempt to present a relatively complete overall picture of the progress being made to integrate all of the important factors affecting the structural behavior of solid propellant rocket motor grains. A complete literature review will not be presented in these reports as it is believed this has been adequately presented in the excellent and comprehensive Final Report of the work at GALCIT by M. L. Williams, P. J. Blatz, and R. A. Schapery.

The general mechanical properties of composite polyurethane propellants and the related stress analysis of rocket motor charges will be treated on an unclassified and non-proprietary basis; where necessary to show application to specific motor development problems, a classified second part will be prepared.

The research work in Azusa was coordinated by K. W. Bills and included work on response properties by K. W. Bills and W. D. Hart, on basic polymer behavior by H. R. Lubowitz, and on cylinder deformation under pressure by F. S. Salcedo and G. D. Nesheim. In Sacramento, strain measurements on cycling motors were performed by R. B. Farnham and D. J. Dougherty, variability of properties and improvement of testing methods was studied by I. G. Hazelton, R. D. Steele, and L. W. Martin under the direction of H. P. Briar, the behavior of propellant under pressure was measured by C. C. Surland, and the change of volume with strain was measured by P. C. Colodny and G. J. Svob under the direction of T. B. Lefferdink. Also in Sacramento, theoretical analysis of stress and strain in finite elastic cylinders was performed by R. E. Leary and A. Messner; an alternative solution to include a star configuration is under

FOREWORD (cont.)

study by A. F. Fraser and C. A. Wagner; nomographic solutions were performed by T. O'Callaghan, K. Egupov, and F. Kinsley; photoelastic analysis and gelatin studies were being carried out by R. C. Sampson and J. D. Dixon; and correlation of data on failure as related to motors was performed by W. T. Milloway and J. H. Wiegand. The broad problem of an integrated method was under joint study by J. S. Billheimer, R. Lou, K. W. Bills, T. B. Lefferdink, T. O'Callaghan, and J. H. Wiegand. The failure studies under combined loading being performed under subcontract to the Massachusetts Institute of Technology are being performed by G. Leon under the direction of Professor Norman C. Dahl.

TABLE OF CONTENTS

| | <u>Page No.</u> |
|--|-----------------|
| I. Introduction | 1 |
| II. Phase 1 – Mechanical Property Determination | 2 |
| A. Composition Factors Affecting Response Behavior | 3 |
| 1. Effect of Oxidizer Surface | 3 |
| 2. Effect of the Polymeric Binder | 4 |
| B. Measurement of Response Behavior | 7 |
| 1. Effect of Sample Size | 7 |
| 2. Effect of Filler Parameters | 10 |
| 3. Tensile Measurements Under Superimposed Hydrostatic Pressure | 14 |
| 4. Volume Change Under Uniaxial Deformation | 18 |
| 5. Effect of Repeated Strain | 26 |
| 6. Improved Preparation of JANAF Tensile Specimen | 29 |
| III. Phase 2 – Mathematical Representation of Mechanical Behavior | 33 |
| A. Propellant Classification | 33 |
| 1. Particle Packing | 33 |
| 2. Dewetting Phenomenon | 35 |
| 3. Nature of the Yield Band | 36 |
| 4. Highly Dewetted Propellant System | 39 |
| 5. Classification System | 39 |
| IV. Phase 3 – Theoretical and Experimental Stress Analysis | 42 |
| A. Theoretical Calculation of Stresses and Strains | 42 |
| 1. Computer Calculation of Stresses and Strains | 42 |
| 2. Nomograph for Calculation of Stresses and Strains | 44 |
| B. Experimental Temperature Cycling of Propellant Cylinders | 47 |

TABLE OF CONTENTS (cont.)

| | <u>Page No.</u> |
|---|-----------------|
| C. Experimental Pressurization of Propellant Cylinders | 49 |
| 1. Test Results | 50 |
| 2. Precision of Pressure Test Methods | 57 |
| 3. Analytical Correlation of Data with Mechanical Properties | 58 |
| 4. Mechanical Property Measurements Required for Analysis | 60 |
| D. Experimental Studies of Photoelastic Materials | 60 |
| E. Development of New Methods of Strain Measurement | 62 |
| V. Phase 4 - Failure Criteria | 62 |
| A. Batch Variability of Failure Behavior | 63 |
| B. Correlation of Failure Data with Motor Failures | 70 |
| C. Graphical Representation of Failure Behavior | 75 |
| D. Mechanism of Failure | 75 |
| E. Failure Studies Under Combined Loading (MIT) | 78 |
| VI. Phase 5 - Integrated Design Approach | 81 |
| VII. Summary and Conclusions | 88 |
| List of Symbols | 89 |
| Bibliography | 91 |

TABLE LIST

| <u>Table No.</u> | | <u>Page No.</u> |
|------------------|---|-----------------|
| 1 | Original Data on Sample Tests | 9 |
| 2 | The Stress at Break for Notched Propellant Specimens Tested at 80°F | 38 |
| 3 | Comparison of Uniaxial and Biaxial Failure Stresses of a Class 2 Propellant at Several Temperatures | 77 |

FIGURE LIST

| <u>Figure No.</u> | | <u>Page No.</u> |
|-------------------|---|-----------------|
| 1 | Comparison of the Effect of Sample Size upon the Mechanical Properties of a Polyurethane Propellant (NH ₄ ClO ₄ Filler) | 11 |
| 2 | Comparison of the Effect of Sample Size upon the Mechanical Properties of a Polyurethane Propellant (NH ₄ ClO ₄ Filler) | 12 |
| 3 | Comparison of the Effect of Gage-Length Upon the Mechanical Properties of a Polyurethane Propellant (NH ₄ ClO ₄ Filler) | 13 |
| 4 | Comparison of the Effect of Filler Upon the Mechanical Properties of a Polyurethane Propellant | 14 |
| 5 | Tensile Stress-Strain with Superimposed Hydrostatic Pressure | 15 |
| 6 | Stress-Strain Data for Uniaxial Tensile with Superimposed Hydrostatic Pressure Using Jones' Correlation | 17 |
| 7 | Effect of Pressure on Elongation at Failure | 19 |
| 8 | Effect of Pressure on Nominal Stress at Failure | 20 |
| 9 | Log Volume Change vs Log Extension Ratio for Several Glass Bead - Polyurethane Composites | 22 |
| 10 | Correlation of Yield Strain with Volume Fraction of Glass Beads | 23 |
| 11 | Uniaxial Stress vs Strain Glass Bead - Polyurethane Composites | 24 |
| 12 | Tensile Test Under Water Compared with that in Air or Silicone Oil Showing Behavior After Yield Strain | 25 |

FIGURE LIST (cont.)

| <u>Figure No.</u> | | <u>Page No.</u> |
|-------------------|--|-----------------|
| 13 | Log Volume Change vs Log Extension Ratio for a 50.7 Vol % Glass Bead Filled Polyurethane Rubber in a Cycling Test | 27 |
| 14 | Stress-Strain Behavior of Class 2 Propellant at a Test Temperature of 77°F and a Strain Rate of 0.74 min ⁻¹ for Repeated Cycles with Rest of 13 Days After Run No. 11 | 28 |
| 15 | Machining of First Side of Block of Propellant Using Vacuum to Hold Block in Place | 31 |
| 16 | Machining Other Face of Propellant Block Using Vacuum to Hold First Machined Surface on Formed Aluminum Section | 32 |
| 17 | Typical Packing of a Propellant System (65 Vol% Filler* - Strained 8%) | 34 |
| 18 | Dewetting of Class 2 Propellant | 37 |
| 19 | Dewetting in a Class 1 Solid Propellant (Dark Areas Indicate the Formation of Cavities about the White Oxidizer Particles) | 40 |
| 20 | Effect of b^2/a^2 on Maximum Strains Observed in Subscale Motors | 48 |
| 21 | End of Grain at Zero Pressure as Seen Through 1.5-in. -Thick Lucite Plate Showing Grids on the Plate and on the End of the Grain | 48 |
| 22 | End of Grain Shown in Figure 21 at Interval Pressure of 300 psig | 52 |
| 23 | Tangential Strains at Inner Wall of Cylinder, as Measured by Water Volume and by Grid on End of Grain, and Tangential Strain at Outer Wall as Measured by Strain Gages | 53 |
| 24 | Tangential Strain at Various Radii of Pressurized Hollow Cylinder Calculated from Movement of Grid at Top of Cylinder Plotted Against Radii and $1/(\text{Radius})^2$ | 55 |
| 25 | Propellant Case Interface Pressure Produced by the Internal Pressure for a Case Modulus of 10^7 psi | 56 |

FIGURE LIST (cont.)

| <u>Figure No.</u> | | <u>Page No.</u> |
|-------------------|---|-----------------|
| 26 | Correlation of Failure Strain at 180°F with that at 77°F for Same Batch | 65 |
| 27 | Correlation of Failure Strain at 0°F with that at 77°F for Same Batch | 66 |
| 28 | Correlation of Failure Strain at -40°F with that at 77°F for Same Batch | 67 |
| 29 | Correlation of Failure Strain at -75°F with that at 77°F for Same Batch | 68 |
| 30 | Effect of 2 Months Storage at 0°F on the Initial and Final Break Elongations at -75°F of Several Batches of a Class 2 Polyurethane Propellant | 69 |
| 31 | Relation of Failure in Tensile Specimens to Cracking of Subscale Tubular Case Bonded Grains at -75°F for one Class 1 and two Class 2 Polyurethane Propellants | 71 |
| 32 | Relation of Failure in Tensile Specimens to Cracking of Subscale Tubular Case Bonded Grains at -75°F for one Class 1 and two Class 2 Polyurethane Propellants | 73 |
| 33 | Sketch of Very Low Rate Tester (VLRT) | 74 |
| 34 | Hypothetical Propellant Properties Related to Motor Strain | 76 |
| 35 | Predicted Values of Variation of Modulus with Density Compared to Test Data on Initial Loading | 80 |
| 36 | Diagram of General Process of Grain Development Showing Interrelation of Major Development Efforts | 85 |
| 37 | Growth of Reliability (or Performance) of a Given Propulsion System | 87 |

I. INTRODUCTION

The relation of the mechanical properties of solid propellants to the structural behavior of solid propellant charges in motors has not been established quantitatively, though general property relationships have been used qualitatively by propellant development chemists and the designers of charge configurations. The use of mechanical property criteria as acceptance criteria is rare, though rejection for defects, lack of cure, and ballistics are customary. This same problem exists in general in the plastics and elastomer field and reflects the complexity of the mechanical property behavior with time and temperature of such materials, as well as the unsuitability of the usual stress analysis procedures in dealing with such linear or nonlinear viscoelastic materials.

Recent progress in analytical procedures, coupled with the capacity for high-speed numerical computation in large IBM calculators, has now brought some of these problems facing the stress analyst within reach of solution. It was proposed that a concerted attack be made on the problem by empirical and theoretical methods, using the newer methods of measuring pertinent properties. The results would be confirmed by cycling and pressurization experiments on simpler tubular case-bonded charges of solid propellant. If the methods proved applicable, the more complex case of star perforations would then be attempted.

The availability of a rational procedure of treating the structural problem would lead to its use as a part of an integrated method of propellant charge design capable of producing an optimum charge for given requirements*. The program as a whole incorporates the four phases pertinent to structural design—mechanical-property measurement, representation of the properties in a form suitable for use, theoretical and experimental stress analysis, and development of failure criteria—and a fifth phase that integrates structural design with propellant development and ballistic configurational analysis. The report will discuss the work done under each of these phases and show the development of the integrated design method.

*By optimum charge is meant one for which the several types of reliability—ballistic performance, performance without malfunction, reproducibility, etc.—are about the same.

II. PHASE 1 — MECHANICAL PROPERTY DETERMINATION

The broad objective of this phase is to measure the response behavior in terms of properties necessary to structural analysis. Specifically, several batches of live and inert propellants will be studied over a wide range of strains, strain rates, and loads at a wide range of temperatures under both uniaxial and multiaxial conditions. Improvements in apparatus and technique will be required to give measurements of the desired accuracy, and to allow assessment of the variability of the propellant. Measurements of this type are valuable for gaining insight into the causes of behavior as well as for providing the numerical values needed in structural analysis. The results of theoretical and experimental studies on the mechanical behavior and failure properties of solid propellants, liners, and propellant-liner bonds should be interpreted into practical goals and procedures for research and development chemists. This will provide the parametric relations, with their chemical and physical interpretations, which are pertinent either to currently produced propellant materials or to totally bonded and totally dewetted propellant materials, even though such materials are not now produced.

Theoretical and experimental studies of solid propellants, liners, and propellant-liner bonds should also be directed towards the provision of those mechanical response relations and failure properties most useful to the design engineer or stress analyst. The first approach in making the measurements suitable for design use will be to assume that the classical theory of elasticity, as modified by viscoelasticity considerations, is sufficiently accurate to describe propellant behavior. In solid grains the major portion of the charge appears to fit this description, but in regions of high stress concentrations, locally yielded material is produced by the very large local strains. Hence, for the solid propellant in the high strain region, both the time-dependent viscoelastic parameters and the properties of the unit-yield band of localized yielding are required. This would not be true for the cases of totally wetted or totally dewetted propellants, since in those cases the unit band of

II, Phase 1 — Mechanical Property Determination (cont.)

localized yielding does not occur and the classical properties of materials may be sufficient for reasonable characterization. The second approach will be to assume the necessity of the finite theory of elasticity for grain design and analysis. Here the large strain viscoelastic parameters and the unit band of localized yielding properties would both be required except for the totally wetted or totally dewetted propellants where the unit yield band does not apply.

A. COMPOSITION FACTORS AFFECTING RESPONSE BEHAVIOR

It has been found that the mechanical properties of a propellant are determined by the following major factors: (1) the polymeric binder; (2) the filler; and (3) interactions between (1) and (2). Normal propellant development employs variations in the first two factors to control the mechanical behavior of the propellant. It is now known that the third factor, in particular the polymer-to-filler bond, significantly regulates the mechanical behavior of the propellant. It has been shown that wide ranges in mechanical properties are possible by proper control of these factors.

1. Effect of Oxidizer Surface

To understand the role of the polymer-binder bond on the propellant properties a study was initiated to determine the effect of totally wetted and totally dewetted oxidizer. Propellants that partially dewet the oxidizer will be studied later in the program. One of the methods used to obtain a totally dewetted oxidizer is the modification of the oxidizer surface.

In an effort to provide suitable oxidizer, three 100-gram batches of NH_4ClO_4 , coated with Viton, barium stearate and E-39*, have been prepared for preliminary evaluation in experimental filled-polymer batches. These coated particles should provide low bond strengths with the polymer.

* Union Carbide proprietary coating.

II, A, Composition Factors Affecting Response Behavior (cont.)

2. Effect of the Polymeric Binder

From a survey of work on solid filled elastomers, the following generalizations on filler release, or dewetting can be seen:

When the heat of adsorption of the elastomeric polymer on the solid filler surface is less than or of the same order of magnitude as the potential energy barrier of free rotation around single bonds of the polymer, the solid-filled polymeric system will exhibit the stress-strain properties (to 200% elongation) which are characteristic of the polymer with deviations predicted (up to 10% by volume of solid filler) by an equation which considers only the volume fraction of the solid filler and the bulk modulus of the polymer.

The work on filled elastomers in the open literature mainly deals with cases wherein the conditions given by the above generalization are fulfilled. The elastomers are usually hydrocarbons which do not adhere strongly to most solid fillers because of their chemical composition.

Nevertheless, there are cases wherein the stress-strain data cannot be reproduced through the use of the formula which contains the volume fraction of the solid-filler and the bulk modulus of the polymer as parameters. These exceptions include the very important cases wherein carbon black is used as the solid filler for hydrocarbon elastomers containing double bonds. One explains these exceptions by saying that the bulk modulus of the polymer can no longer be equated to the bulk modulus of the polymeric moiety of carbon-filled elastomers. The discrepancy between the bulk modulus of the polymeric moiety and the pure polymer is ascribed to the formation of chemical bonds between the carbon black and the elastomer which thereupon increases the crosslink density of the polymeric moiety over that of the pure polymer. The modified modulus must then be utilized in the standard formula in order to reproduce the experimental data.

II, A, Composition Factors Affecting Response Behavior (cont.)

Although the formation of chemical bonds between carbon black and unsaturated hydrocarbons can be considered as chemisorption, a phenomenon wherein the heat of adsorption of the polymer to the solid filler exceeds the potential barrier of free rotation around single bonds, this case is considered to be a special case of solid filled elastomeric systems wherein the interaction of the filler and the polymer is weak. This consideration can be made because the number of active sites available on carbon black for chemisorption with the elastomer are few compared to the total number of surface atoms. Thus, the molecular weight of the elastomeric binder between crosslinks remains relatively high. As a result, the chain segments are relatively unrestricted, and there is no increase in the magnitude of the potential barrier around single bonds. Another way of viewing this case is to consider that along a hydrocarbon chain which is chemisorbed to the carbon black filler certain carbon atoms are snugly anchored to the carbon filler while the adjacent hydrocarbon segments are left relatively free. The effect of carbon is thus analogous to the increasing of the crosslink density of elastomers through the use of chemical reagents.

The above situations are in marked contrast to what is considered to occur when a salt such as ammonium perchlorate (NH_4ClO_4) is placed in a polyether polymer instead of in a hydrocarbon polymer. From the foregoing discussion, one can predict the properties which filled elastomeric systems of salts such as ammonium perchlorate in a hydrocarbon binder will yield, because the interaction between filler and binder is low. In general, the physical properties of the filler system should be characteristic of the properties of the binder. For example, polybutadiene exhibits a high resistance to embrittlement at low temperatures, and the same holds for the propellant. It is predicted that the stress-strain curve of the above filled system below one tenth volume fraction of solids can be characterized by considering the solid volume fraction and the polymer

II, A, Composition Factors Affecting Response Behavior (cont.)

modulus as parameters. Corrected formulas which consider solid-solid interaction must be used for cases involving higher solid volume fractions. However, in the case of salts such as ammonium perchlorate in a polyether binder, the heat of adsorption of filler to binder, due to the formation of hydrogen bonds between filler and binder will exceed the potential energy of free rotation of single bonds of the polyether elastomer. This situation cannot be considered as a special case of weak solid-binder interaction in the manner that chemisorbed hydrocarbon binder on carbon black was considered. Rather than relatively few surface active sites, all of the surface molecules of the salt must be considered to be labile to strong interactions with the polyether binder. Conversely, the polyether contains a great multiplicity of active sites (the oxygens which are separated by a few methylene groups) which are labile to strong interaction with the surface molecules of the salt. The result is a solid-filled elastomeric system wherein the effective volume fraction of the solid filler is greater than its actual volume fraction.

As the amount of binder unaffected by salt surface decreases with increasing solid loadings, the physical properties of the salt-filled polyether system will markedly deviate from the physical properties of the polymer. Thus, for example, polyurethane binders obtained from polytetramethylene glycols, which form strong elastomers with high recoverable elongations and excellent low temperature properties, yield propellants containing high solids loading that are stiff and brittle. Because the physical presence of moisture in polyurethane propellant will enhance the interaction between binder and filler, the moisture content of polyurethane propellant (discounting the interfering role it plays in the cure reaction) becomes a much more important matter than in the case wherein hydrocarbons are used as binders in producing solid propellants. Polyether binders will also dissolve a greater quantity

II, A, Composition Factors Affecting Response Behavior (cont.)

of the salt filler than will hydrocarbon binders, thus introducing salt dissolution and crystallization considerations in interpreting physical properties. However, this phenomena can be viewed as a special case of binder-filler interaction.

Four polymer systems (polyethylene, polybutylene-, poly-epichlorohydrin-, and polystyrene glycols cured with various isocyanates) have been selected for use. These binders will be used with various fillers to provide the parametric relations and interpretations discussed above which are pertinent to propellant conditions where the oxidizer ranges from totally wetted to totally dewetted.

B. MEASUREMENT OF RESPONSE BEHAVIOR

Mechanical properties testing of solid propellants provides an adequate tool for the determination of material parameters required for solid propellant research and development. It is known, however, that the mechanical properties response behavior of the propellant in the large motor is not simulated under these test conditions. Methods, therefore, must be developed to determine dimensional relationships for which the mechanical properties of solid propellant are independent of sample size.

1. Effect of Sample Size

A peripheral statistical analysis of variance was designed to study the effects of sample configuration and specimen size on the mechanical response of filled polymer systems. The mechanical response behavior (uniaxial tensile) considered here was obtained from specially prepared, over-size, milled barbell specimens containing sodium chloride (NaCl) and potassium chloride (KCl) fillers in the same polymer formulation. Four combinations of two gage lengths (2.7 and 4.0 in.) and two cross-sectional areas (0.56 and 1.21 sq in.) were used. The sample shape was that of JANAF composite

II, B, Measurement of Response Behavior (cont.)

propellant type, 0.5 in. thick, with a 0.50-in. radius at the shoulder. The general formulation was filler: 74 wt%, fuel additives: 1 wt%, and polyurethane fuel: 25 wt%. The test was run on duplicate samples on a standard Instron at a crosshead rate of 2 in./min at 77°F. Five values were taken from the Instron record of each specimen, strain at nominal maximum stress (ϵ_m), strain at break (ϵ_b), nominal maximum stress (S_{nm}), nominal stress at break (S_{nb}), and elastic modulus (E).

There are certain problems encountered in the statistical analysis of stress-to-failure data which add to the complexity of the analysis. The standard analysis of variance assumes normally distributed and homogeneous errors which probably holds approximately for nominal stress and strain before break but which would probably not hold for nominal stress and strain at break values. Because of the limited number of specimens of each size, the possible types of distributions involved could not be determined and the standard procedure was used as the best choice.

In analyzing the data, it was found that the experimental errors of the tests made on material containing NaCl were in general considerably larger than those encountered with material containing KCl. It was necessary, therefore, to analyze the data separately for each salt. The original data, together with the mean and standard error for each salt, are given in Table 1.

The statistical analyses for KCl and NaCl, respectively, are shown in the form of analysis of variance tables for each variable and each salt, and are also summarized in Table 1. Significant mean squares are starred and the corresponding mean values are shown. Significance indicates that effects as large as those obtained would be unlikely to occur by chance alone considering the experimental error involved. Significance at the 5% level is taken here as an indication that the effect probably exists.

TABLE 1

ORIGINAL DATA ON SAMPLE TESTS

KCl Filler

| Gage, in. Area, sq. in. | 2.9 | | 4.0 | | Average | Estimated Std. Dev. | %Std. Error of Estimate |
|----------------------------|--------|--------|--------|--------|---------|------------------------|----------------------------|
| | 0.56 | 1.21 | 0.56 | 1.21 | | | |
| ϵ_m | 0.1418 | 0.1473 | 0.1572 | 0.1368 | 0.1464 | 0.00355 | 2.42 |
| ϵ_b | 0.2073 | 0.2398 | 0.1812 | 0.1590 | 0.1965 | 0.01427 | 7.26 |
| S_{nm} | 149 | 145 | 143 | 139 | 144.5 | 2.67 | 1.85 |
| psi | 145 | 150 | 145 | 140 | | | |
| S_{nb} | 97.1 | 80.6 | 109 | 119 | 96.5 | 13.8 | 14.3 |
| psi | 54.0 | 87.2 | 108 | 117 | | | |
| E | 2020 | 1800 | 1730 | 1830 | 1820 | 95 | 5.21 |
| psi | 1860 | 1960 | 1660 | 1700 | | | |

NaCl Filler

| | | | | | | | |
|--------------|--------|--------|--------|--------|--------|--------|------|
| ϵ_m | 0.3681 | 0.3795 | 0.2488 | 0.4325 | 0.3279 | 0.0853 | 26.0 |
| ϵ_b | 0.2256 | 0.2694 | 0.3990 | 0.3000 | 0.7487 | 0.2167 | 29.0 |
| S_{nm} | 1.3330 | 0.8111 | 0.6215 | 0.4675 | 74.1 | 16.8 | 22.7 |
| psi | 55.3 | 65.6 | 88.9 | 63.1 | | | |
| S_{nb} | 69.2 | 96.2 | 64.0 | 90.2 | 38.8 | 9.84 | 25.3 |
| psi | 17.8 | 39.3 | 41.1 | 41.0 | | | |
| E | 23.8 | 48.6 | 31.1 | 67.9 | 644 | 251 | 39.0 |
| psi | 417 | 611 | 857 | 474 | | | |
| psi | 747 | 879 | 313 | 853 | | | |

Summary of F Ratio Values from Variance Analysis

| | Gage Length | | Area | | Interaction | |
|--------------|-------------|-------|------|-------|-------------|------|
| | KCl | NaCl | KCl | NaCl | KCl | NaCl |
| ϵ_m | 0.31 | 0.33 | 0.60 | 0.34 | 23.6** | 0.01 |
| ϵ_b | 27.3** | 9.50* | 0.38 | 0.20 | 3.34 | 2.97 |
| S_{nm} | 8.52* | 0.18 | 1.13 | 0.63 | 2.17 | 0.55 |
| S_{nb} | 11.8* | 3.43 | 0.84 | 8.89* | 0.00 | 0.10 |
| E | 7.21* | 0.05 | 0.01 | 0.46 | 0.93 | 0.05 |

* Significant at 5% level
** Significant at 1% level

II, B, Measurement of Response Behavior (cont.)

The results on the KCl filled system show all variables except ϵ_m being sensitive to gage length. This would indicate that holding specimen area constant does not ensure that measurements will be independent of size. The testing errors for the NaCl filled system were so large that they masked almost all effects.

As a result of the tests with inert filler, an additional statistical design has been prepared and initiated on the mechanical response behavior of oversize specimens of a live propellant. The relationship of the area-to-gage ratio will be considered in this analysis to evaluate further the effect of sample design upon the mechanical properties of the propellant system. A summary of the conditions to be considered is:

| <u>Gage Length, in.</u> | <u>Area, sq in.</u> | <u>A/G</u> |
|-------------------------|---------------------|------------|
| 4.00 | 7.58 | 1.89 |
| 2.70 | 5.05 | 1.87 |
| 1.35 | 2.56 | 1.89 |
| 4.00 | 2.56 | 0.64 |
| 2.70 | 1.70 | 0.63 |
| 1.35 | 0.90 | 0.64 |

Testing and initial data reduction, preliminary to statistical analysis, has been completed on the above specimens. These data are presented in Figures 1, 2, and 3. Preliminary analysis of the data indicates that both area and gage length have an effect upon the measured parameters. Specific conclusions await completion of the statistical analysis.

2. Effect of Filler Parameters

In order to evaluate properly the mechanical response behavior of solid propellants, the effect of filler type, particle size distribution, particle surface type, etc., upon the stress-strain properties, volume change, and

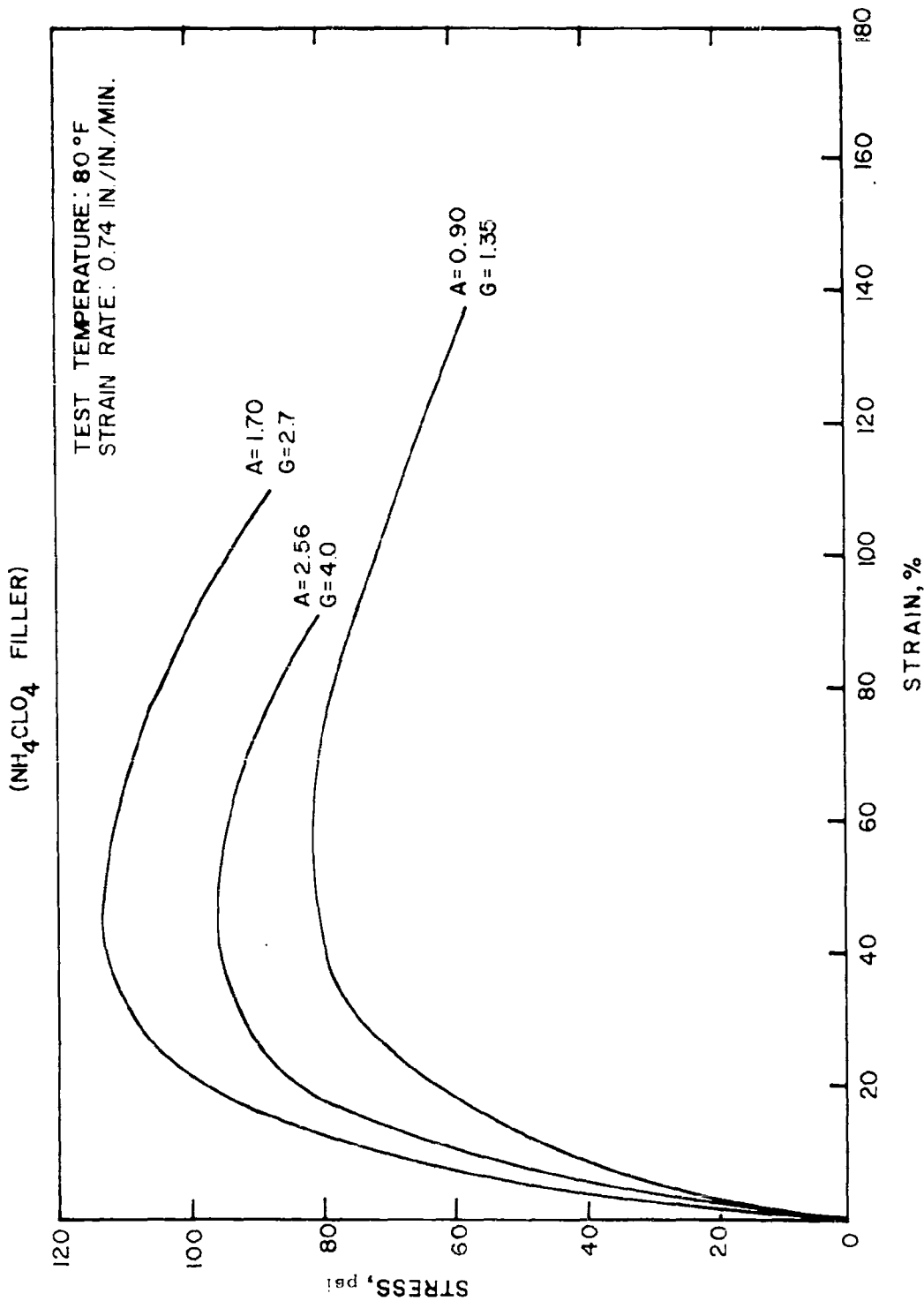


Figure 1: Comparison of the Effect of Sample Size upon the Mechanical Properties of a Polyurethane Propellant (NH₄ClO₄ Filler)

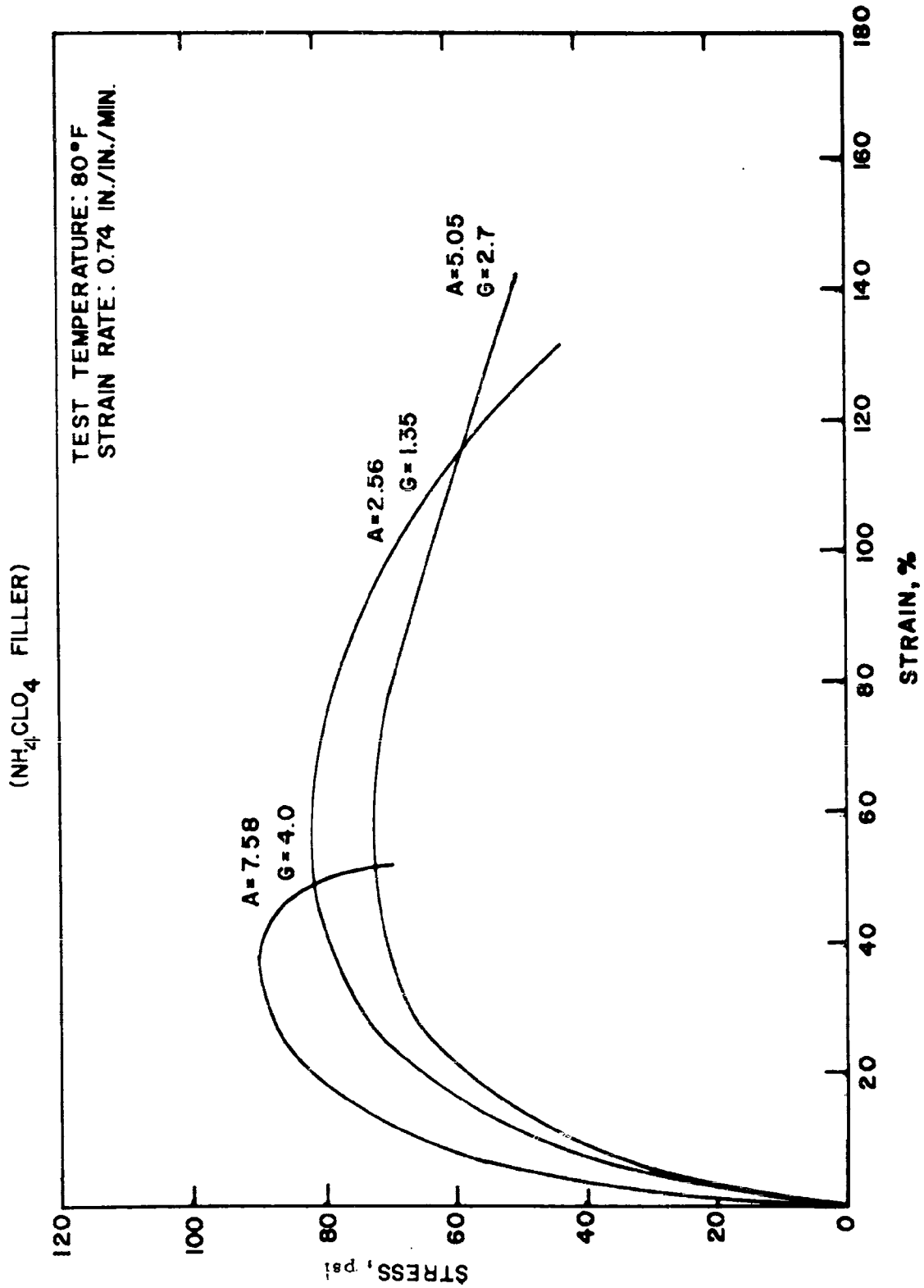


Figure 2: Comparison of the Effect of Sample Size upon the Mechanical Properties of a Polyurethane Propellant (NH₄ClO₄ Filler)

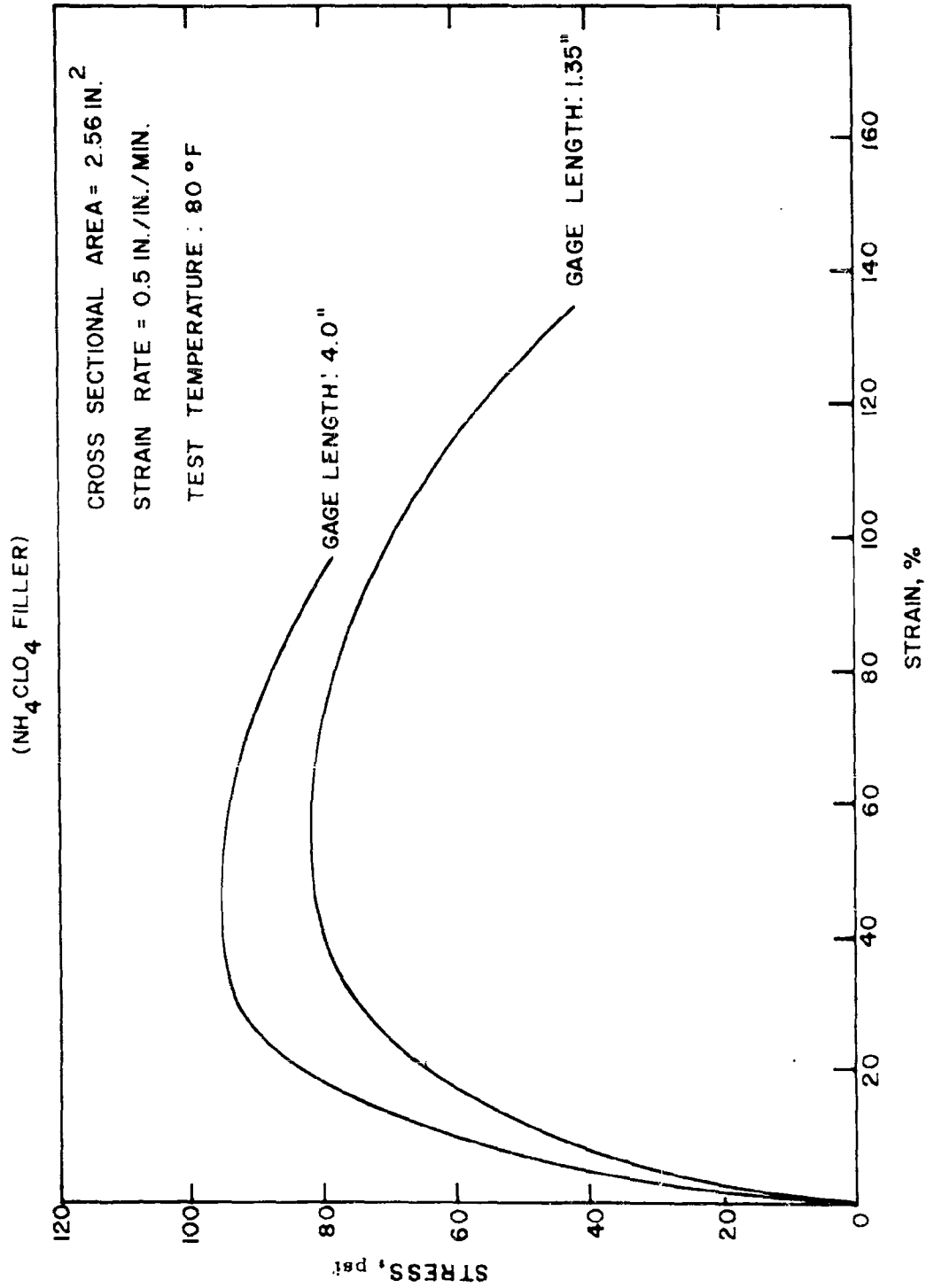


Figure 3: Comparison of the Effect of Gage-Length Upon the Mechanical Properties of a Polyurethane Propellant (NH₄ClO₄ Filler)

II, B, Measurement of Response Behavior (cont.)

failure properties must be known. Batches of polymer containing oxidizer salt (NH_4ClO_4), inert salts (NaCl, KCl) and glass beads as fillers have been made. Some testing of these batches has been done on oversize specimens. The stress-strain curves for batches with KCl, NaCl, and NH_4ClO_4 salts as fillers are plotted in Figure 4. Sample dimensions were the same for all specimens.

It can be seen that great differences exist in properties of the various materials. Variations in batch cure alone would not be expected to produce this significant behavior. From the discussion of binder-filler interaction, it is not surprising that such large differences exist. In an effort to understand these differences, studies are in process to determine the surface structure of the filler, its interaction with the polymer, and the other parameters expected to affect the response behavior.

3. Tensile Measurements Under Superimposed Hydrostatic Pressure

One of the factors which affects the dewetting process is pressure. Under superimposed hydrostatic pressure, which simulates the effect of motor pressure on the dewetting process, the failure level of inert propellant (DP-16) was found to be considerably raised for specimens tested in simple tension in the presence of hydrostatic pressure, confirming the data of Vernon (14). The tensile strain at nominal maximum stress was more than doubled when the test pressure was raised from atmospheric to 250 psig at 77°F. The nominal maximum stress was raised from 120 psi to 180 psi under the same conditions. Figure 5, a composite plot of the nominal stress versus strain curves, shows the effect on the nominal maximum and on the failure values. Figure 6 shows these same curves plotted as $S_n \lambda^2$ versus $\ln \lambda$, a method of plotting suggested by Jones (4). The change of slope of the stress-strain data reduced by this method appears to

STRAIN RATE: 0.74 in./in./min
TEST TEMPERATURE: 80°F

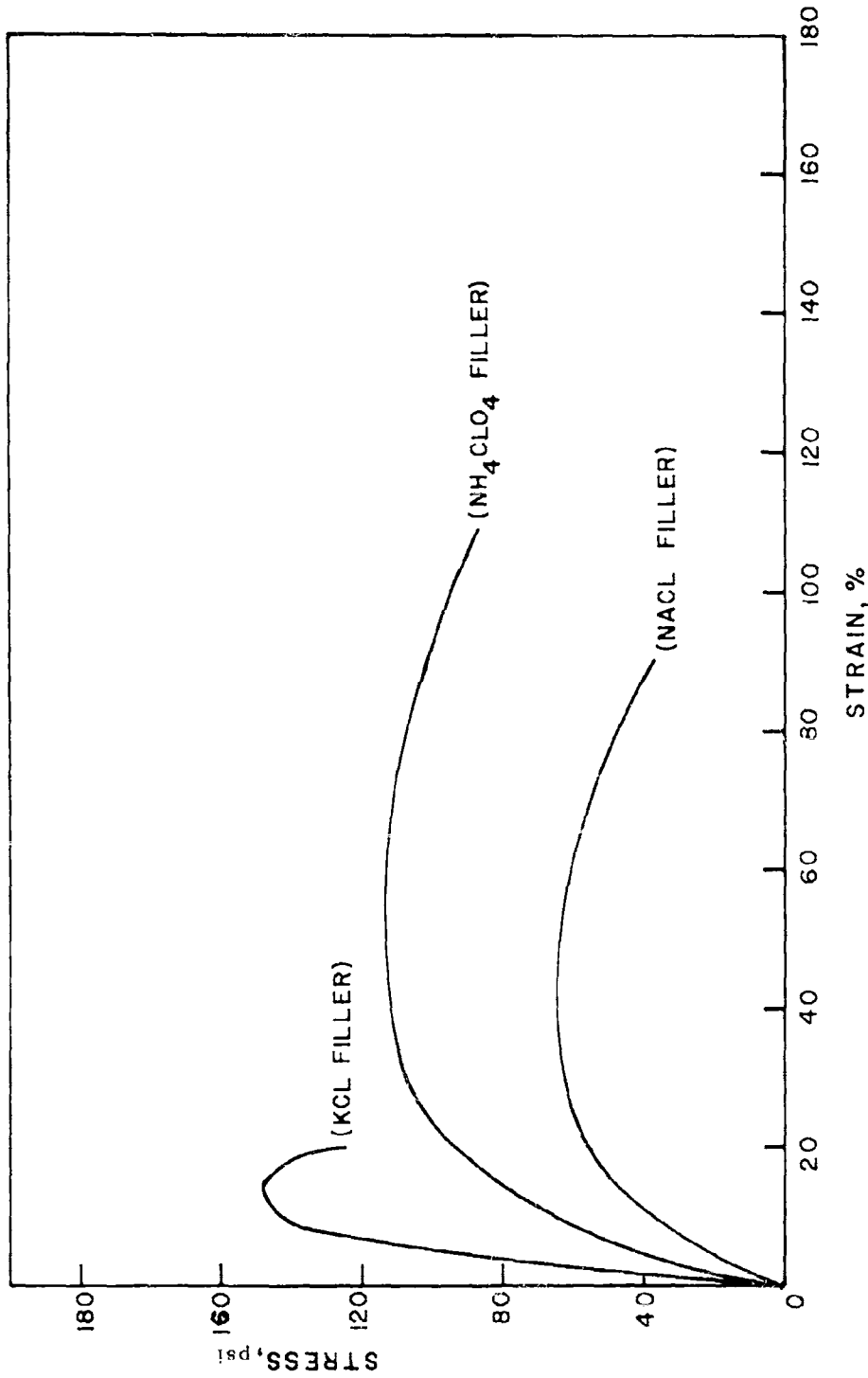


Figure 4: Comparison of the Effect of Filler Upon the Mechanical Properties of a Polyurethane Propellant

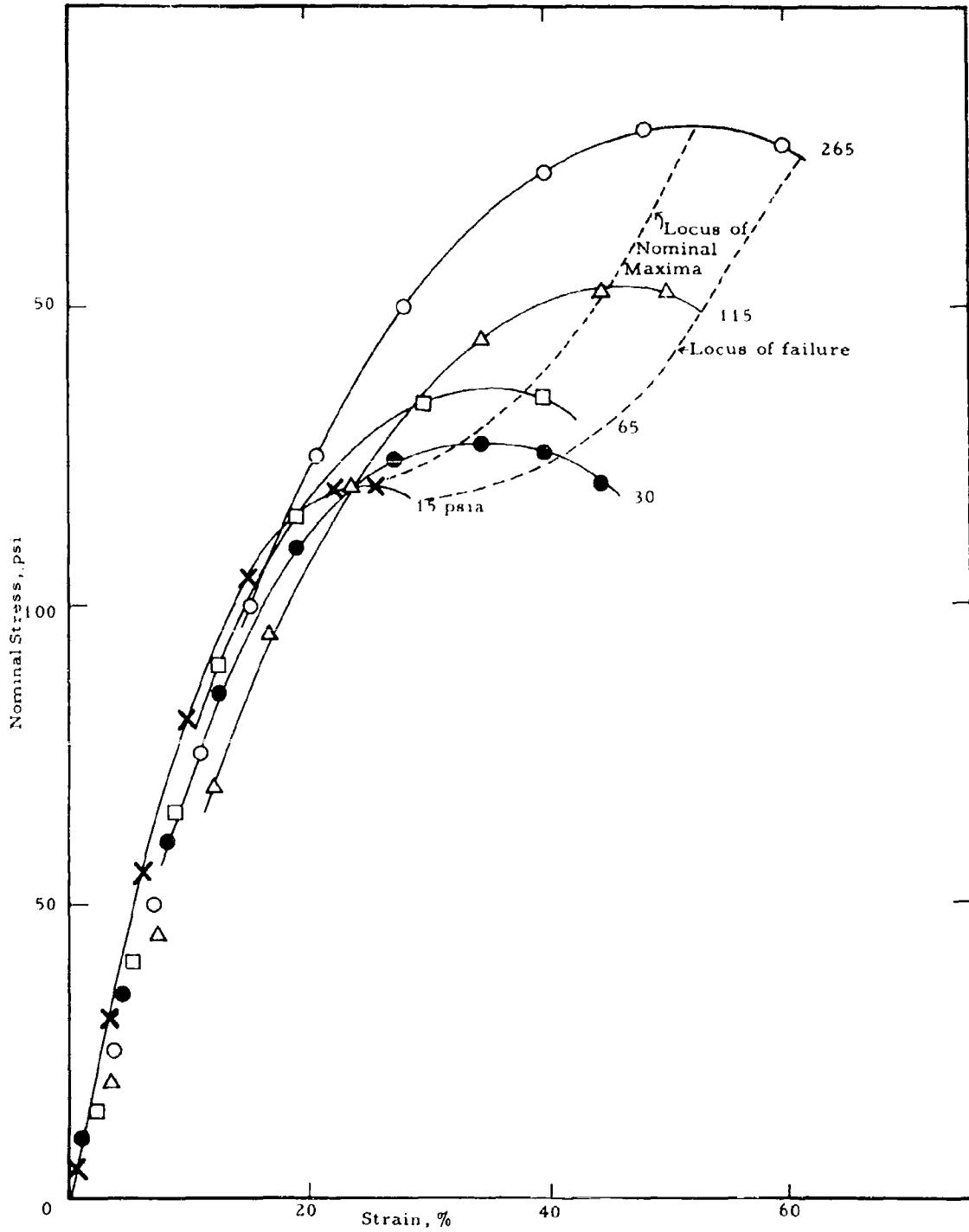


Figure 5: Tensile Stress-Strain with Superimposed Hydrostatic Pressure

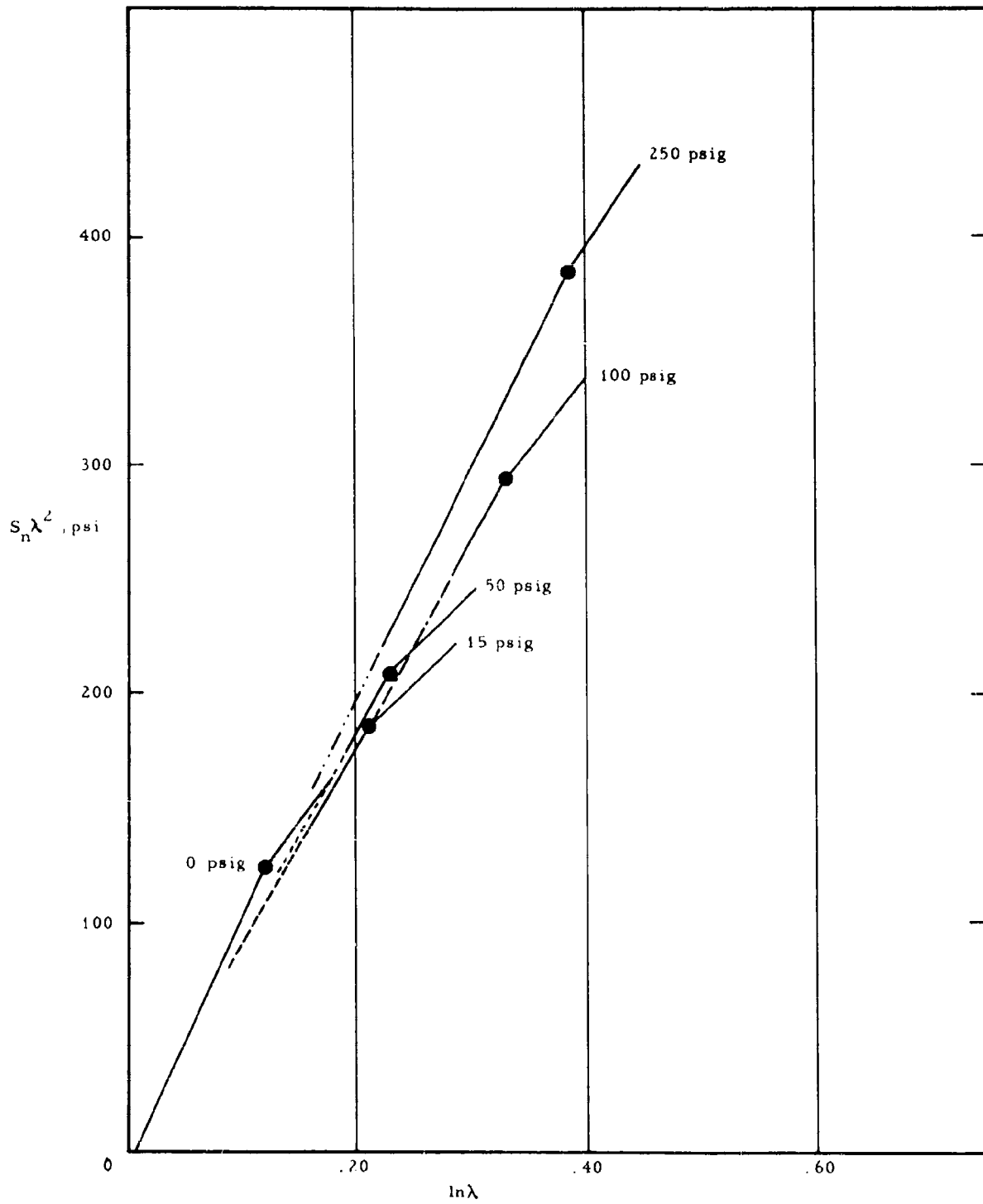


Figure 6: Stress-Strain Data for Uniaxial Tensile with Superimposed Hydrostatic Pressure Using Jones' Correlation

II, B, Measurement of Response Behavior (cont.)

be a regular function of the superimposed hydrostatic pressure, occurring at higher elongations as the pressure is increased. The initial elastic response of the composite did not seem to be appreciably changed by superimposed hydrostatic pressure. That is, the Young's Modulus of Elasticity calculated from the initial slope of the stress-strain curve was essentially constant regardless of the pressure of testing. This would be expected at the low strains before dewetting of the oxidizer has occurred.

Four live polyurethane propellants, showing Class II behavior as discussed in Phase 2, have also been tested in the same way and an analysis made of the effect of hydrostatic pressure on nominal stress at break and elongation at break. The results, shown in Figures 7 and 8, suggest a similar effect of pressure on failure stress but not on failure strain. These studies are being improved by adding a measurement of cross section during strain, and further discussion will await such data.

4. Volume Change Under Uniaxial Deformation

Specimens 1/4- by 1/4- by 2-in. are subjected to small strains and the volume change measured by a buoyancy technique. According to Thor Smith ⁽¹¹⁾, the volume change that occurs during a tensile or compressive deformation is given by:

$$\frac{d \ln V/V_0}{d \ln L/L_0} = 1 - 2\nu \quad (1)$$

where

V/V_0 = relative volume,

L/L_0 = extension ratio,

ν = Poisson's Ratio.

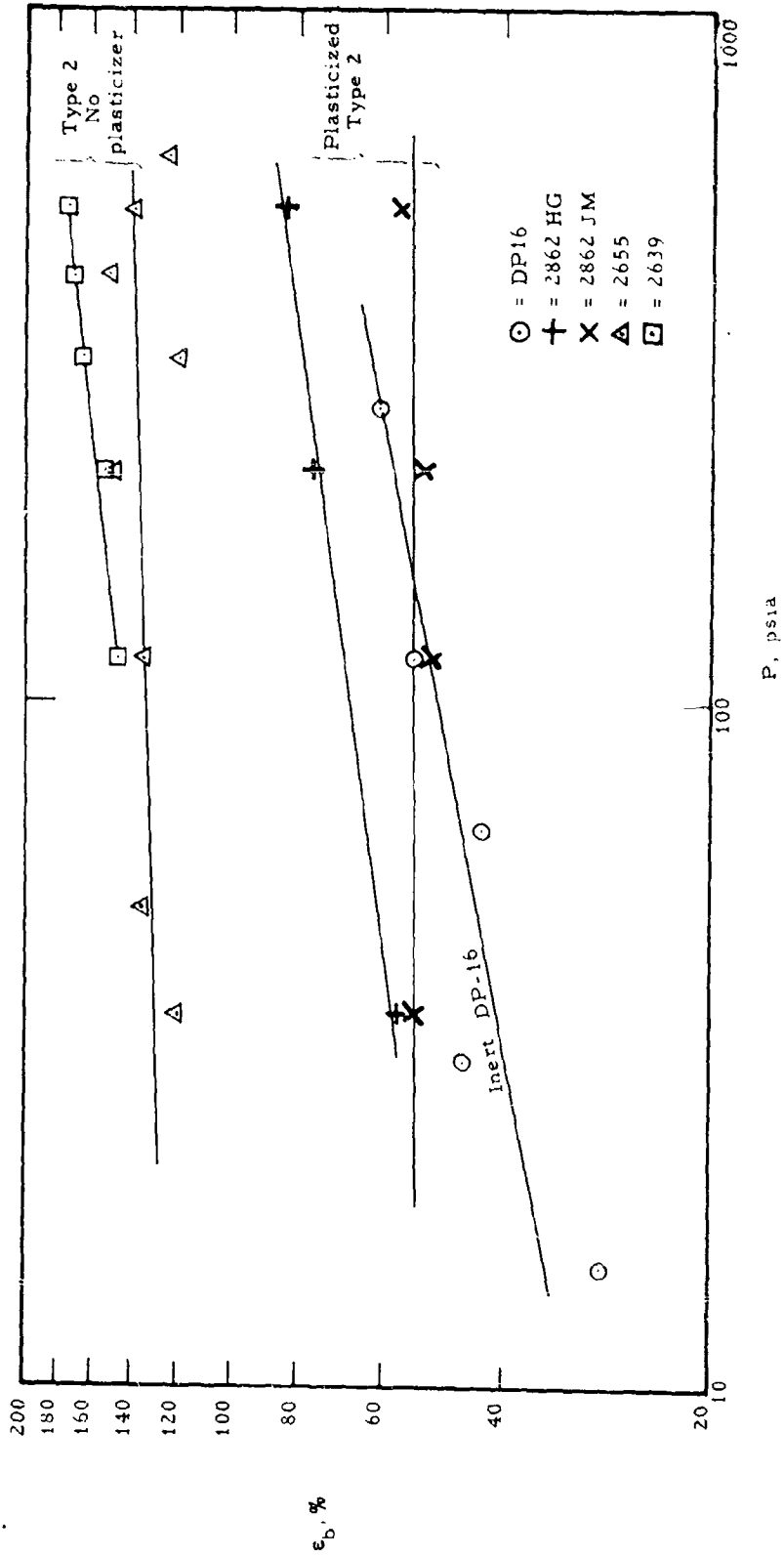


Figure 7: Effect of Pressure on Elongation at Failure

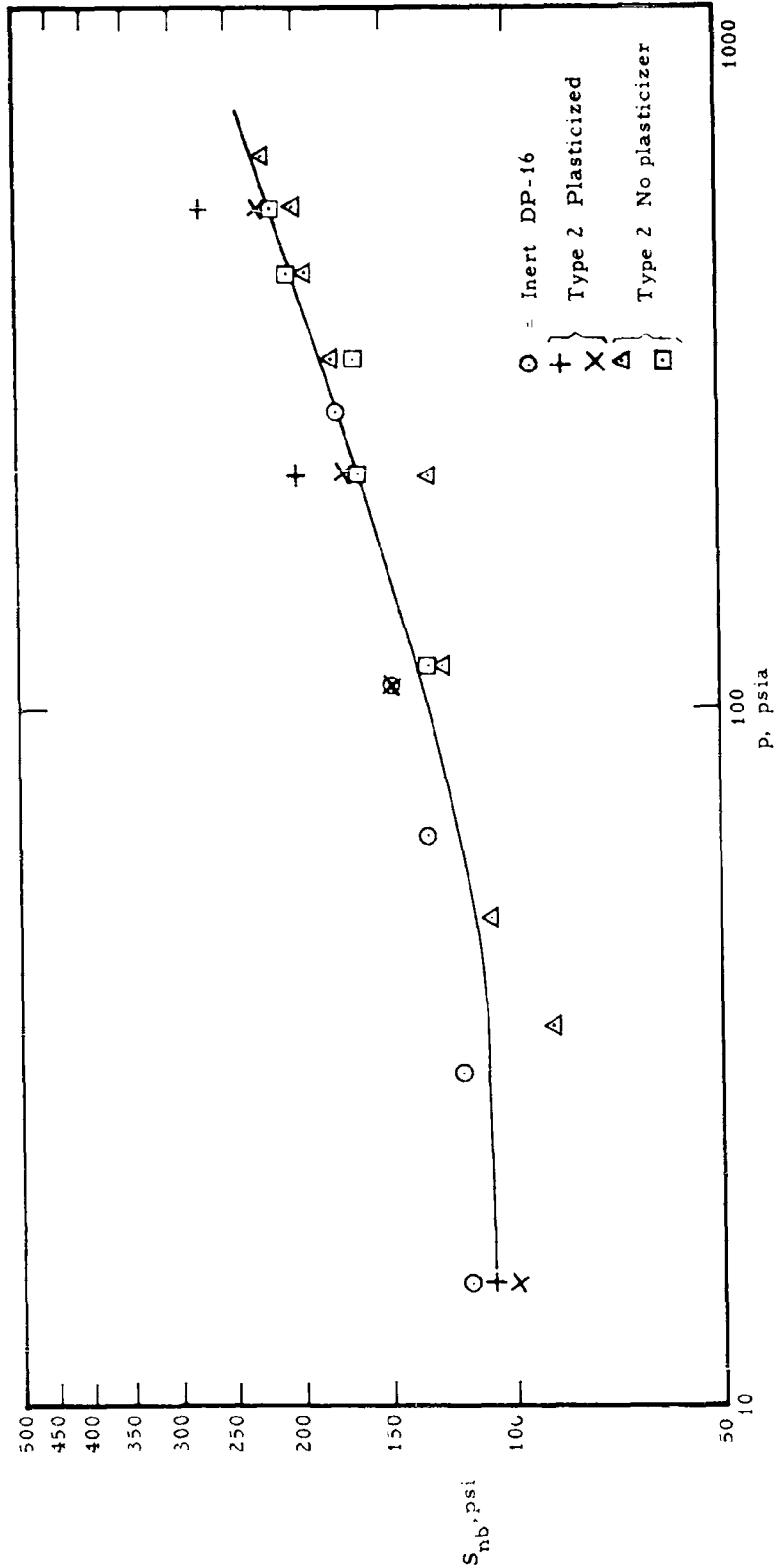


Figure 8: Effect of Pressure on Nominal Stress at Failure

II, B, Measurement of Response Behavior (cont.)

To determine ν graphically, the slopes of the linear portions of the plot of log relative volume versus log extension ratio are equated to $1 - 2\nu$ and calculated. Figure 9 shows these plots and corresponding Poisson's ratio for glass bead polyurethane composites containing 40.8, 50.7, and 58 vol. % glass beads. The extrapolation of the linear portion to $\log V/V_0$ gives a value suggested by Thor Smith as yield strain.

Thor Smith reports that the relationship between this yield strain and volume fraction of filler for this idealized system may be represented by the following equation:

$$\epsilon_c = \epsilon_{r,c} (1 - 1.105 V_f^{1/3}) \quad (2)$$

where

ϵ_c = observed yield strain,

$\epsilon_{r,c}$ = strain in the binder between adjacent filler particles just prior to failure of the adhesive bond,

V_f = volume fraction of glass beads.

A plot of ϵ_c versus $1 - 1.05 V_f^{1/3}$ is presented in Figure 10. The slope, which equals $\epsilon_{r,c}$ is 0.37, or 37% strain. From the stress-strain curves for the unfilled binder in Figure 11, it can be seen that this strain corresponds to a stress of about 50 psi, indicating a rather low bond strength between binder and filler. Figure 11 also shows the stress-strain curves of two of the filled systems taken at 0.74 min^{-1} and 77°F .

Figure 12 shows how the yield strain of propellant (shown in Figure 9) can be found by a different method which produces results that are in good agreement. Two representative tensile curves are shown in Figure 12; one is the tensile curve for the propellant in air or silicone oil and the other is the curve in water. The point of divergence of the curves

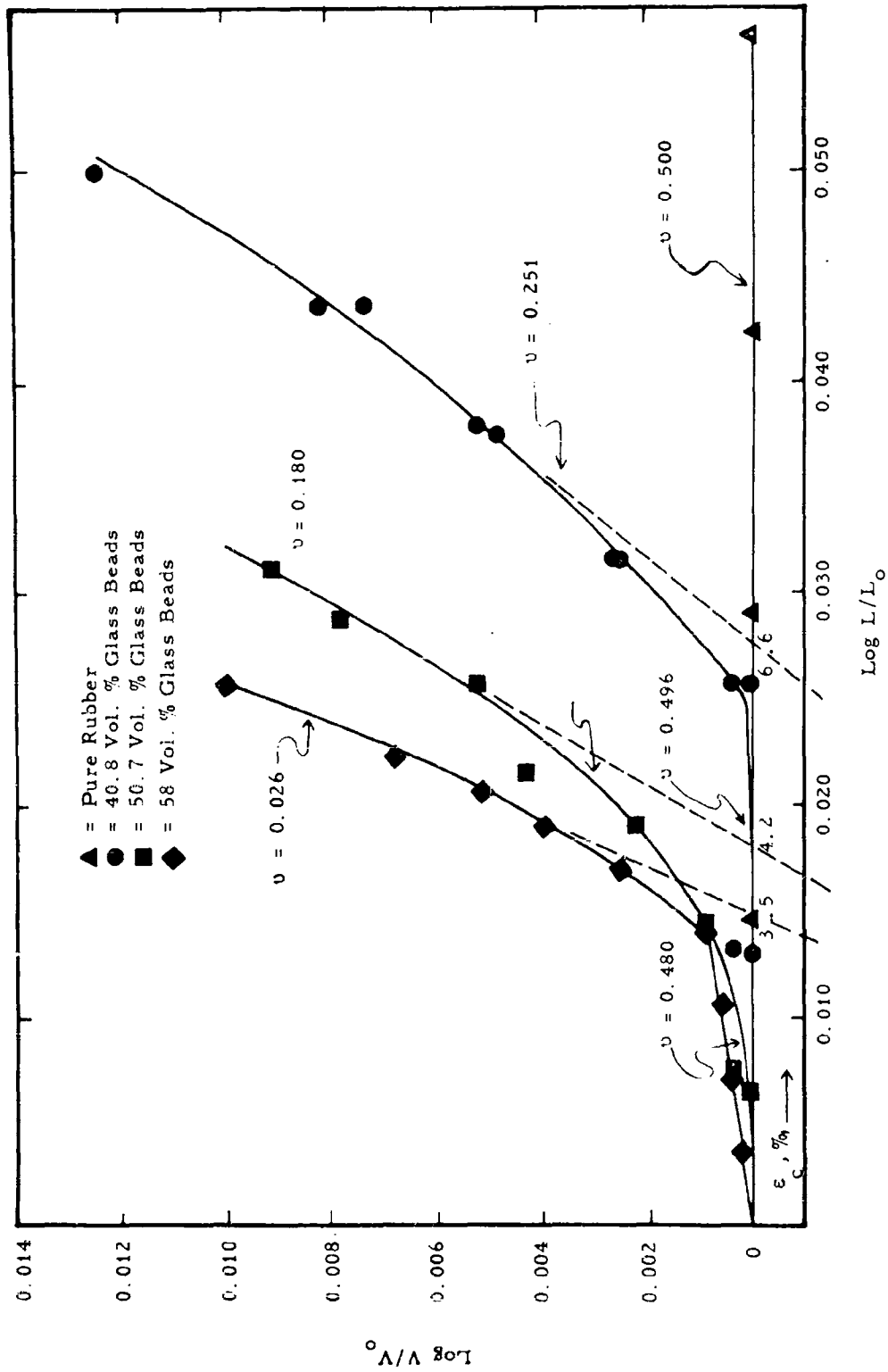


Figure 9: Log Volume Change vs Log Extension Ratio for Several Glass Bead - Polyurethane Composites

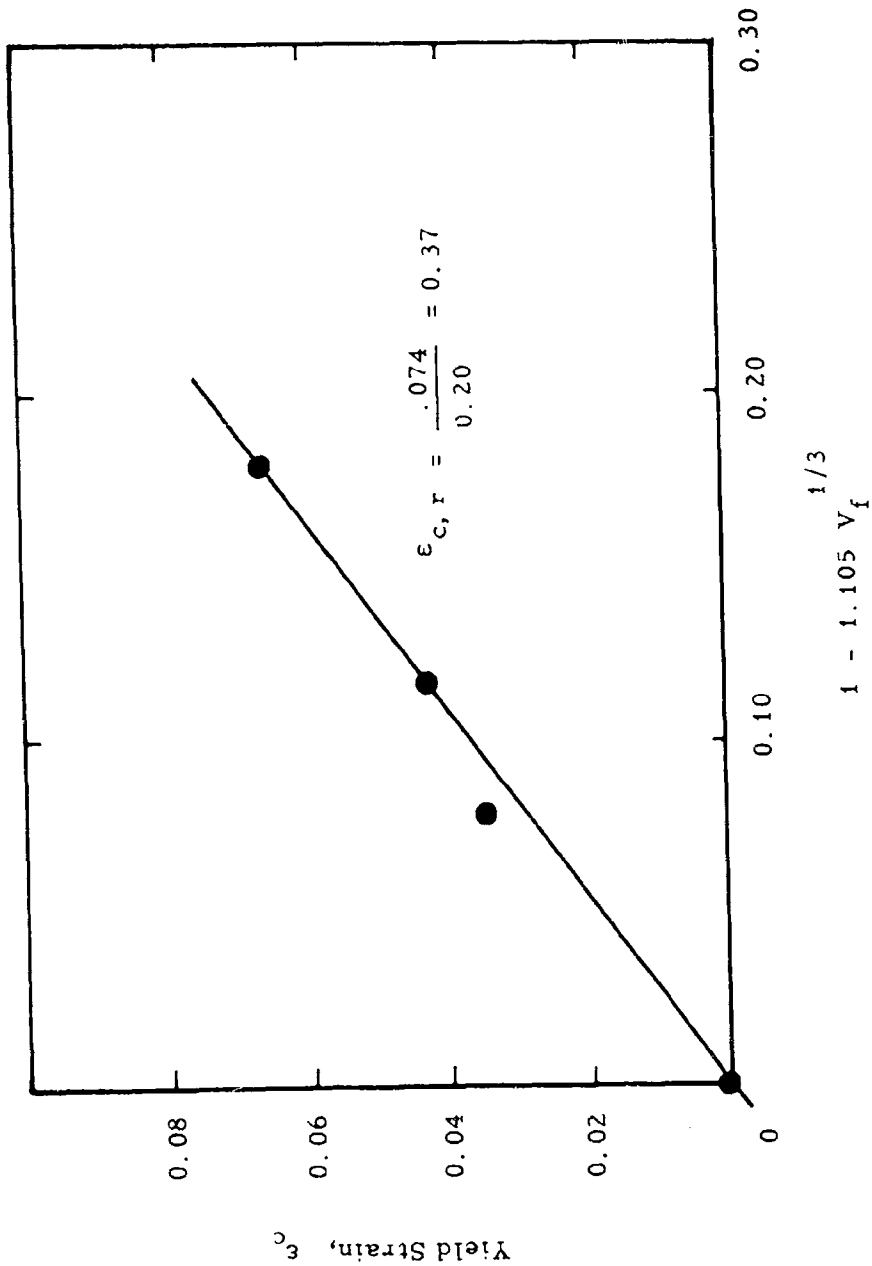


Figure 10: Correlation of Yield Strain with Volume Fraction of Glass Beads

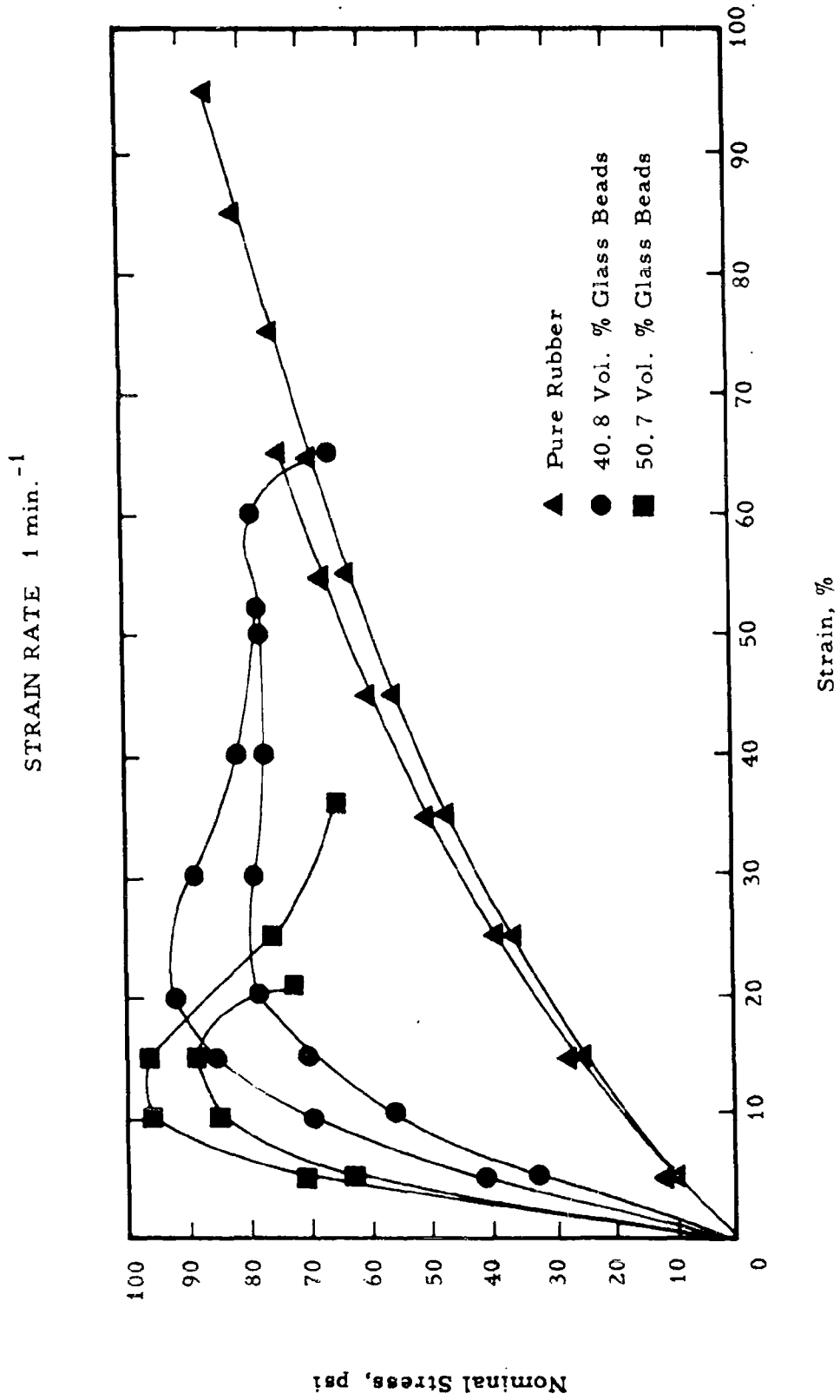


Figure 11: Uniaxial Stress vs Strain Glass Bead - Polyurethane Composites

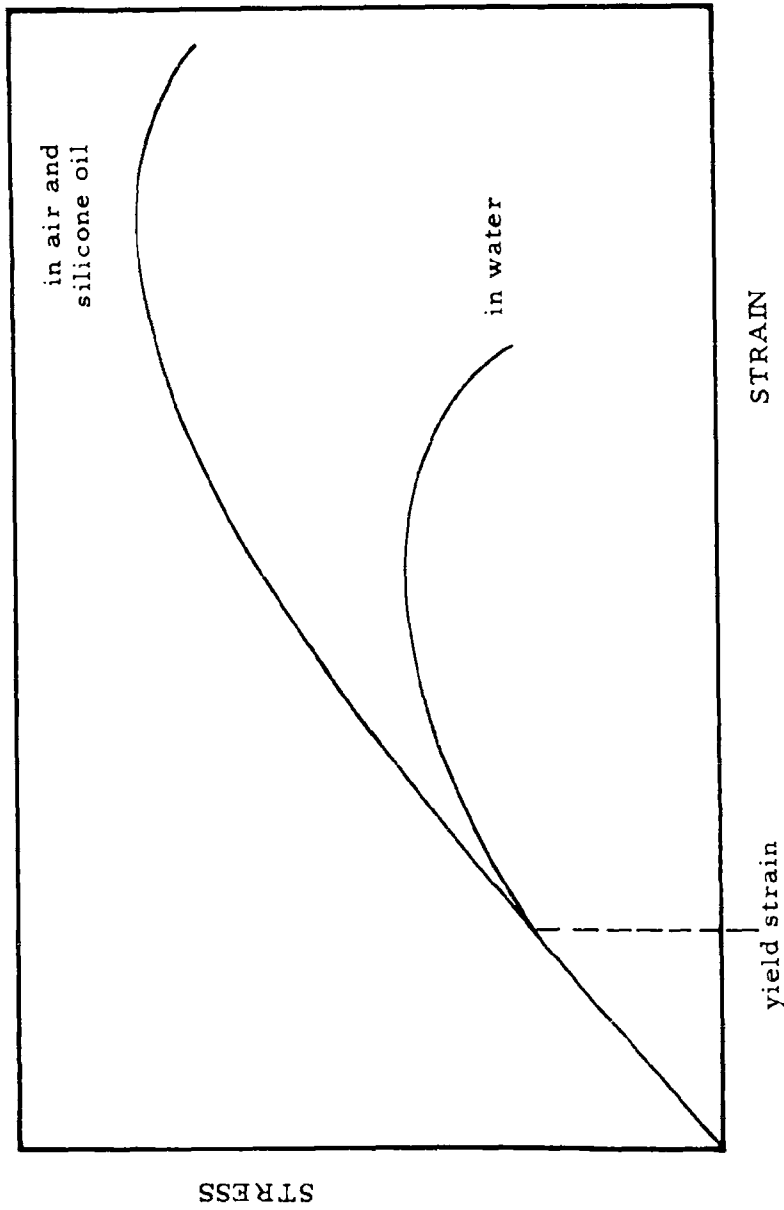


Figure 12: Tensile Test Under Water Compared with that in Air or Silicone Oil Showing Behavior After Yield Strain

II, B, Measurement of Response Behavior (cont.)

indicates the yield strain, since this is also the point at which the propellant becomes permeable to water. The considerably lower S_{nm} and ϵ_m of the "water" curve past the "yield strain" should be noted. The role of water in modifying the behavior of polyurethane propellants is being studied intensively in a related program ⁽³⁾ and will not be discussed in detail here.

5. Effect of Repeated Strain

The dewetting, or release of the binder-filler bond, appears to be the dominant factor in response behavior of composite propellants. Further information on the nature of this bond is provided by examining volume change behavior on repeated loading of specimens.

Figure 13 shows the $\log V/V_0$ versus $\log L/L_0$ plots for a specimen containing 50.7% volume glass beads cycled three times between 0 and 11% strain. In going from cycle 1 to 3, it should be noted that the "forward" halves of the cycles approximate more closely the "recovery" halves, in which Poisson's ratio is independent of extension. This behavior may be explained by assuming that initially there exists a mechanical bond between the binder and filler particles and a certain critical strain level must be reached before these bonds begin to rupture with the formation of voids around the glass beads. As the strain is increased, more voids form and those already formed increase in size. When the applied strain is reduced, the volume uniformly decreases as the voids become smaller analogous to the behavior of a foam.

The breaking of these bonds may be analogous to the breaking of the adhesive bond of pressure sensitive adhesives. This is suggested by the preliminary data of Figure 14. A live propellant with a plasticized polyurethane binder was repeatedly strained at 77°F at a rate

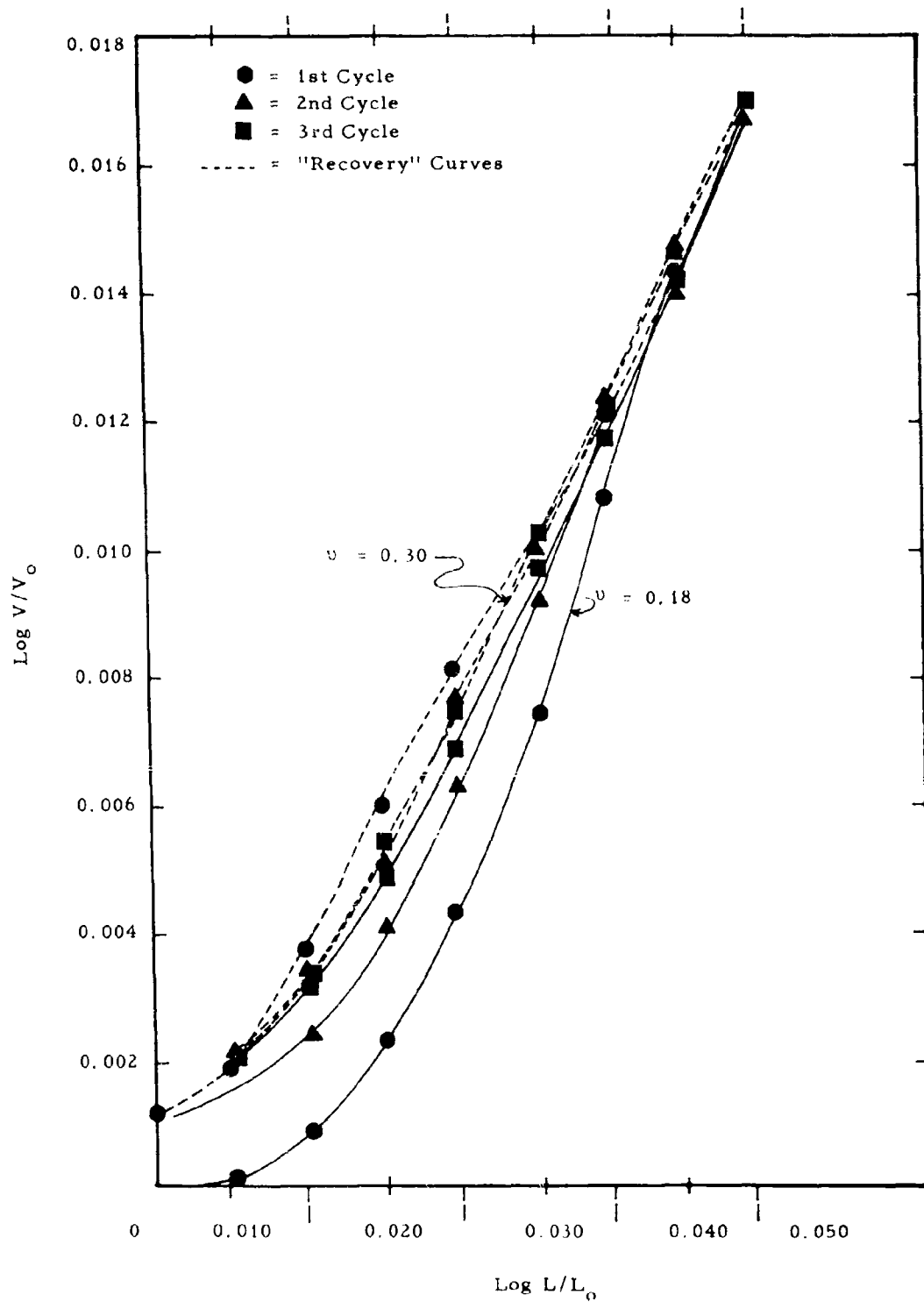


Figure 13: Log Volume Change vs Log Extension Ratio for a 50.7 Volume % Glass Bead Filled Polyurethane Rubber in a Cycling Test

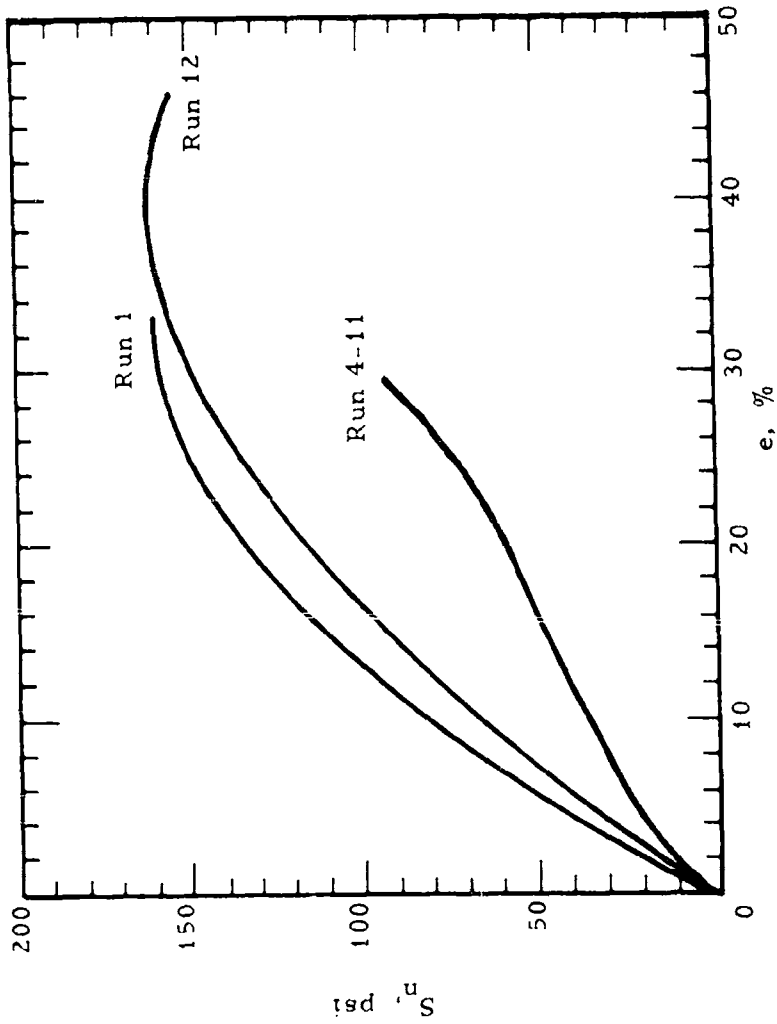


Figure 14: Stress-Strain Behavior of Class 2 Propellant at a Test Temperature of 77°F and a Strain Rate of 0.74 min⁻¹ for Repeated Cycles with Rest of 13 Days After Run No. 11

II, B, Measurement of Response Behavior (cont.)

of 0.74 min^{-1} to about 30%, reversing the Instron to remove the load after each cycle. The first 11 runs were performed on one day, after which the specimen rested for 13 days before the 12th run. The essential recovery of initial properties suggests that the filler-binder bond was reestablished. A test of these results with volume change measurements will be performed.

6. Improved Preparation of JANAF Tensile Specimen

A widely used method of sample preparation for the JANAF Instron sample uses a die cutter pressed hydraulically through a precut slab of propellant. This is a fast and simple method of sample preparation, but it gives several undesirable effects:

a. Nonparallel faces in the gage section of the bar make the sample trapezoid shaped, and because of this it is extremely difficult to measure cross sectional area with less than 3 to 5% variation. The trapezoid shape of the shoulders of the specimen also causes it to bow in the fixtures while testing, resulting in a nonuniaxial test and a strain rate gradient throughout the cross section of the specimen. Further, the trapezoid shape of the specimen in the shoulder and gage sections causes the strain rate to be non-linear due to seating effects and irregular area changes, resulting in inaccurate strain readings and low modulus readings.

b. The sample must undergo considerable compressive stresses and strains while being cut.

c. The surface of the sample is often rough and scarred as though it was torn and not cut which may cause premature failure.

d. The gross irregularities in the specimen together produce high variances in the data so that many samples have to be tested before obtaining values what have significant meaning statistically.

II, B, Measurement of Response Behavior (cont.)

A method of machining Instron specimens using a fly cutter had been tried here. Good quality specimens were obtained with a significant reduction of variance of the measured parameters. Although such methods for machining samples have been available, no adequate methods for holding the material while it was being machined were available except for limited production. Vise-type gripping fixtures with abrasive surfaces work adequately if great caution is used by the operator. With this type of holding mechanism, the sample must undergo considerable compressive forces and strains in order to be held rigidly enough for milling, and because of the low flexure modulus of most propellants, the material tends to bulge making it difficult to machine specimens within good tolerances. Vise-gripping of the material also minimizes the surface one can machine.

It was decided to hold the material with vacuum while machining. A fixture was designed using several vacuum ports with a machined aluminum section to support the gage section. Grit cloth over the vacuum ports provides an abrasive surface at the propellant-fixture interface resulting in high shear between the propellant and the fixture. The fixture is mounted on a mill, and a water aspirator with a vacuum reservoir to act as a surge tank, is incorporated to provide a means of displacing the free air in the fixture. Reducing the air pressure in the fixture and surge tank to 5 inches of Hg provides adequate holding force for milling without producing more than 0.0001 in. reduction in thickness of the specimen because of atmospheric pressure. The machining of the first face of the specimen section is shown in Figure 15, the reverse face is then machined while the specimen section is held on top of the machined fillet as shown in Figure 16. After both faces have been completed, the section is sliced into individual bars on a Do-All saw.

Approximately 200 samples have been prepared in this manner and the width of the specimen has a range of 0.006 in., equivalent to a range of area values of 1.6%.

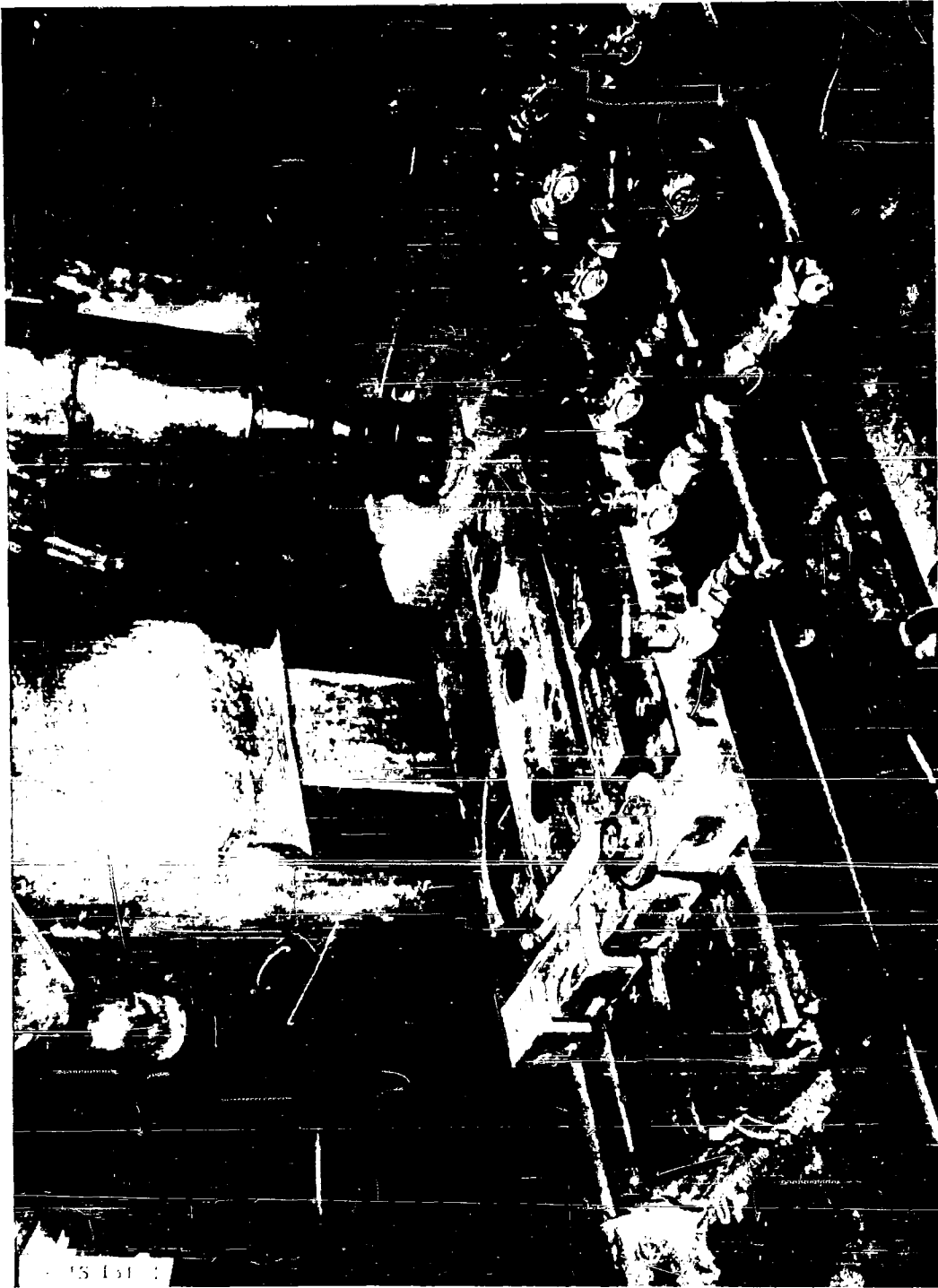


Figure 15: Machining of First Side of Block of Propellant Using Vacuum to Hold Block in Place

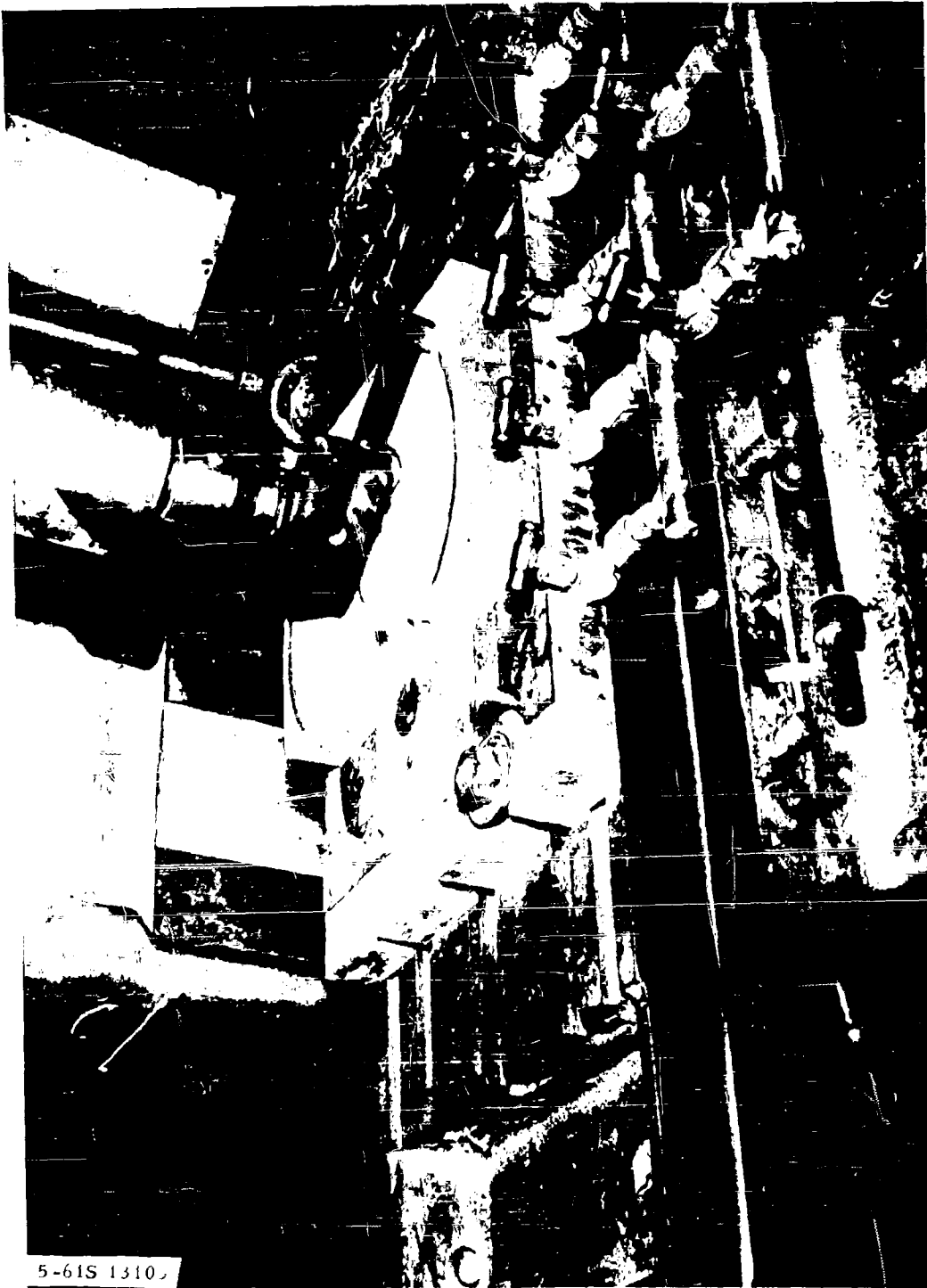


Figure 16: Machining Other Face of Propellant Block Using Vacuum to Hold
First Machined Surface on Formed Aluminum Section

III. PHASE 2 — MATHEMATICAL REPRESENTATION OF MECHANICAL BEHAVIOR

The objectives of this phase are to systematize the methods for correlating results from the various experimental tasks, and to find the mathematical relationships which best approximate the observed mechanical behavior of solid propellants.

A. PROPELLANT CLASSIFICATION

The development of a systematic means for classifying and correlating experimental results requires an analysis of the types of mechanical properties observed in solid propellants. Consideration of the factors affecting these properties leads to a rational classification system.

1. Particle Packing

The problem of particle packing in solid propellant results from loadings in excess of 50 volume percent filler, frequently as high as 63 volume percent or more, used in most solid propellants. As seen in Figure 17 for the special case of a bimodal system, the filler particles are closely packed and irregularly shaped. The finer particles are seen as small nodules in the photo on the left of Figure 17. This complex and non-homogeneous character of solid propellant suggests that the mechanical distortion of this material, involving in turn relative movement of these particles with respect to one another, should reflect this close packing and nonuniform character. A study was made of this problem using the specimen shown in Figure 17. Points on two of the large particles were used to determine the angle of intersection of lines extending through these points. The angles were measured at various tensile strain levels and compared with calculated values obtained on the assumption of a homogeneous incompressible material. The results are:



SCHEMATIC OF LARGE
PARTICLE PACKING

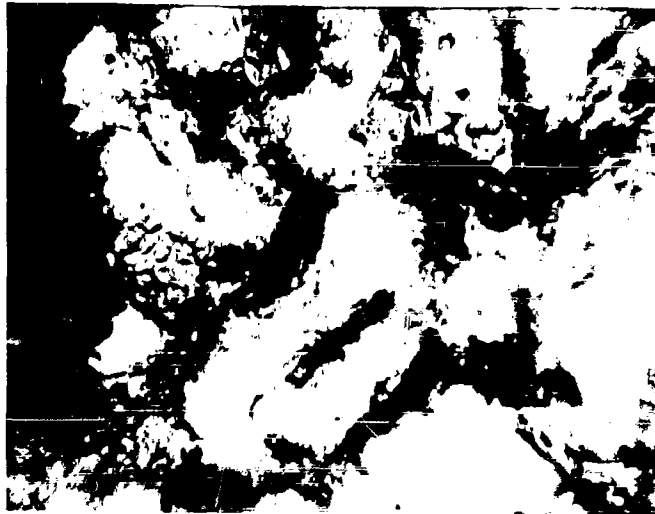


PHOTO SHOWING DEWETTING

x 48 VOL. % 470 - 500H
17 VOL. % 45 - 55H

Figure 17: Typical Packing of a Propellant System (65 Vol% Filler* - Strained 8%)

III; A₇ Propellant Classification (cont.)

| <u>Strain, %</u> | <u>Angle of Intersection, degrees Measured</u> | <u>Calculated</u> |
|----------------------|--|-----------------------|
| 1 | 44.7 | 44.7 (starting point) |
| 3 | 42.9 | 44.15 |
| 6 | 36.1 | 42.88 |
| 8 | 34.9 | 42.05 |

One of the particles chosen for this measurement was closely aligned to the direction of straining. The reduction in the angle of intersection with strain indicates that the second particle is being moved nonuniformly leading to an exaggerated rotation. Examination of the behavior of other particles shows that the degree of rotation experienced is affected by many factors, such as shape, influence of adjacent particles and orientation.

2. Dewetting Phenomenon

The effect of particle rotation on strain is to produce a repacking of the particles which leads to the formation of voids within the medium resulting from the failure, or dewetting, of the bond between the binder and the filler.

The behavior of highly filled elastomers will vary greatly with changes in bond strength between the filler particles and polymeric matrix. For zero bond strength, the filler-polymer bond fails immediately upon straining and small voids are created next to a particle. Since there is no physical reinforcement, this type of material is weak and highly extensive. Alternatively, if the bonds are strong, the filled material exhibits a relatively high modulus with considerable reduction in the ultimate elongation.

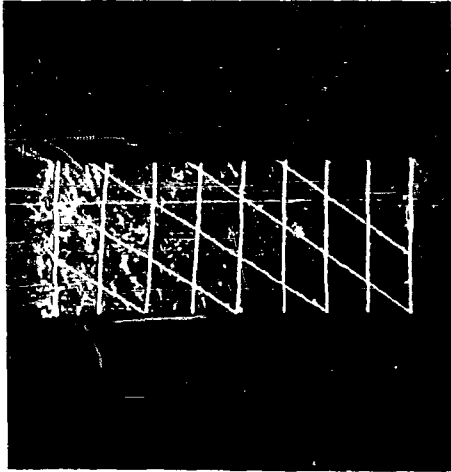
III, A, Propellant Classification (cont.)

It is in those systems where the adhesive bond is of intermediate value that the problem of localized failure appears. As the specimen undergoes tensile loading, the weakest bond strengths are first exceeded. The filler particles thus released, transmit a higher stress to the neighboring polymer-particle bonds, resulting in a band of released particles perpendicular to the direction of strain. If the applied load occurring after this phenomenon does not exceed the bond strength of the remaining intact bonds, the polymer along this line experiences very high strains and eventually fails. The implication of the above behavior is that the stress-strain data in simple tension obtained after localized yielding occurs can no longer be related to the overall behavior of the material.

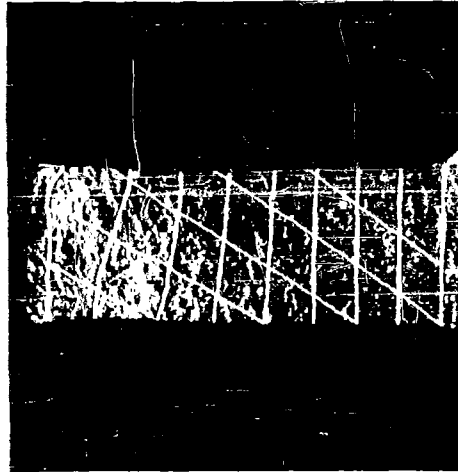
The extremely localized behavior of the dewetting process is well exemplified in Figure 18. This localized effect is not easily seen by the naked eye at low strain levels. Measurement of the grid on Figure 18 shows that between 34.5 and 49% strain the uppermost portion of the specimen exhibits numerous white bands which permit the elongation while the three bottom portions of the specimen grid show no change in dimension.

3. Nature of the Yield Band

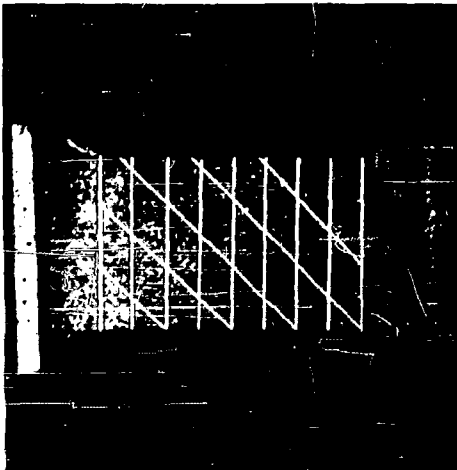
The contribution of the yield band to the behavior of the propellant is demonstrated by the following experiment. Consider tensile specimens which have been machined through one-half of their cross section to provide various radii at the tips of the machined notch. The specimens were clamped to give uniform loading and pulled in tension at constant rate. The reduction of the cross-section to one-half ensures that negligibly small deformations will be obtained except at the end of the notch. It was expected that the narrowest cross-section of the specimen would produce just one yield band, in which case the elongation required to break the specimen would be nearly independent of the radius at the tip of the notch. The data of Table 2



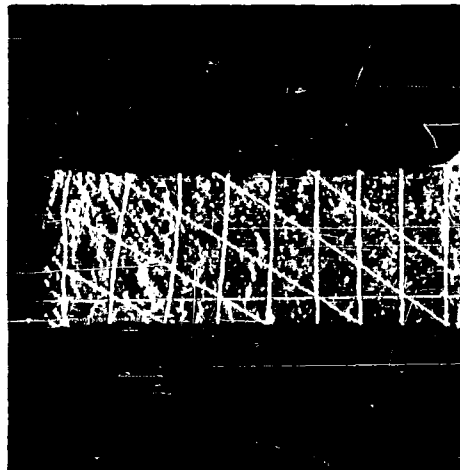
$\epsilon = 34.5\%$



$\epsilon = 49\%$



$\epsilon = 0\%$



$\epsilon = 44.5\%$

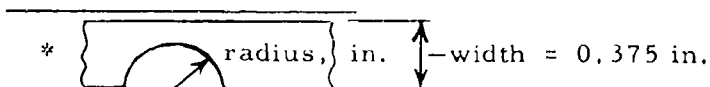
Figure 18: Dewetting of Class 2 Propellant

0 1 1730

TABLE 2

THE STRESS AT BREAK FOR NOTCHED PROPELLANT
SPECIMENS TESTED AT 80°F

| Radius at tip of cut, in.* | Propellant A | | | | Propellant B | | | |
|-------------------------------|--------------|------------------------------------|------------------|--------------------------------|--------------|------------------------------------|------------------|--------------------------------|
| | Δl | $\frac{\Delta l_o^{**}}{\Delta l}$ | S_{nb}' psi | $\frac{S_{nb}}{S_{nbo}^{***}}$ | Δl | $\frac{\Delta l_o^{**}}{\Delta l}$ | S_{nb}' psi | $\frac{S_{nb}}{S_{nbo}^{***}}$ |
| 0.01 | 0.51 | 3.5 | 115 | 1.09 | 0.15 | 4.4 | 125 | 0.68 |
| 0.094 | 0.605 | 3.0 | 109 | 1.04 | 0.20 | 3.3 | 143 | 0.77 |
| 0.115 | 0.67 | 2.7 | 107 | 1.02 | 0.20 | 3.3 | 159 | 0.86 |
| 0.125 | 0.665 | 2.7 | 111 | 1.06 | 0.20 | 3.3 | 178 | 0.96 |
| 0.145 | 0.71 | 2.5 | 109 | 1.04 | 0.22 | 3.0 | 157 | 0.85 |
| 0.165 | 0.625 | 2.9 | 107 | 1.02 | 0.215 | 3.1 | 159 | 0.86 |
| 0.190 | 0.67 | 2.8 | 118 | 1.12 | 0.215 | 3.1 | 174 | 0.94 |
| 0.220 | 0.665 | 2.8 | 109 | 1.04 | 0.345 | 1.9 | 185 | 1.00 |
| 0.245 | 0.685 | 2.6 | 115 | 1.09 | 0.37 | 1.8 | 175 | 0.95 |
| Av. | | 2.83 | | 1.057 | | 3.02 | | 0.874 |
| Std. Dev. | | 0.29 | | 0.035 | | 0.78 | | 0.102 |
| Std. Estimate of Error, % | | 10.3 | | 3.3 | | 25.9 | | 11.6 |



** Δl_o = elongation at failure of unnotched specimen
= 1.8 in. for Prop. A; = 0.66 in. for Prop. B

*** S_{nbo} = nominal stress at break of unnotched specimen
= 105 psi (av. of range 100-110) for Prop. A
= 185 psi (av. of range 170-200) for Prop. B

III, A, Propellant Classification (cont.)

confirm this expectation for the two propellants shown. The data suggest further that these two propellants normally produce three yield bands. A statistical test of differences of average values for the two propellants gave $t = 0.679$, not significant, for the $\Delta L_o / \Delta L$ values, and $t = 5.13$, which is significant at 95% level, for S_{nb} / S_{nbo} .

The first conclusions to be drawn from this experiment is that the elongation to break of the standard specimen (2.7 in. gage) is equivalent to about three times the elongation of one yield band, thus emphasizing the high elongation capabilities of locally yielded material. The second conclusion is that the elongation at failure is essentially controlled by the nature and amount of the dewetted material.

4. Highly Dewetted Propellant System

The data available on these highly filled systems suggest that only propellant structures capable of considerable dewetting can produce large deformations and offer a practical means for benefiting from the superior characteristics of some binder systems. This is illustrated in the photomicrographs of Figure 19 of a strained propellant exhibiting a high degree of dewetting. The photomicrographs show that the dewetting can be made to increase quite uniformly with elongations.

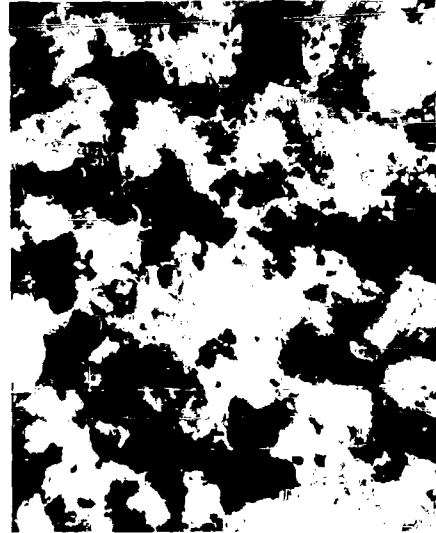
5. Classification System

The classification proposed for composite propellants is based upon dewetting behavior. Four classes of propellants are proposed as follows:

44 X MAGNIFICATION S S/MA DIAM.



25 % STRAIN



50% STRAIN



75 % STRAIN

Figure 19: Dewetting in a Class 1 Solid Propellant (Dark Areas Indicate the Formation of Cavities about the White Oxidizer Particles)

III, A, Propellant Classification (cont.)

| Class | | |
|-------|--|---|
| I | Essentially complete dewetting is observed as the break point is reached | Linear relation of $\log V/V_0$ to $\log \lambda$ |
| II | Dewetting occurs in two or more bands throughout the gage length of the specimen | Typical of that shown in Figure 18 for filled systems |
| III | Dewetting occurs generally only in one narrow band | Similar to Class II but only one band occurs |
| IV | No dewetting occurs up to the break point, typical of propellants below their glassy point | Essentially no volume change to failure |

The mathematical descriptions of response behavior to be developed will utilize this classification system.

IV. PHASE 3 - THEORETICAL AND EXPERIMENTAL STRESS ANALYSIS

The objective of this phase is to use the data representations of Phase 2 for the calculation of strains in a simple tubular, case bonded, charge, as well as in a typical star configuration. The end configurations of these charges will be simple for ease of analysis and test. Charges satisfying the boundary conditions of the analysis will be prepared and tested and the strains measured will be compared with predicted values.

A. THEORETICAL CALCULATION OF STRESSES AND STRAINS

1. Computer Calculation of Stresses and Strains

A method for computing stresses and strains using the infinitesimal linear theory of elasticity was perfected for use on the IBM 7090 computer (7). The technique uses the special stress functions introduced by Southwell for axisymmetrical solids of revolution. It can be applied to determine stresses and strains caused both by pressurization and by thermal cycling. The method in its present form is applicable to the analysis of a case-bonded finite circular cylindrical grain with a hollow bore, given the Young's Modulus E and the Poisson's Ratio ν of the propellant. The allowance for the constraint of the motor case is such that the anisotropic properties of filament wound chambers can be treated just as readily as can constraint by an isotropic metal chamber.

The method was applied to a tubular, case-bonded grain, cooled from a uniform temperature of 110°F down to a uniform -40°F. Computed values of the maximum hoop strain at the inner bore, which occurs at the center of the grain, turned out to be essentially independent of the Young's Modulus of the propellant, as shown in the following tabulation of inner bore hoop strain with Poisson's Ratio and propellant Modulus of Elasticity.

IV, A, Theoretical Calculation of Stresses and Strains (cont.)

MAXIMUM INNER BORE HOOP STRAIN, %

| E, psi | ν | | |
|--------|-------|-----|------|
| | 0.3 | 0.4 | 0.5 |
| 500 | 2.8 | 4.2 | 11.6 |
| 3775 | - | 4.4 | 11.1 |

While the inner bore hoop strain is relatively insensitive to variations in the value of Young's Modulus, the hoop stress at the midplane is sensitive as the following tabulation shows:

INNER BORE HOOP STRESS, psi

| E, psi | ν | | |
|--------|-------|-----|-----|
| | 0.03 | 0.4 | 0.5 |
| 500 | 19 | 23 | 72 |
| 3775 | | 210 | 540 |

While the approximate propellant Poisson's ratio can be determined from the bore hoop strain, the equivalent propellant Young's Modulus can be determined from the strain of the case since the interfacial radial pressure, σ_r , and shear stress at the case depend markedly both on ν and on E. This is brought out for σ_r by the following tabulation:

INTERFACE RADIAL STRESS AT THE MIDSECTION OF THE GRAIN AS A FUNCTION OF PROPELLANT E AND ν

| <u>E</u> | <u>ν</u> | <u>σ_r, psi</u> |
|----------|-------------------------|-----------------------------------|
| 500 | 0.3 | 8 |
| | 0.4 | 12 |
| | 0.5 | 35 |
| 3775 | 0.3 | - |
| | 0.4 | 90 |
| | 0.5 | 240 |

IV, A, Theoretical Calculation of Stresses and Strains (cont.)

The interfacial shear stress is not listed at the mid-plane as it is zero there. Since the radial stress at the case can be calculated from strain measurements on the case, a means is available for determining the equivalent propellant Poisson's ratio from test results.

An alternative technique was initiated for computing stresses and strains in propellant grains, making use of the displacement equations of equilibrium for three-dimensional linear infinitesimal elasticity. The reason for the two-pronged approach on the infinitesimal elasticity grain analysis problem is that the numerical analysis with certain boundary conditions will be simpler using the displacement equation approach. There will be fewer nonzero terms, i. e., more zero terms in the matrix equations, with a resultant freeing of storage space in the computer and the possibility of obtaining a finer mesh. The displacement equations have been cast in finite difference form. The finite cylinder with flat bonded ends and a star bore, consisting of radial sides and circular arcs at root and tip, subjected to internal pressure is being analyzed by means of these equations. A special instance (rigid case, rigid ends) has been programed to check the equations; investigation of initial results shows that a finer grid may be necessary in future analyses. Initial grid size on the check case was three radial divisions, three circumferential divisions, and twelve longitudinal divisions.

2. Nomograph for Calculation of Stresses and Strains

A nomographic method for analyzing stresses and strains in an internally pressurized long cylindrical propellant grain with a circular bore was developed during the quarter. The nomograph is now being finalized and a report written describing its utilization. The possibility of using a nomograph became evident when the results of an analysis based on a large deformation theory proposed by Blatz were being examined⁽¹⁾; it was found that the differential equations derived by Blatz could be cast into a particularly useful

IV, A, Theoretical Calculation of Stresses and Strains (cont.)

dimensionless form, thus facilitating the use of a nomograph for their solution⁽⁸⁾. The theory used is based on a parameter, ν_B , which can be measured photographically during the conventional tensile testing of propellant samples. If the longitudinal strain of a propellant sample in an Instron test is denoted by ϵ and the concurrent lateral contraction by ϵ_1 , then the experimental quantities

$$\lambda = 1 + \epsilon \quad (3)$$

$$\lambda_1 = 1 + \epsilon_1 \quad (4)$$

can be related by a relationship of the type.

$$\lambda^2 = \frac{1}{1 + 2\nu_B(\lambda - 1)} \quad (5)$$

where ν_B is an experimental constant somewhat akin to a Poisson's ratio; ν_B differs from the conventional Poisson's ratio in that it remains relatively constant up through large strains.

When this concept is applied to an internally pressurized, infinitely long cylinder of propellant with a circular bore and the large deformation strain energy function theory of Rivlin is applied⁽⁹⁾, the following differential equation, connecting tangential and radial strains, results:

$$\frac{d\lambda_r}{d\lambda_\theta} = -\frac{\lambda_r}{\lambda_\theta} \cdot \frac{1 + (1 - 2\nu_B)\lambda_r\lambda_\theta}{1 + (1 - 2\nu_B)\lambda_r^2} \quad (6)$$

with $\lambda_r = 1 + \epsilon_r = 1 + \frac{du}{dr}$ (7)

$$\lambda_\theta = 1 + \epsilon_\theta = 1 + \frac{u}{r} \quad (8)$$

IV, A, Theoretical Calculation of Stresses and Strains (cont.)

where u is the radial displacement of the cylindrical surface originally at r .
If a number B is introduced, defined as the Blatz Number,

$$B = 1 - 2\nu_B \tag{9}$$

then the differential equation given above can be put in the dimensionless form and independent of propellant-property,

$$\frac{d\lambda_r^*}{d\lambda_\theta^*} = - \frac{\lambda_r^*}{\lambda_\theta^*} \cdot \frac{1 + \lambda_r^* \lambda_\theta^*}{1 + \lambda_r^{*2}} \tag{10}$$

with $\lambda_r^* = \sqrt{B} \cdot \lambda_r$ Blatz radial extension measure (11)

$\lambda_\theta^* = \sqrt{B} \cdot \lambda_\theta$ Blatz tangential extension measure. (12)

The nomograph is based on this dimensionless strain equation.

A computer program was written to establish numerical results.
A check case was run for the following values of the parameters

- a = Bore Radius = 5 in. t = Case Thickness = 0.10 in.
- b = Inside Case Radius = 27 in. E = Case Modulus = 5×10^6 psi
- ν = 0.36 $\nu_{\text{case}} = 0$ (filament wound)
- μ = Propellant Shear Modulus = 370 psi

The results contrast with those of infinitesimal elasticity theory as follows:

| | Blatz Characterization | Infinitesimal Elasticity |
|-----------------------------------|---------------------------|-----------------------------|
| Percent Radial Strain at Bore | -38% | -37.5% |
| Percent Tangential Strain at Bore | +52% | +36% |
| Radial Stress at Case | 67 psi | 37 psi |

IV, Phase 3 – Theoretical and Experimental Stress Analysis (cont.)

B. EXPERIMENTAL TEMPERATURE CYCLING OF PROPELLANT CYLINDERS

Small tubular, case-bonded cylinders of live propellant showing essentially Class 1 dewetting behavior were cycled from the cure temperature, 110°F, to 0°F and to -75°F. The maximum strain which occurred at the center of the grain, was determined by measuring the bore several times at each temperature and taking the difference of the average measurements. The cylinders were bonded in heavy-walled steel casings of 5 in. inside diameter, and the length-to-diameter ratio of the bonded section was 2.1. One of the bonded ends was chamfered at 45 degrees, the other end of the grain was released 2.25 in. The lack of symmetry at the ends did not shift the maximum strain position significantly from the center of the grain. The data are shown in Figure 20 for the various values of outer to inner diameter ratio tested. The strains in such a case from simple geometry should be essentially proportional to b^2/a^2 , to the temperature difference, and to the difference in the coefficients of thermal expansion, of the propellant and the case, $a_p - a_c$, if the propellant is an incompressible material and the ends of the grain are unrestrained.

$$\epsilon_{\text{mm}} (1 + \epsilon_{\text{mm}}/2) = (b^2/a^2) (a_p - a_c) (110 - T) \quad (13)$$

For ends restrained to the lengthwise strain of the case, this equation becomes

$$\epsilon_{\text{mm}} (1 + \epsilon_{\text{mm}}/2) = \left(\frac{3}{2} \frac{b^2}{a^2} - \frac{1}{2} \right) (a_p - a_c) (110 - T) \quad (14)$$

The data of Figure 20 have not been corrected for the change of inner diameter caused by cooling from 110°F to T, which increases the right hand side of Equations (13) and (14) by the amount $a_p (110 - T)$. Values of

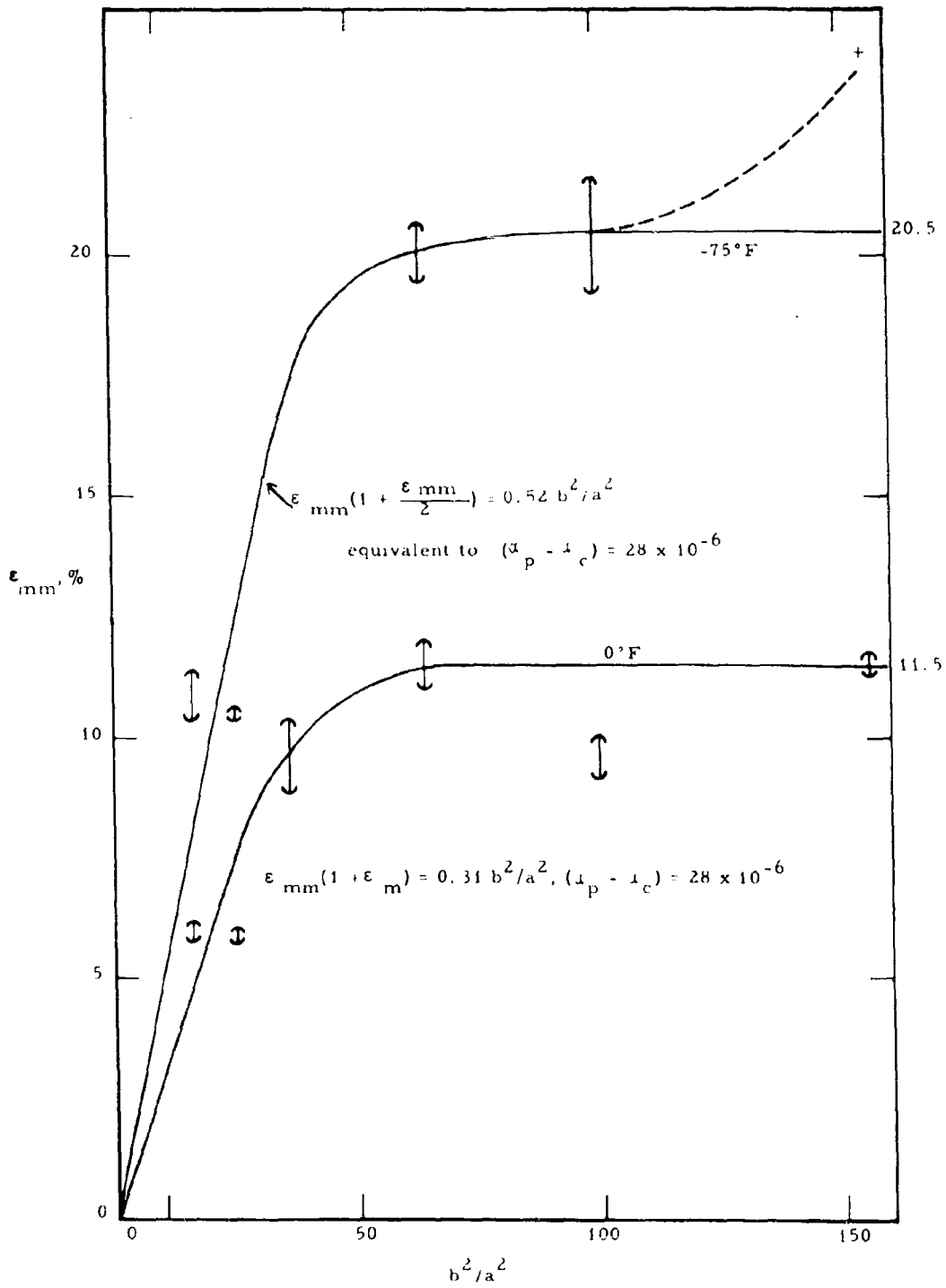


Figure 20: Effect of b^2/a^2 on Maximum Strains Observed in Subscale Motors

IV, B, Experimental Temperature Cycling of Propellant Cylinders (cont.)

$a_p = 53 \times 10^{-6}$ (in.)/(in.)(°F), and $a_c = 6.3 \times 10^{-6}$ (in.)/(in.)(°F) are typical for these propellants. At 0°F this correction factor is 0.6% and at -75°F is 1.0%. The best line through the lower b^2/a^2 values of Figure 20 correspond to a value of $a_p - a_c = 28 \times 10^{-6}$; a line through highest value of range at the lowest b^2/a^2 value would correspond to $a_p - a_c = 38 \times 10^{-6}$. The use of the value of $a_p - a_c = 47 \times 10^{-6}$ calculated from the coefficients of expansion of propellant and metal given above would thus overestimate the strain and give conservative values.

The departure of the data from the expected curves at values of $b^2/a^2 \sim 40$ is presumably related to the dilatation at higher strain levels caused by void formation. The curve at 0°F shows the dilatation increasing steadily once 10% strain is reached with the net effect of preventing strains much above 11.5%. However, when the temperature is lowered further to -75°F, a higher strain level is apparently reached without a significant amount of further dewetting, since the start of dilatation occurs at the same b^2/a^2 as at 0°F, and the increase of limiting strain at higher b^2/a^2 values (except for the one observation at $b^2/a^2 = 155$) above that at 0°F is essentially proportional to the further increase of temperature difference from equilibrium. This conclusion suggested by these cycling data will be studied further by volume change measurements at low temperature under Phase 1.

C. EXPERIMENTAL PRESSURIZATION OF PROPELLANT CYLINDERS

The purpose of this investigation is to formulate a method with which the stress and strain distribution can be predicted in the propellant grain of a solid rocket motor. For the present, this is limited to the specific area of stresses and strains at the interior of a long hollow cylinder of cased propellant under internal pressure. The approach used is to observe the deformations of cased, subscale inert propellant cylinders under controlled pressure

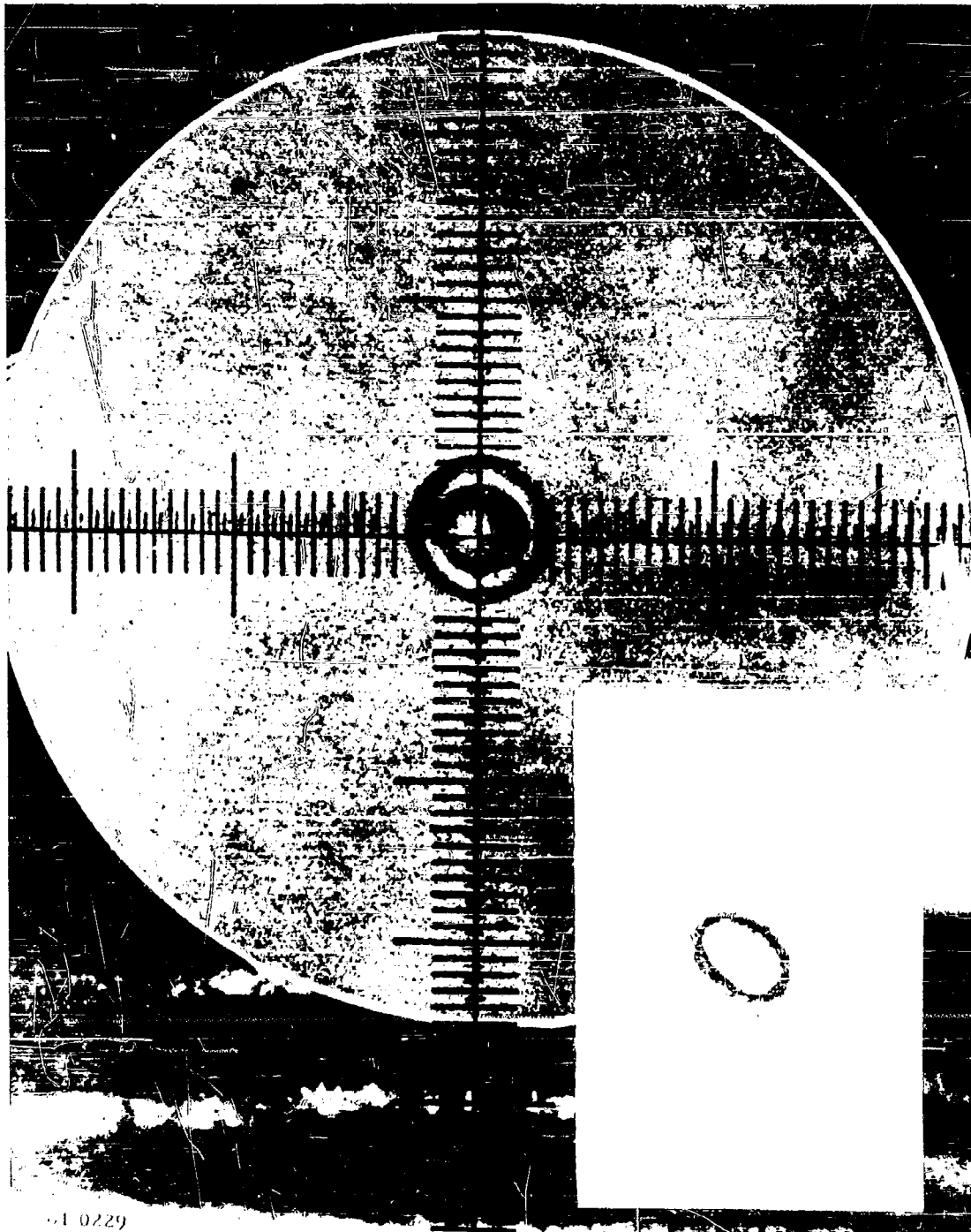
IV, C, Experimental Pressurization of Propellant Cylinders (cont.)

conditions and in a plane strain condition. Parallel with this, the mechanical properties of this same material are measured in a laboratory. Analytical methods will then be developed to provide the connecting link between mechanical properties and observed deformations. These analytical methods can then be tested out on larger specimens or on actual rocket motors. It is felt that the simple configuration of a cylindrical inner bore should be studied first to develop the technique. Later, modifications can be made to allow for the effect of a star shape.

The first phase of the test program has been initiated. A hollow cylinder of DP-16 inert propellant was tested to an internal pressure of 300 psi. The cylinder was 1.00 in. inner diameter, 6.00 in. outer diameter, and was a slip fit in an aluminum case of 0.060 in. wall thickness. Internal radius measurements were made by two independent methods; one was to monitor the flow of water into the pressure bladder inside the cylinder, the second was to photograph the end of the sample through a 1 1/2-in. thick Lucite plate. Photographs at zero and 300 psig pressure are shown in Figures 21 and 22. The tangential strain at the case was measured by three strain gages mounted in line one inch apart; a modulus of 10^7 for the case was used to convert strains to stresses.

1. Test Results

The tangential strains at the inside boundary calculated from volume of water, at the outside boundary calculated from the strain gage measurements, and at the inside boundary measured from the grid photographs are shown in Figure 23. A water leak was observed in the bladder at 100 psi which sealed itself with additional pressure. A discontinuity in the strain curve at the inside boundary due to the leakage is corrected for by the dashed curve to give approximately a 55% strain at 300 psi pressure. The corresponding



61 0229

Figure 21: End of Grain at Zero Pressure as Seen Through 1.5-in. -Thick Lucite Plate Showing Grids on the Plate and on the End of the Grain

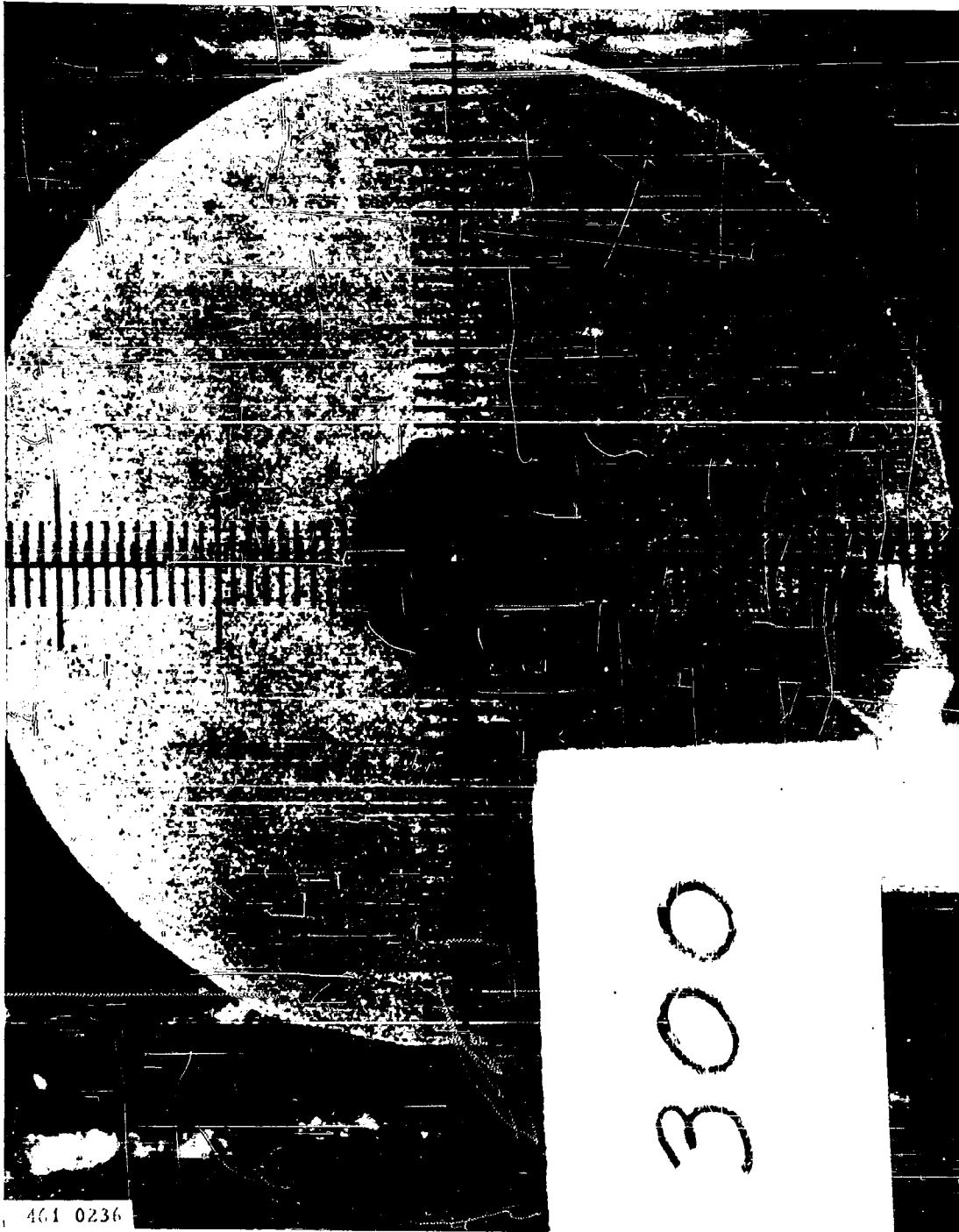


Figure 22: End of Grain Shown in Figure 21 at Interval Pressure of 300 psig.

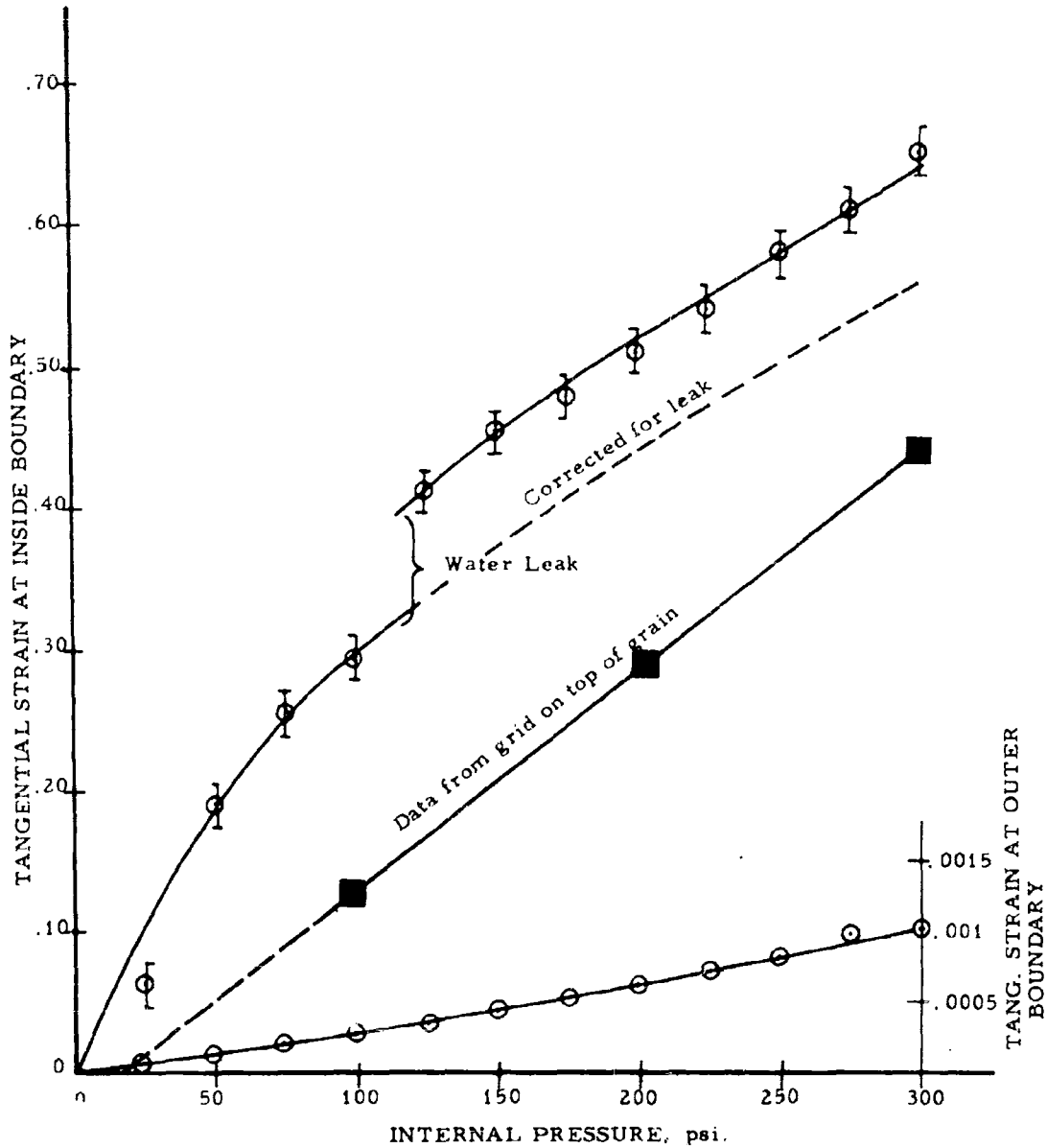


Figure 23: Tangential Strains at Inner Wall of Cylinder, as Measured by Water Volume and by Grid on End of Grain, and Tangential Strain at Outer Wall as Measured by Strain Gages

IV, C, Experimental Pressurization of Propellant Cylinders (cont.)

tangential strain at the outside boundary at 300 psi was 0.1%. The agreement between the two strain values for the inner wall is not satisfactory and is being studied further. Figure 24 shows the distribution of strains through the cylinder at various pressures, obtained by measuring the movement of photographs such as Figures 21 and 22 of the grid painted on the propellant with respect to the grid on the Lucite. These data appear to be linear when plotted against $1/r$,² as would be expected for an incompressible material.

As had been expected, the tangential strain in the propellant changed very rapidly in the region near the inner bore. Attempts were made to fit these curves to linear, infinitesimal theory of elasticity equations to see if some value of modulus of elasticity and Poisson's ratio could be found which would give a match for the boundary conditions and the tangential strain curve in the high strain region within ten percent. The curves demonstrate: (1) the deviations from linearity and the magnitude of the strains are too great to allow such a simplified analytical approach to be used; and (2) the sensitivity of strain levels to small variations in Poisson's ratio presents difficulties in analytically interpreting the curves in a test which allows as little overall volume change as this one does.

Figure 25 shows the effect of internal pressure on the pressure at the propellant-case interface calculated for a modulus of 10^7 for the case. The values are also expressed as the percent of the internal pressure transferred to the case. The large nonlinearity below 50 psi is probably due to the propellant expanding to fill the case.

Certain sources of errors in the above calculations should be mentioned. The bending in the Lucite plate due to the pressure was not taken into account and tests are being performed to determine what errors are involved here. The friction between the propellant and the Lucite plate was assumed

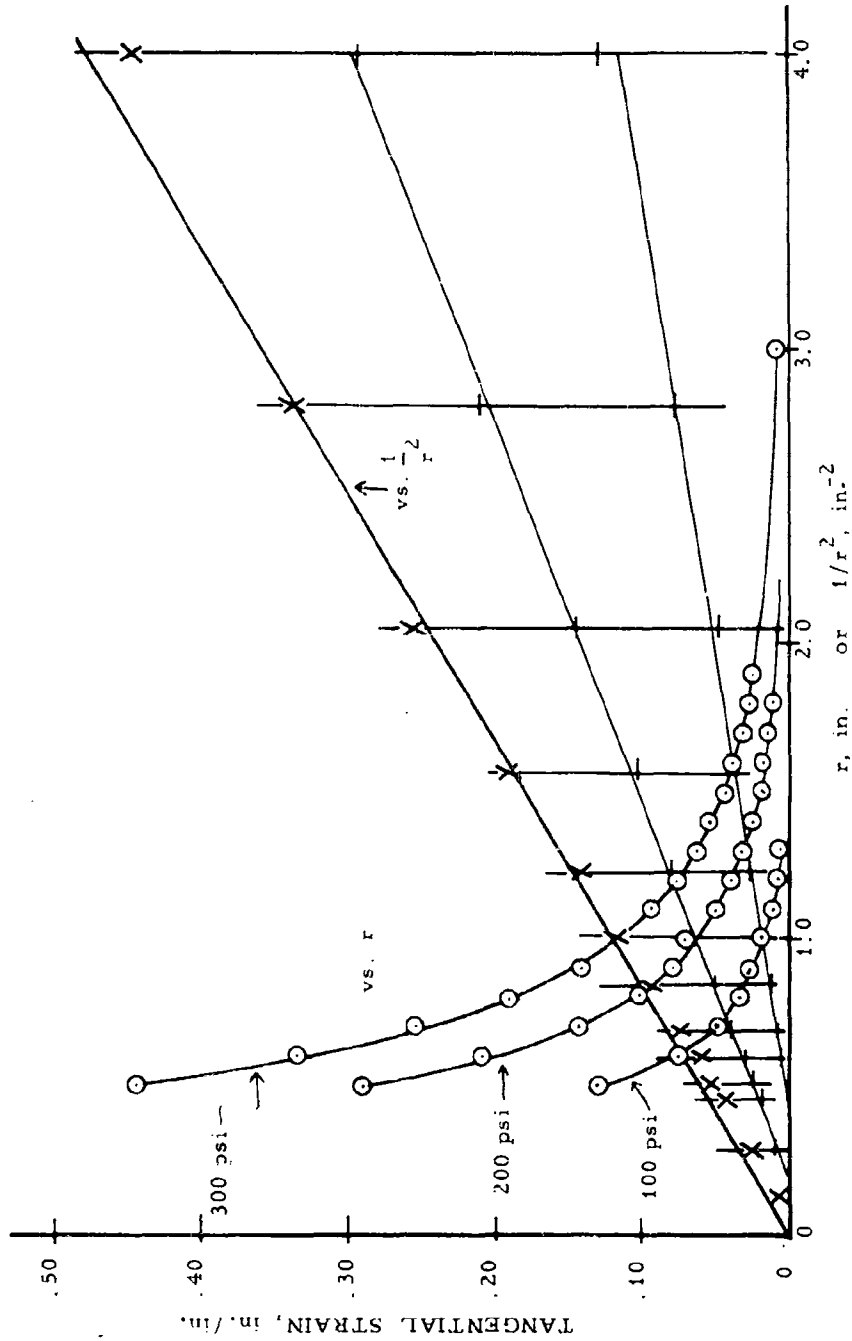


Figure 24: Tangential Strain at Various Radii of Pressurized Hollow Cylinder Calculated from Movement of Grid at Top of Cylinder Plotted Against Radii and 1/(Radius)²

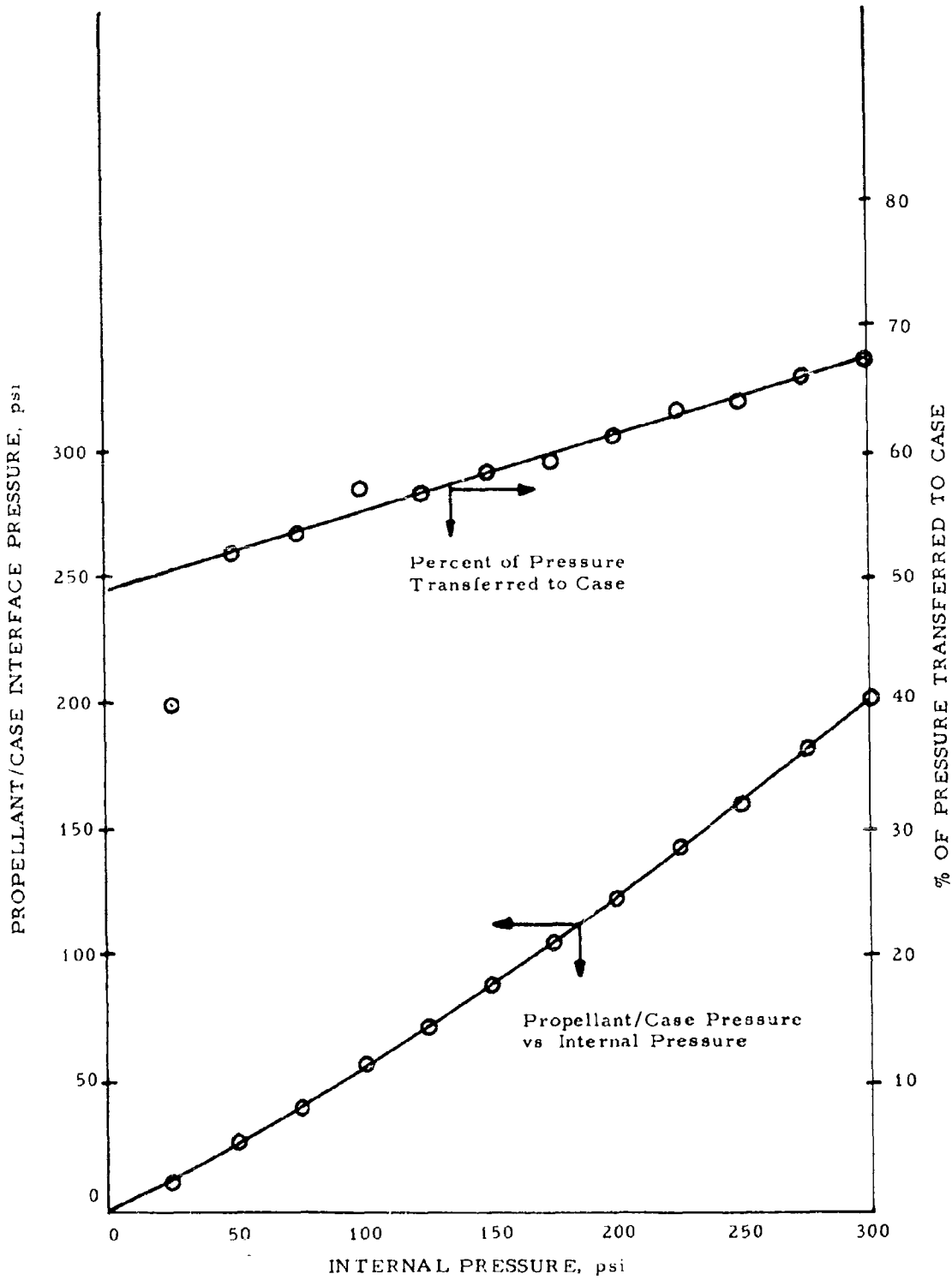


Figure 25: Propellant Case Interface Pressure Produced by the Internal Pressure for a Case Modulus of 10^7 psi

IV, C, Experimental Pressurization of Propellant Cylinders (cont.)

negligible, since the propellant surface was coated with a silicone grease. If there is no friction, then the sample would remain cylindrical under pressurization. This assumption is being tested through additional measurements along the length of the core.

The immediate points for concern are three; the first is to gain assurance that the precision of measurements and the assumption of plane strain conditions during the pressure tests are of sufficient accuracy; the second is to find a correlating analytical method which can be used satisfactorily with a nonlinear viscoelastic material; and the third is to ascertain the type of mechanical property measurements which are needed to fit into the analysis.

2. Precision of Pressure Test Methods

The test measurements include direct measurement of internal pressure by a pressure gage, measurement of hoop strain in the metal case by strain gages, measurement of the change of volume enclosed by the inner bore of the specimen by means of water level measurements on the supply reservoir, and direct measurements of radial deformation of the end of the specimen made through the transparent end plate. The internal pressure measurement accuracy is dependent on the accuracy of the gage and gage readings. This should easily fall within two or three percent of the true values, and hence should present no problems or particular limitations. The same can be said of the strain gage readings on the outer case. Since there exists a possibility of nonuniformity of deformation at different points along the axis, three strain gages are being used located an inch apart. Thus far, the readings of these gages have compared quite closely. Since the elastic properties of the metal (aluminum) case are well known, the external pressure on the specimen can easily and accurately be calculated from the case strains. The severest limitations on accuracy of measurement probably lie in attempts to determine the tangential strain at the inner bore and in the region near the inner bore. Internal strain as deduced

IV, C, Experimental Pressurization of Propellant Cylinders (cont.)

from volumetric change will tend to be high, since the rubber bladder does not completely fill the void in the specimen at low pressures. Change in strain with change in pressure at high pressure levels (in excess of 100 psi), is accurate to within 2% however. In making radial deformation measurements through the end plate, it is difficult to obtain accuracies of strains any better than $\pm 8\%$ of the true value. As the strain level drops to ten percent, the accuracy of measurement drops to about $\pm 25\%$ of the true value.

In a test of this nature where the propellant is confined within a relatively inextensible case, the assumption of plane strain must be closely questioned. The change in the volume bounded by the case and the end plates is strongly affected by bending of the end plates and stretching of the bolts connecting the end plates as well as the extension of the case itself. Tests to be conducted in the future will be using highly extensible cases to allow such effects to be neglected.

3. Analytical Correlation of Data With Mechanical Properties

In formulating an analytical approach to this problem, the appearance of the test data and the general information known about the characteristics of the propellant material needs to be taken into consideration. It is proposed to use an approach somewhat different from that already described for study on the IBM 7090. There are two significant observations that can be made about the test data. First, it is apparent that the magnitude of the strains that can be expected at and near the inner radius of the propellant cylinder is extremely large. Second, the variation of this strain with radius is very large, particularly in the region near the inner radius. It would be expected that the stress would exhibit a corresponding variation. The material is well known to have very nonlinear stress-strain relationships particularly at large strain levels. Both dilatation and shear deformations can be expected to exhibit extreme strain dependency under load. Since a large part of these property

IV, C, Experimental Pressurization of Propellant Cylinders (cont.)

variations can be attributed to the progressive breaking of the bonds between oxidizer particles and the filler material, it was felt desirable to try an analysis which does not require that this nonlinearity be expressed in an algebraic form. It is proposed, therefore, to subdivide the propellant cylinder, for the purpose of analysis, into several concentric cylindrical segments, each having a fairly uniform tangential strain across their radial dimension. Each of these segments will be in a tension-compression-compression stress field with high tangential and radial strains and zero longitudinal strain. Hence, the mechanical properties used in the analysis of each segment must be correct for this type of stress-strain field.

For each cylinder, an estimate of the final tangential strain level under load is estimated. Mechanical properties are then selected for each cylinder based on these estimated strain levels. These properties are introduced into conventional equations relating stresses to strains at the inner and outer boundaries. The equations for the different cylinders are then related to each other through compatibility of tangential strains and equilibrium at the interface. It can be seen that regardless of any peculiarities encountered in material properties, these compatibility and equilibrium conditions must exist. The resultant will be a system of equations, two for each cylinder, that can be solved simultaneously when the inner and outer boundary conditions for the entire system is known. This solution will yield the radial stresses and tangential strains at each interface. New mechanical properties can now be selected on the basis of these resultant strains and the above procedure repeated until the resultant strains are compatible with the mechanical properties.

IV, C. Experimental Pressurization of Propellant Cylinders (cont.)

4. Mechanical Property Measurements Required for Analysis

As has been noted, the key to the application of the described analytical technique is the establishment of mechanical property information under conditions closely approximating those met under the applied loads. It may be that specimen tensile tests under hydrostatic pressure will provide satisfactory information. This type of test can be closely controlled yielding quite accurate measurements. The test conditions differ from the environmental conditions in that the principal compressive stresses are equal in the first, whereas in the latter, they differ somewhat. Only by conducting tests under both conditions will it be possible to determine if this difference is significant. It is hoped that a series of tests soon to be conducted will resolve this problem. In these tests, a thin-walled hollow cylinder of propellant will be pressurized while confined in a case which can be expanded to control the external pressure on the specimen. The plane strain condition will be maintained as before. The complexity of this method with its attendant precision of measurement problems does not make it appear too desirable as a means in itself of determining mechanical properties. However, it is felt that a close correlation will be achieved with the tensile tests under hydrostatic pressure.

D. EXPERIMENTAL STUDIES OF PHOTOELASTIC MATERIALS

Propellants can be simulated to a first or second approximation by photoelastic materials. At room temperature it is possible to vary the elastic and viscous properties considerably. At the elevated temperatures required for stress freezing, photoelastic materials are almost perfectly elastic; no introduction of viscous properties is possible in the latter instance.

IV, D, Experimental Studies of Photoelastic Materials (cont.)

To better understand propellant behavior, plane photoelastic model tests would be run under various biaxial and uniaxial stress conditions. Propellant binder would be simulated by photoelastic plastic material and oxidizer by rigid circular disks. A study would be made of effective elastic properties (E , ν) and the stress distribution around rigid inclusions. With such data, proposed theories of mechanical behavior could be checked, and better insight into actual propellant behavior would be attained. The major variables in such a program are inclusion packing density, bonded or unbonded inclusions, and average strain level. Similar experiments with perforated flat plates without inclusions have been conducted (10).

The second major phase for concentration of photoelastic effort is the simulation of three dimensional propellant grains, somewhat idealized for generality, subject to thermal restraint by a relatively rigid casing. No temperature gradients would be involved, but only a temperature discontinuity at the grain-case interface. The major variables in this study would be length-to-diameter ratio, bore-to-outer diameter ratio, and end configuration.

Closely related to the use of photoelastic materials with properties similar to those of propellant is the use of material with quite different properties, such as gelatin. The much lower viscosity and rigidity of gelatin allow studies to be made at an effectively accelerated time scale. This type of scaling study has received a great deal of experimental attention in geology and civil engineering. The use of gelatin for creep studies appears worth preliminary experimental study, utilizing the good birefringence exhibited by gelatin. (2)

IV, Phase 3 -- Theoretical and Experimental Stress Analysis (cont.)

E. DEVELOPMENT OF NEW METHODS OF STRAIN MEASUREMENT

The Baldwin-Lima-Hamilton Company was asked for suggestions on methods of measuring strains inside solid propellants. They have offered two experimental gages of a helical wire type that they have developed; one of these was accidentally destroyed in first tests but the other was cast in PR-1910 plastic*. The gage was found to have a linear response and good electrical output for compressive strains up to 27%. Approximate dimensions of the unit are 1 in. long with a 0.25-in. diameter of the helix.

A stress-meter for measuring stresses in propellant grains is also being developed. Two preliminary tests were conducted in live propellant as a result of which improvements are being made. Dimensions of this unit are 0.170 in. thick and 0.5 in. in diameter.

V. PHASE 4 -- FAILURE CRITERIA

The objective of this phase is to carry out such theoretical and experimental studies as are needed to establish failure criteria applicable to the simple charges studied in Phase 3, and evaluate these criteria by carrying those charges to failure. The concept of failure necessarily includes a study of the behavior of those members of the population most likely to fail. The usual measurement of properties and correlation of data, as in Phases 1 and 2 of this program, centers around consideration of mean behavior with estimates of variability being made to assess the measurement quality. Stress and strain calculations also focus on the use of mean values of the parameters and comparison with the mean of observed deflections. Failure, however, is concerned with the likelihood of a particular stress or strain occurring at the point where the material properties are least adequate. The formation of yield bands in Class 2 and Class 3 propellants gives particular point to this

*PR-1910 is made by the Products Research Co., Burbank, Calif.

V, Phase 4 -- Failure Criteria (cont.)

problem. The data on these classes suggest that as the strains increase, yield bands occur and change the distribution of strains to produce regions in which failure will occur before further strain is produced in the unyielded regions. Thus, the calculations of Phase 3 and the use of techniques such as photoelasticity, do not directly lead to predictions of failure.

A. BATCH VARIABILITY OF FAILURE BEHAVIOR

The large variability associated with propellant properties suggests that certain batches, and certain portions of these batches, will be more susceptible to failure than others. A related hypothesis is immediately suggested for experimental testing: the failure behavior under different types of stress-strain environments are related such that those batches with the highest incidence of failure in one environment will have the highest incidence in another. It is clear that we lack the knowledge at this time to define failure mechanisms in detail for different batches or even different compositions. The generalization of four classes of propellant in Phase 2 has agreed with experimental observations to date in that each of these classes is consistent in the type of failure observed, and that motors using these classes show differences in failure behavior consistent with this classification system. The major problem in testing the hypothesis offered above lies in obtaining sufficient statistical information on full motors and on the same batches of propellant going into these motors. An alternative procedure is to compare property measurements with small-scale motors, and validate the results as full-scale motor data become available. It is evident that during the validation process, the small-scale motor data and the property data would become increasingly firm as a basis for acceptance criteria.

V, A, Batch Variability of Failure Behavior (cont.)

The production of propellant for several programs at the Sacramento Solid Rocket Plant of the Aerjet-General Corporation offers the possibility of taking data on different batches of propellant and determining the correlation between failure values of different mechanical property tests. Instron data at one strain rate are taken from -75° to 180° F in these several programs. A study has been completed in this program of data on one carton from each of 40 batches of a Class 2 propellant. Figures 26 to 29 show correlation graphs of the elongation at failure at 77° F vs the same value at the other test temperatures for each of the cartons studied. The data were also analyzed numerically to give the correlation coefficient shown on each figure. Except for -75° F, the data gave high correlations, and in particular, the three cartons giving highest elongations and the two giving lowest elongations (except as shown in Figure 29 for -75° F) were the same in all cases. This would indicate that a test at any one of the test temperatures would have screened out the same extreme cartons of the population as any other test temperature except 75° F. The -75° F data are in question at this time because of a particularly strong effect of pretest humidity exposure on -75° F test results; these tests were run on specimens experiencing a fairly wide range of humidity prior to being placed in -75° F conditioning for test. Further cartons from these batches will be tested to assess within batch variability.

Limited results of a different type on another Class 2 propellant are shown in Figure 30 for Instron data taken at -75° F after storage for various periods at temperatures at or near 0° F. This latter test is a measure of embrittlement which occurs to a greater or lesser degree in all composite propellants, and is characterized by an increase of modulus and a decrease of elongation at failure. The same general behavior is observed that the ordering of the batches with respect to each other was the same under both test conditions. The paucity of data for this long exposure prevents adequate statistical assessment and more data will be required.

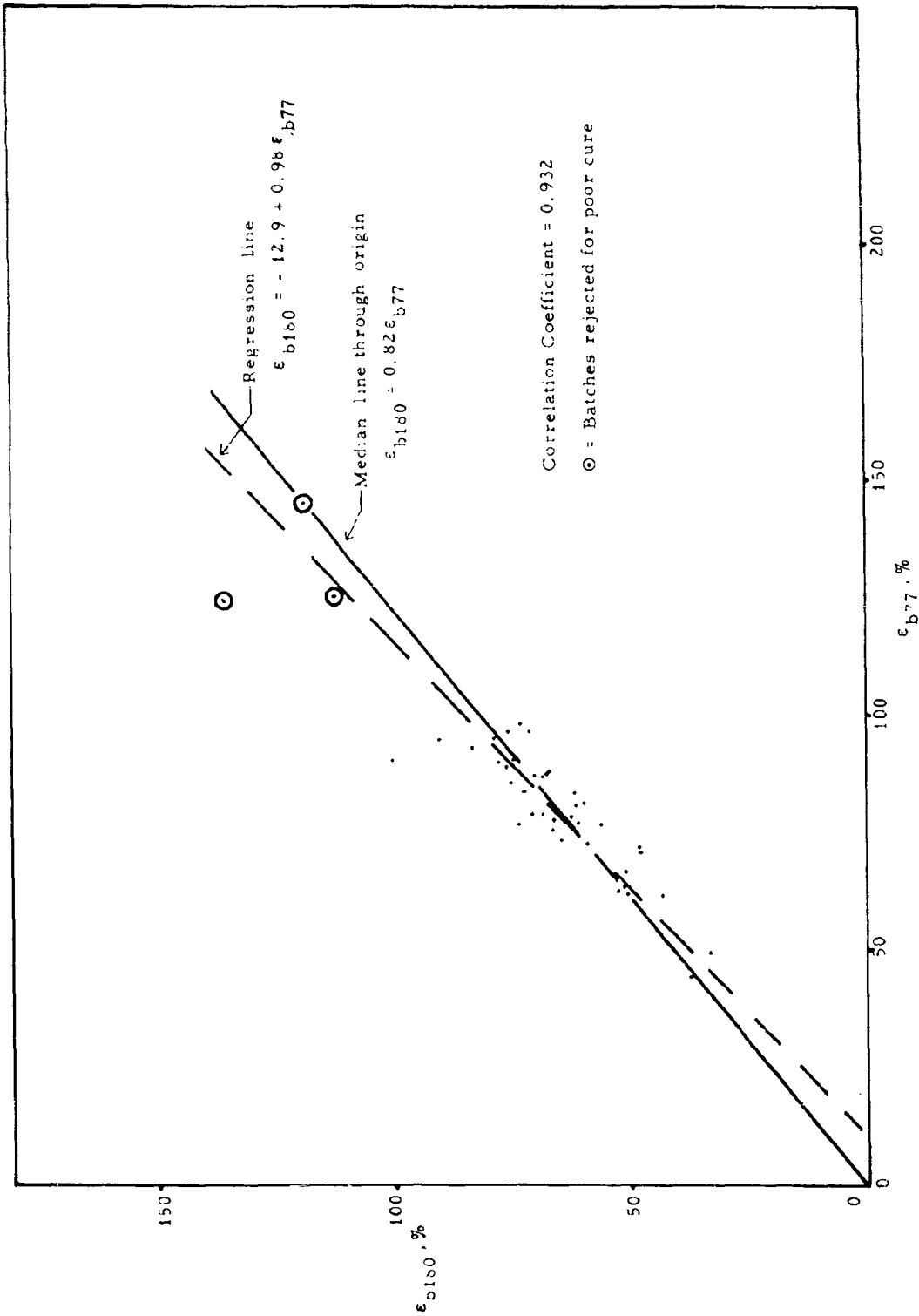


Figure 26: Correlation of Failure Strain at 180°F with that at 77°F for Same Batch

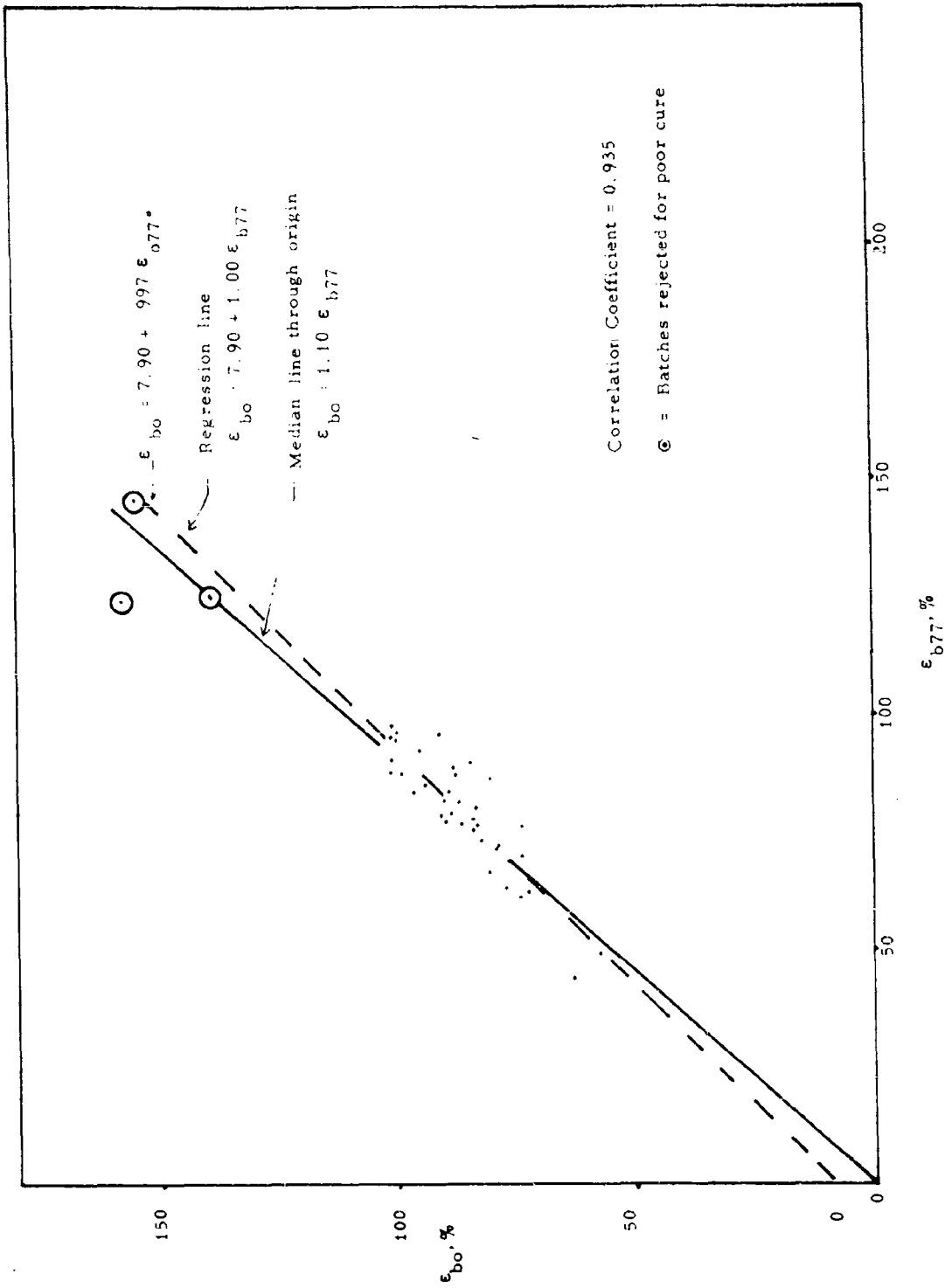


Figure 27: Correlation of Failure Strain at 0°F with that at 77°F for Same Batch

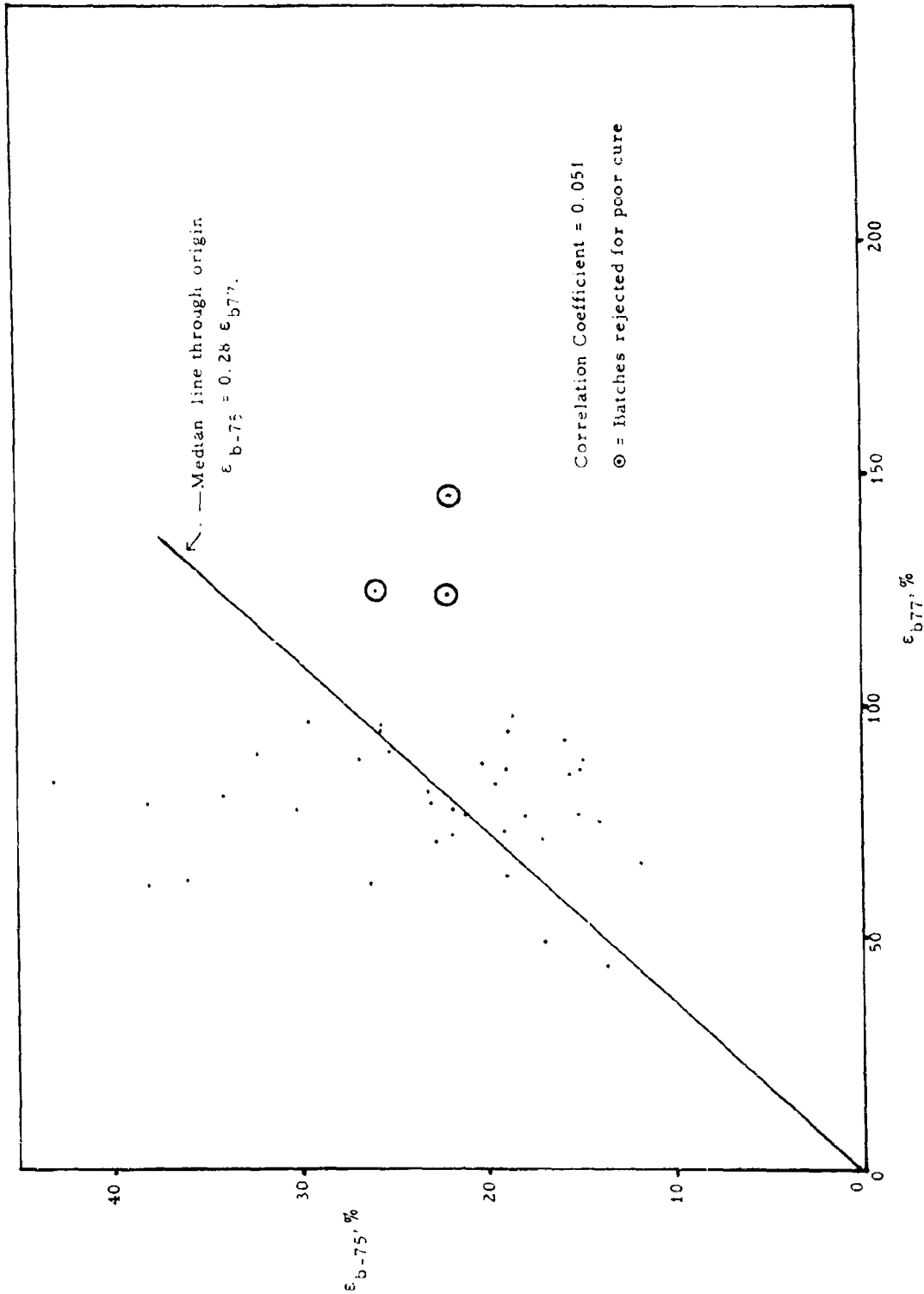


Figure 29: Correlation of Failure Strain at -75°F with that at 77°F for Same Batch

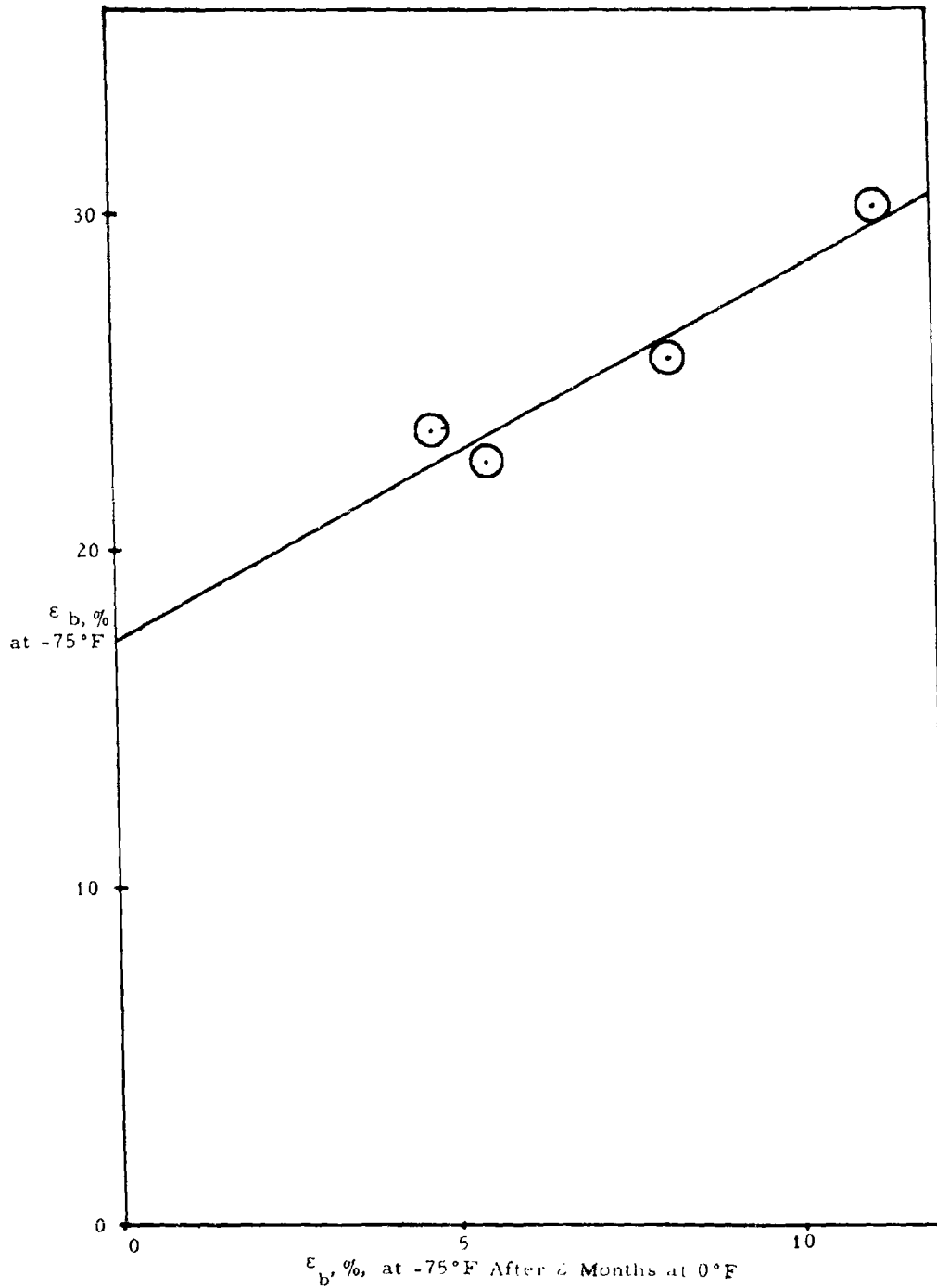


Figure 30: Effect of 2 Months Storage at 0°F on the Initial and Final Break Elongations at -75°F of Several Batches of a Class 2 Polyurethane Propellant

V, Phase 4 -- Failure Criteria (cont.)

B. CORRELATION OF FAILURE DATA WITH MOTOR FAILURES

The small motors with cast-in-case cylindrical grains discussed in Phase 3 have been used for studies of strain produced in motors and some of these motors have experienced failures. It appeared possible to test the failure hypotheses in a different way by study of these failures. A survey was made of 41 small case-bonded motors that had been thermally cycled to -75°F ; b/a ratios from 4 to 12.5 were tested. Of these 41 motors, 15 failed by longitudinal cracking of the propellant grain. The strain in the motor, as measured on the first cycle to -75°F was compared to the strain at break of the propellant at -75°F in the standard Instron test with the hope of establishing a correlation between the propellant failure strain under the condition as seen in the motor and the failure strain as encountered in uniaxial tensile tests.

The propellants involved were two of Class 2 and one of Class 1 type. The propellant property used was the lowest tensile strain at break reported from the two or three tensile tests taken at -75°F . Since some of the motors had been stored for various lengths of time at 0°F before cycling to -75°F an estimated correction for embrittlement was added to the strain at break as measured on unembrittled propellant. The strain at break corrected for embrittlement was divided by the measured strain in the motor on its first cycle to -75°F , to give a ratio called $\epsilon_b / \epsilon_{mm}$. The ratio of $\epsilon_b / \epsilon_{mm}$ is shown plotted against the percent of motors cracking at that ratio in Figure 31. When the ratio $\epsilon_b / \epsilon_{mm}$ was one or less all of the motors failed, when the ratio was two or more none of the motors failed. The region between one and two is the expected area of doubt caused by the wide distribution of propellant properties.

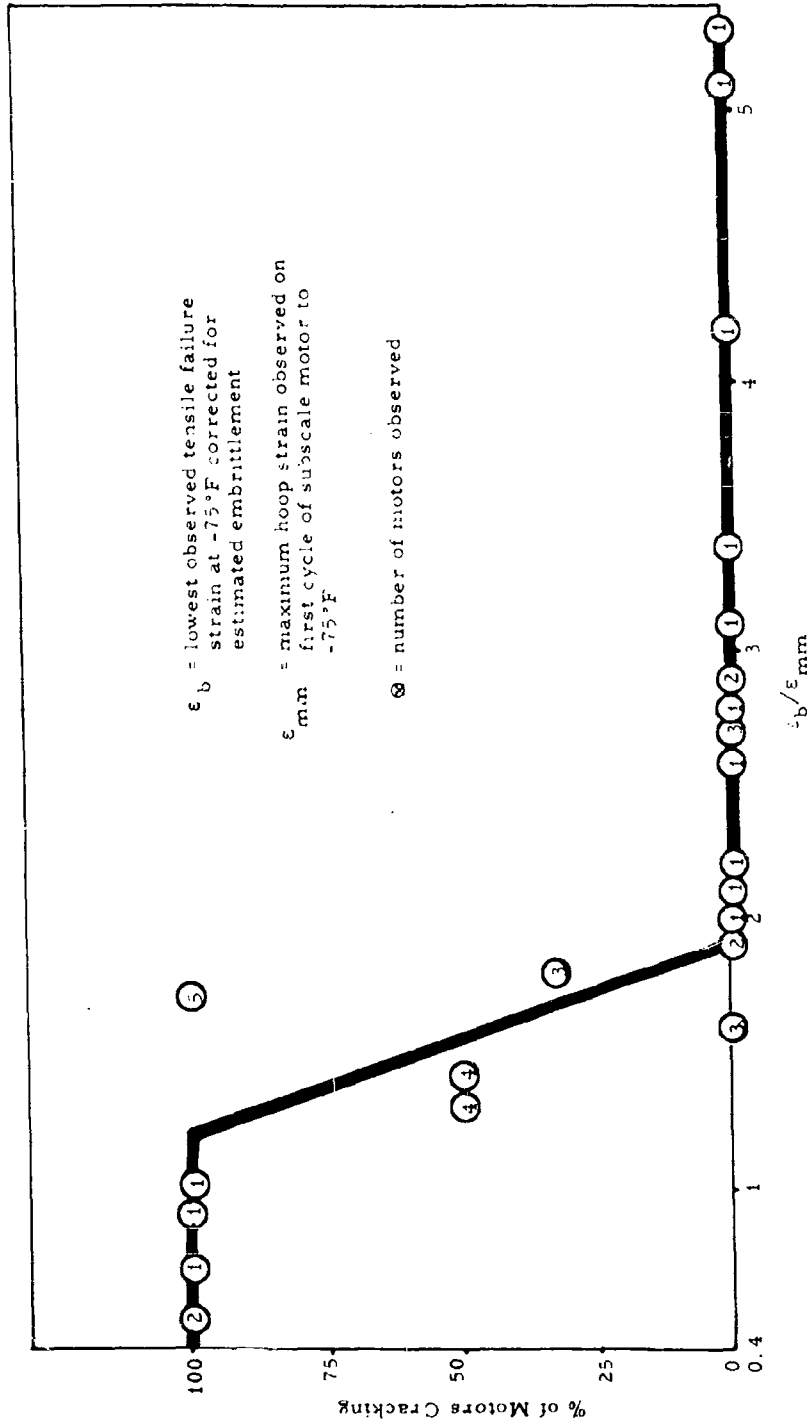


Figure 31: Relation of Failure in Tensile Specimens to Cracking of Subscale Tubular Case Bonded Grains at -75°F for one Class 1 and two Class 2 Polyurethane Propellants

V, B, Correlation of Failure Data With Motor Failures (cont.)

The embrittlement corrected value of strain at maximum stresses was also divided by the measured strain of the motor on the first cycle to -75°F and plotted against the percent of motors failed as shown in Figure 32. As is evident by comparing Figure 32 with Figure 31, the strain at break would appear to be a much more discriminating value to use for predicting failure due to thermal cycling.

The correlation shown in Figure 31 using the relation $\epsilon_b / \epsilon_{\text{mm}}$ emphasizes the importance of adequate data on ϵ_b within and between batches, and the probable importance of measuring ϵ_b under environmental conditions closely approaching those in the motor. The success of the correlation with uniaxial data suggests that a concentration on uniaxial failure behavior is warranted for correlation with failure data on small charges having unrestrained ends. The data on yield bands also suggest that study of the number of yield bands produced in tubular grains is pertinent in this type of correlation, as well as a general study of the production of yield bands at various temperatures; or more specifically, the formation of such bands in tensile specimens due to simultaneously straining and changing temperature.

The requirement for failure studies covering larger numbers of specimens and under environmental conditions similar to those in the motor has led to the development of the very low rate tester (VLRT) shown in Figure 33 now under construction. Through gear reduction, a speed range of 0.002 to 0.0005 in. /min can be obtained, equivalent to a time of failure range of 5 to 30 hr. Provision for mounting up to 11 standard specimens is provided. Break time of individual specimens will be measured from the steps in the total load time curve; if this does not give sufficient precision, separate instrumentation will be set up to measure individual break times.

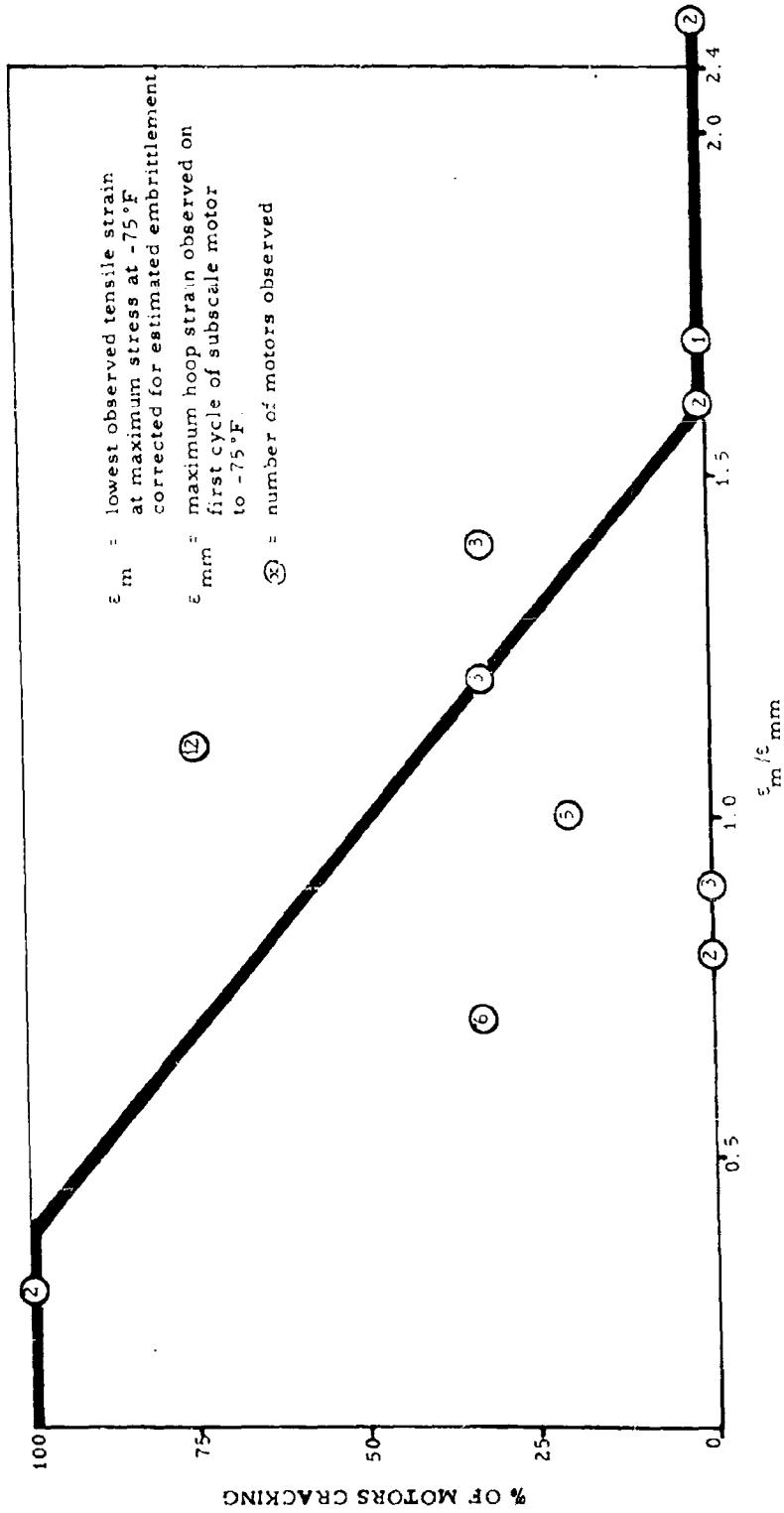


Figure 32: Relation of Failure in Tensile Specimens to Cracking of Subscale Tubular Case Bonded Grains at -75°F for one Class 1 and two Class 2 Polyurethane Propellants

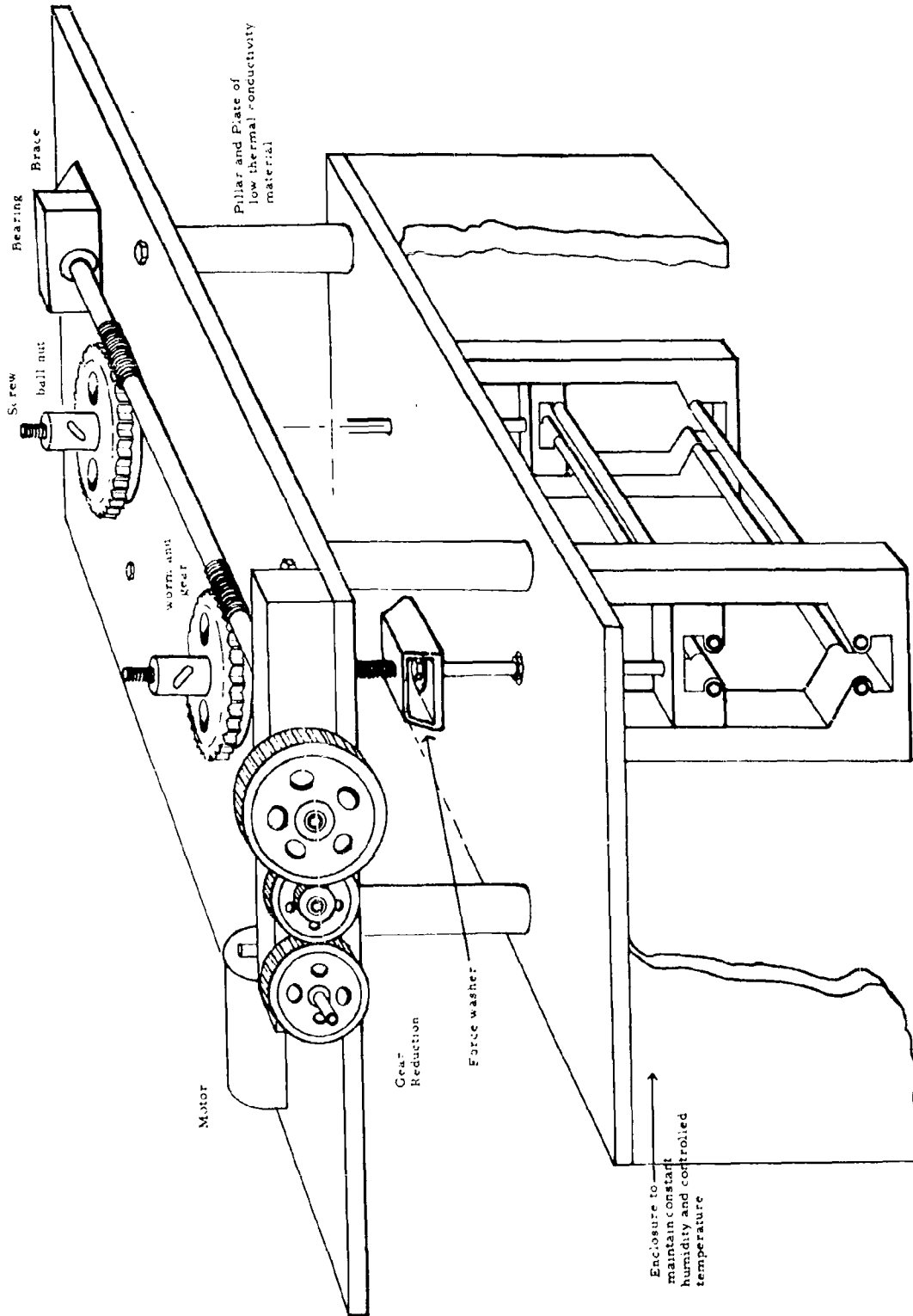


Figure 33: Sketch of Very Low Rate Tester (VLRT)

V, Phase 4 - Failure Criteria (cont.)

C. GRAPHICAL REPRESENTATION OF FAILURE BEHAVIOR

The distribution of failure elongations at the various measurement temperatures can be combined with the expected strain in the motor as shown in Figure 34 to give a graphical representation of the expected failure behavior. This figure is drawn using the lower 3σ limit of individual failures values to describe the failure value expected in the poorest batch used in the motors. From the correlation of Figure 31, the intersection of the lower 3σ curve with the line corresponding to twice the maximum expected motor strain should be the highest temperature, T_f , at which failure could be expected. Similarly, the intersection with the calculated strain in the motor of the lowest failure elongation expected from the best batch of propellant, ϵ_{bm} , would give the lowest temperature, T_{uf} , to which any of the motors could be expected to cycle before failure. The expected statistical distribution of motor failures between T_f and T_{fm} is now under study using the available data on failure elongation given in Figures 26 to 29.

D. MECHANISM OF FAILURE

A preliminary study of the available test data for Class 2 solid polyurethane propellants was made for comparisons with the known failure relations for metals. None of these relations were found to apply to the solid propellants. However, an unexpected correlation was observed as shown in Table 3, indicating that the maximum tensile stress which a specimen will support is nearly independent of the lateral loading condition. (After due consideration for sample size and shape and loading rate) It was concluded that the Class 2 solid propellant does not demonstrate isotropic failure characteristics.

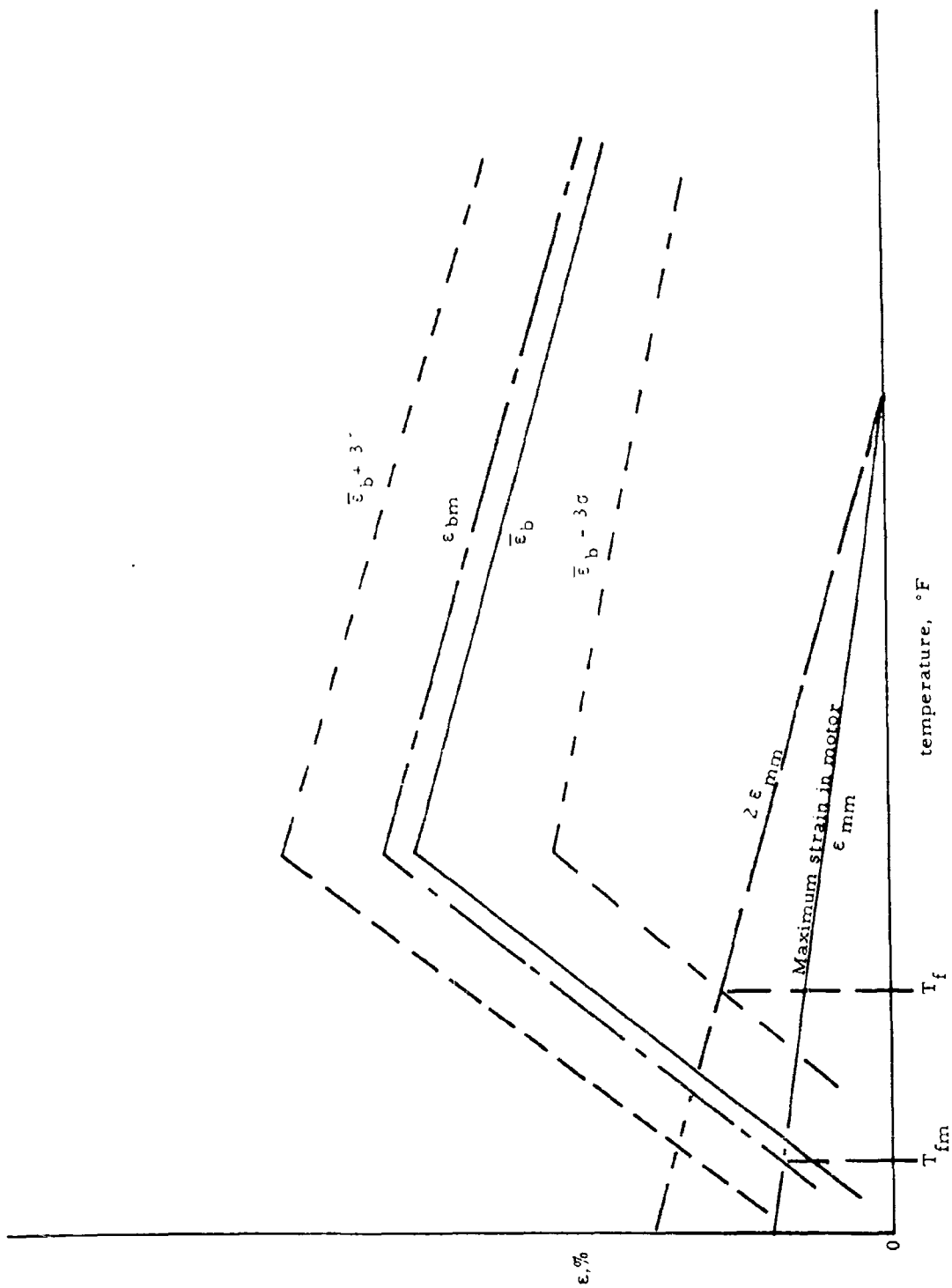


Figure 34: Hypothetical Propellant Properties Related to Motor Strain

TABLE 3

COMPARISON OF UNIAXIAL AND BIAxIAL FAILURE STRESSES
OF A CLASS 2 PROPELLANT AT SEVERAL TEMPERATURES

| Temperature °F | Nominal Stress at Failure, psi | |
|-------------------|-----------------------------------|---------------------------------|
| | Uniaxial, 0.74 min. ⁻¹ | Biaxial, 1.0 min. ⁻¹ |
| 180 | 63 | 52 |
| 140 | 68 | 48 |
| 110 | 79 | 58 |
| 80 | 84 | 62 |
| 40 | 110 | 99 |
| 0 | 124 | 127 |
| 40 | 188 | 224 |
| -60 | 224 | 216 |
| -75 | 470 | 485 |

V, Phase 4 - Failure Criteria (cont.)

E. FAILURE STUDIES UNDER COMBINED LOADING (MIT)

Equipment for investigating the failure of solid fuels under combined loadings has been designed at the Massachusetts Institute of Technology to control independently the levels of hydrostatic tension and shear or distortion. Calculations have been carried out, during this period, on models to predict and evaluate the results of this type of testing. Because a realistic model of such composite materials is so complex, the analysis is not ready for application at present. However, an approach has been established with the work done so far that can be developed to give insight into failure mechanisms and which will help in correlating observed results.

The approach used in the analysis is based on the premise that, for dense packing, the region connecting adjacent particles will be the critical area for failure. In these ligaments the strains in the matrix will be much greater than the macroscopic average for the specimen and the stresses will similarly be much higher than the nominal stresses.

If the loading is rapid so that the response is essentially elastic, the stresses in these regions will tend to exceed the bonding strength between matrix and filler. When this happens, the modulus will be expected to decrease, the Poisson ratio will decrease and the structure will behave more like a fibrous material. Of particular importance in this process is the nominal hydrostatic stress, which, because the material is relatively incompressible before separation occurs, can be superimposed on the local stresses resulting from distortion in a ligament. This loading will decrease, if tensile, or increase, if compressive, the nominal stress or strain at which separation occurs.

V, E, Failure Studies under Combined Loading (MIT) (cont.)

Another possible sequence of failure may result from very slow loading, particularly with hydrostatic compression, in which the bonding strength between the matrix and filler is not exceeded. In this case, however, voids would tend to form in the matrix at the ligaments where the total strains would be many times greater than on the gross scale.

To evaluate these effects, the stresses between two paraboloids of revolution, representing the surfaces of filler particles have been analyzed. At present the material is considered as elastic and incompressible. This analysis shows, as would be expected, very large changes in stress level which are affected by the proximity of the surfaces. To check the validity of this approach, the modulus for spheroids of this type arranged in a simple cubic array were estimated and compared with available tensile data for different densities of filler as shown in Figure 35. Since no effort was made to compensate for variations in size or spacing of the particles, the correlation with the limited data on hand is encouraging. The analysis for stresses in the ligaments becomes inexact as the separation between the particles increases. This probably explains the difference between the data and predicted values of modulus at the lower densities.

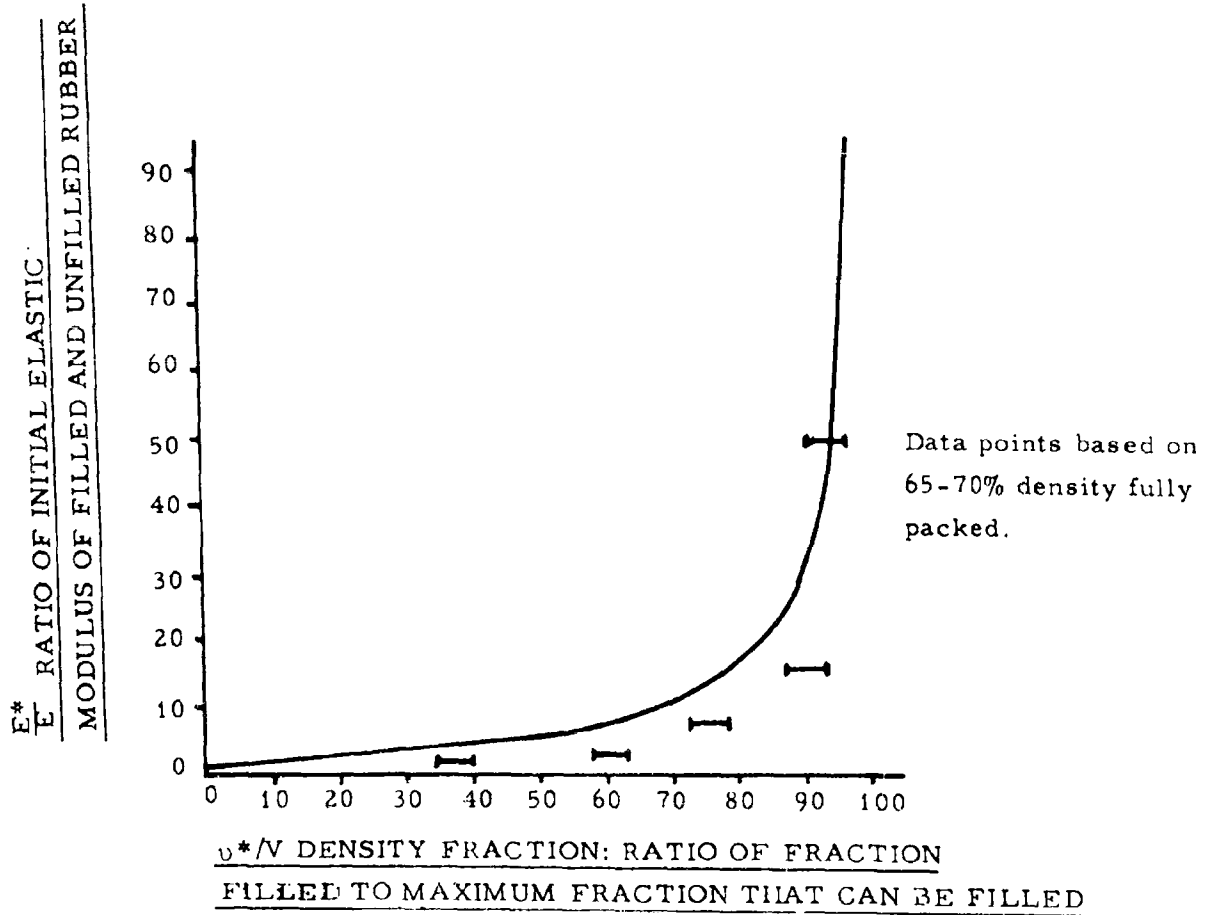


Figure 35: Predicted Values of Variation of Modulus with Density Compared to Test Data on Initial Loading

VI. PHASE 5 - INTEGRATED DESIGN APPROACH

The objective of this phase is to integrate the methods of the first four phases with propellant development and change design and develop a philosophy for optimum development of a charge design capable of meeting both structural and ballistic requirements. In seeking a method of approach to this problem, the Program Evaluation Research Task (PERT) method of network analysis appeared promising, and the PERT concept has been used as a basis of discussion for this phase of the program. The difficulties of program evaluation and analysis for this type of activity are recognized by the Special Projects office of the Bureau of Naval Weapons; "three factors, however, set research and development programming apart. First, we are attempting to schedule intellectual activity as well as the more easily measurable physical activity. Second, by definition, research and development projects are of a pioneering nature. Therefore, previous, parallel experience upon which to base schedules of a new project is relatively unavailable. Third, the unpredictability of specific research results inevitably requires frequent change in program detail. These points are acknowledged by all experienced research people.

"Yet, even though it be ridiculous to conceive of scheduling research and development with the split-second precision of an auto assembly line, it is clear that the farther reaching and more complex our projects become, the greater is the need for procedural tools to aid top managers to comprehend and control the project. At the very least, such a method can improve over the random 'how goes it' examination if only by providing

"Orderliness and consistency in planning and evaluating all areas of the project,

"Automatic identification of all potential trouble spots arising in a complex project as a result of failure in one area,

"Speed in integrating progress evaluation,

VI, Phase 5 — Integrated Design Approach (cont.)

"And throughout runs the requirement for faithful portrayal of the rapidly changing research endeavor."⁽¹³⁾

It was felt that the PERT approach offered a means of describing the elements one analyses consciously, or unconsciously, in arriving at an estimate of any job, whether it be how long to get a Ph.D. degree, to write a book, etc., e.g., how hard is the job in terms of the available ability, and about how long should it take to get to some objective. To estimate the difficulty of the job, one might look at the problem in terms of previous similar work and the relative progress of the field towards some ultimate objective or limit. Thus a bacterial population tends to a limit which can be calculated even if the limit can't be readily measured. In that example, the rate of approach to this limit is proportional to how far one is from the limit, leading to a Fourier type of equation, $dy/dt = k(y-y)$. At the same time, the objective one visualizes may not truly be the ultimate and a sudden advance in the technology or body of scientific knowledge may suddenly shift the whole state of art forward and also increase the objective. The approach to the objective can be described by a learning curve, which can be expressed as reliability (or performance) as a function of units of activity, such as batches made, experiments run, etc. The units of activity depend in turn on the level and quality of support of manpower, material, and equipment to the activity and the number of parallel lines of activity being pursued simultaneously. The rapidity of advance depends upon the talent available, facilities, etc. The rate of progress may not necessarily be in terms of time; completeness of the unit of activity will also determine the increase of reliability accomplished by each unit.

The completeness of the unit of activity refers to adequacy of provision of all elements necessary to a unit. An example of a lack of completeness would be the development of an item without a pertinent means of evaluating performance of items under development. Another example of lack of completeness is inadequate provision for the coordination of interrelated activities within the unit. This latter point directly relates to the use of PERT, for which the most significant points are

VI, Phase 5 – Integrated Design Approach (cont.)

suggested by Malcolm as: "First, it represents a fundamental operational approach to R and D planning by describing the R and D process as a network of interrelated activities. This will cause a very pervasive change in our planning methodology since it faces up to the coordination problem involved in an R and D program. Secondly, PERT has focused attention on and offers the promise for better integrated planning methods in the cost and performance areas."⁽⁵⁾

Malcolm further states that the orderly application of PERT involves the following steps: (with additional steps suggested for this program inserted in parenthesis)

1. "Selection of specified identifiable events."
2. "Determine activities necessary to achieve events."
3. (Determine kinds and quality of talent needed)
4. (Determine major characteristics of activities and the input, output requirements and pertinent interrelationships).
5. "Develop project network of activities and events by properly sequencing events and establishing interdependencies."
6. (Review network for completeness to assure that all necessary activities are present).
7. "Estimate time to complete activities, together with a measure of uncertainty," (including effect of quality of the talent available).
8. "Design and analysis or evaluation procedure to process and manipulate these data."
9. (Determine necessary control and decision points on the several decision lines to insure effectiveness of interrelationship).
10. "Establishment of information channels to bring actual achievement data and change data to the evaluation center."
11. "Application of Electronic Data Processing equipment to the analysis procedure."

VI, Phase 5 - Integrated Design Approach (cont.)

12. "Display and use of the data by management -- -- ."
13. "Maintenance and updating of the planning information to keep up with dynamics of program."
14. (Establish basis for review to assess schedules, assess individual performance, and assess the program strategy and decisions used).

If one considers the development of a propellant charge for a particular application, the process can be visualized in general as shown in Figure 36. Assuming adequate knowledge is available on existing propellants, a morphological analysis of the possible ballistic designs will indicate which, if any, of these propellants can be used, and ballistic calculations will show the performance of the several possible designs. The compatibility of these designs with the environmental conditions can then be estimated by structural analysis using the mechanical properties of the several propellants (assuming the method for doing this is available for each condition). Selection of the best of these designs would require a series of tradeoffs, such as stress concentration against sliver loss in selecting fillet radii, and allow evaluation of deficiencies needing developmental correction. These developments then become the subject of proposal plans and subsequent development effort.

The original analysis may indicate that only modest changes are required, which can be easily handled by introducing available technology into the specific propellant system. Such a change requires only confirmation and little inter-relationship of activities is required. For major advances in propulsion systems, however, the chief effect of the initial morphological, ballistic, and structural analyses is to indicate the inadequacy of existing propellant systems and point up specific deficiencies as objectives for a major propellant development program. This latter situation will receive the major attention in this phase of the program.

The first trial solution of the problem described above may be thought of as defining the areas for study and establishing points of departure and initial

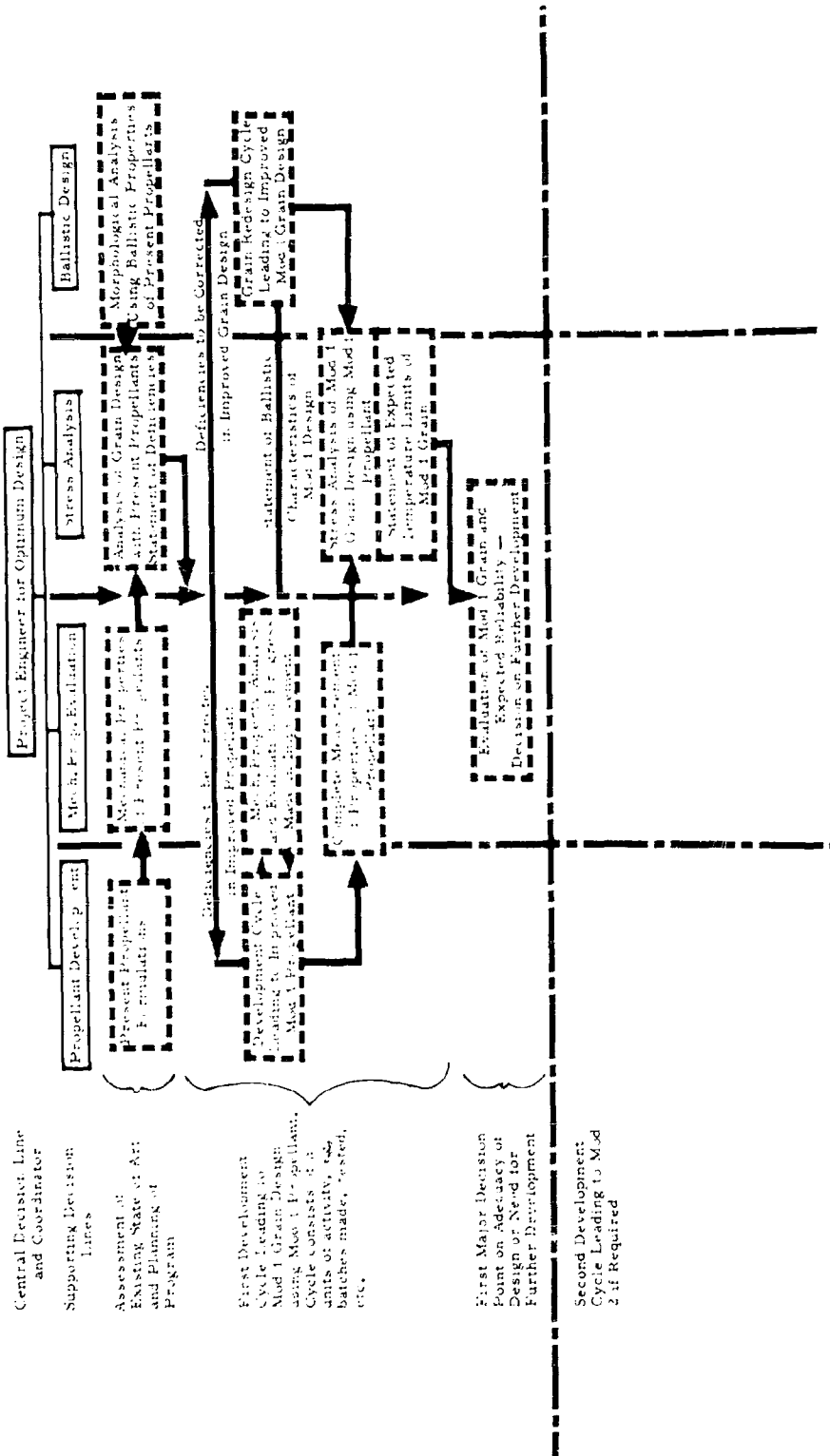


Figure 36: Diagram of General Process of Grain Development Showing Interrelation of Major Development Efforts

VI, Phase 5 -- Integrated Design Approach (cont.)

objectives for the several lines of research and development work. Once started, these lines of work become continuous streams of physical and intellectual activity from which specific products may be removed from time to time for use in the several stages of motors system development. The first of these products may be thought of as the Mod 1 propellant formulation for use in the Mod 1 grain design. Both of these will be modifications of previous items and will be the result of one cycle of the charge development activity. The improvement in performance or reliability in a particular environment due to this cycle of activity is determined roughly by the position of the starting point on the reliability curve of this system as illustrated in Figure 37.

The removal of the Mod 1 products does not generally stop the stream of activity (assuming funding and related problems are not governing) for several reasons. First, the first modification will generally not accomplish all of the desired objectives, particularly under the collapsed time scales prevalent in development work on missiles. Second, a backup effort is generally continued at a reduced pace to overcome expected secondary problems of processing, reproducibility, etc., as Mod 1 goes into scale up and production. Third, a development activity once initiated requires teams of professional personnel that cannot be turned on and off abruptly, though they can be redirected, without serious effect on the development structure as a whole. Finally, the work done to reach Mod 1 has in turn generated new ideas, produced new data, and generally set the stage for further work. Thus even if Mod 1 were to be the final product of this system, it would in turn generate new work on another system for which the Mod 2 of the first system would become the Mod 1 of the second.

This concept of a continuous stream of activity is an essential basis since a program team does not suddenly spring into being but already exists in the continually developing skills of its members. At the same time, it is essential to assess the improvement in reliability resulting from units and cycles of activity

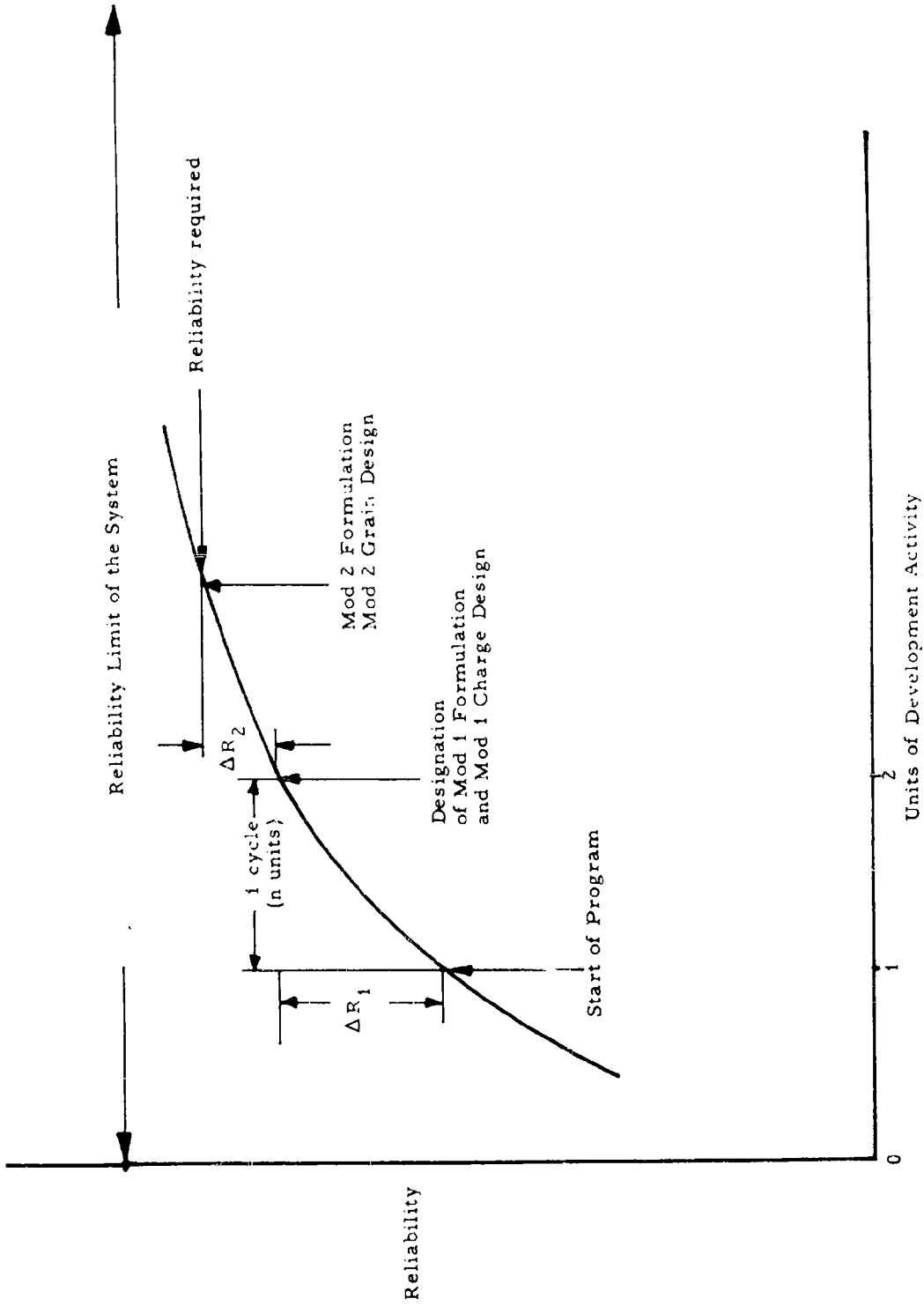


Figure 37: Growth of Reliability (or Performance) of a Given Propulsion System

VI, Phase 5 – Integrated Design Approach (cont.)

and determine whether the available cycles of activity within a program will produce the target reliability specified. In some cases the target reliability may be higher than the ultimate reliability limit of the system in the development stream; then it is essential to recognize that a breakthrough to a new system with greater reliability is required. An example of this was the limitation on low temperature performance for the conventional solid propellant used in thick web designs due to the low failure elongations achievable at low temperatures. The breakthrough of controlled dewetting behavior by new systems established a new reliability growth curve for use.

VII. SUMMARY AND CONCLUSIONS

A program of study leading to methods for optimum grain design incorporates four phases pertinent to structural analysis and property measurement and a fifth phase which integrates these techniques with propellant development and ballistic analysis. The first phase, measurement of mechanical properties has been concerned with improvements in measurement technique leading to better assessment of the binder-oxidizer interaction under the multiaxial conditions expected in motors. The second phase, representation of mechanical behavior, has been concerned with the classification of behavior into several classes characterized by the degree of localization of dewetting with resultant localization of failure. The third phase, theoretical and experimental stress analysis, has been concerned with the suitability of infinitesimal linear theory in predicting stresses and strains and reasonable agreement is found up to strains of the order of 10% above which significant dewetting and dilatation occur. The fourth phase, failure criteria, has been concerned with the variability of failure behavior and a definite ordering of batches from good to bad appears to be effected by low rate tensile tests at different temperatures or by comparing low rate uniaxial elongations at failure with cracking in small tubular, case-bonded grains. The fifth phase, the integrated design approach, has been concerned with selection of a basic point of view and the PERT system of network analysis appears to offer a suitable basis for study.

LIST OF SYMBOLS

| | |
|--------------|--|
| A | Area, sq in. |
| B | Blatz number = $1 - 2\nu_B$ |
| E | Young's Modulus, psi |
| G | Gage length, in. |
| L | Length after strain, in. |
| L_0 | Length before strain, in. |
| P | Hydrostatic pressure, psia |
| S_n | Nominal stress based on original cross section, psi |
| S_{nb} | Nominal stress at break, psi |
| S_{nm} | Nominal maximum stress, psi |
| T | Temperature, °F |
| V | Volume after strain, cu in. |
| V_f | Volume fraction of filler |
| V_0 | Volume before strain, cu in. |
| a | Inside diameter of circular bore of grain, in. |
| b | Outside diameter of cylindrical grain, in. |
| r | Radius at any point in grain |
| u | Displacement of surface at r, in. |
| α_p | Linear coefficient of thermal expansion of propellant, (in.)/(in.)(°F) |
| α_c | Linear coefficient of thermal expansion of case material, (in.)/(in.)(°F) |
| ϵ | Strain |
| ϵ_b | Strain at break |

LIST OF SYMBOLS (cont.)

| | |
|------------------|---|
| ϵ_c | Strain at yield of filler binder bond |
| ϵ_m | Strain at nominal maximum stress |
| ϵ_{mm} | Maximum strain observed in bore of grain |
| ϵ_{rc} | Strain in binder between filler particles just before failure of bond |
| λ | Extension ratio in direction of strain |
| λ_l | Lateral extension ratio |
| λ_r | Radial extension ratio |
| λ_θ | Tangential extension ratio |
| μ | Propellant shear modulus, psi |
| ν | Poisson ratio |
| ν_B | Experimental constant like Poisson ratio, defined by Eq. 5 |
| σ_r | Interfacial radial pressure, psi |

BIBLIOGRAPHY

1. Blatz, P. J., and Nesheim, G. D., "Elastic Stresses in Glass Filament Wound Solid Propellant Motors", Memo 4780-2683, 9 December 1960.
2. Cleve, Merton L., Jr., and Barry, John D., "A Qualitative Photoelastic Gelatin Stress Analysis of the Effectiveness of Various Ground Anchoring Devices", Tech. Report QMRD-5, October 1955.
3. Goldhagen, S., "Study of Methods of Improving Storage Life of Solid Rocket Motors", Contract AF 33(600)-40314.
4. Jones, J. W., and Spangler, R. D., "Application of Experimental Mechanical Property Data to Strain Analysis of Solid Propellant Grains", Bulletin of the Joint Meeting JANAF Panels on Physical Properties and Surveillance of Solid Propellants, PP-13/SPSP-8, August 1960.
5. Malcolm, D. G., "Extensions and Applications of PERT as a System Management Tool", Address delivered at Aerospace Industries Assn., July 1940, Operations Research, Inc.
6. Martin, G. M., Roth, F. W., and Stiehler, R. D., "Behavior of Pure Gum Rubber Vulcanisates in Tension", Trans. Inst. Rubber Ind., Vol 32, pp 189-203, 1956.
7. Messner, A., "Propellant Grain Stress Analyses", Bulletin of 17th JANAF-ARPA-NASA Solid Propellant Group Meeting, May 1961, Denver, Colo.
8. O'Callaghan, T., "Elastic Stresses in Glass Filament Wound Solid Propellant Motors. Dimensionless Presentation of Dr. Blatz' Results for Finite Deformations", Memo 4780-2689, 27 December 1960.
9. Rivlin, R. S., "A Series of Eight Lectures on Finite Elastic Deformations", delivered to the Engineering Division, California Institute of Technology, January and February 1953.
10. Sampson, R. C., "Photoelastic Analysis of Stresses in Perforated Material Subject to Tension or Bending", Bettis Technical Review, April 1960.
11. Smith, Thor, "Volume Changes and Dewetting in Glass Beads - Polyvinyl Chloride Elastomeric Composites Under Large Deformations", Trans, Soc. Rheology, 3, 113-116 (1959).
12. Smith, Thor L., "Ultimate Tensile Properties of Amorphous Polymers", Jour. Soc. Plastics Engrs., 16, No. 11 (1960).

BIBLIOGRAPHY (cont.)

13. Special Projects Office, Bureau of Naval Weapons, "Program Evaluation Research Task, Summary Report, Phase 1", July 1958.
14. Vernon, J. H. C., "The Effects of Confining Pressure on the Mechanical Properties of Solid Propellants", Bulletin of the Joint Meeting JANAF Panels on Physical Properties and Surveillance of Solid Propellants, PP-13/SPSP-8, August 1960.
15. Williams, M. L., Blatz, P. J., and Schapery, R. A., "Fundamental Studies Relating to Systems Analysis of Solid Propellants", Final Report, GALCIT SM61-5, February 1961.

UNCLASSIFIED

UNCLASSIFIED